Title
Epithelial-Mesenchymal Interactions in Intestinal Development

Author
Kosinski, Cynthia Marie

Publication Date
2009

Peer reviewed|Thesis/dissertation

Epithelial-Mesenchymal Interactions in Intestinal Development

by

Cynthia Kosinski

DISSERTATION

Submitted in partial satisfaction of the requirements for the degree of

DOCTOR OF PHILOSOPHY

in

Pharmaceutical Sciences & Pharmacogenomics

in the

GRADUATE DIVISION

of the

UNIVERSITY OF CALIFORNIA, SAN FRANCISCO

DEDICATIONS

To my parents, Pamela and John, who ignited my interest in science so many years ago with a slide box full of mounted sea specimens and a plastic microscope. Their loving support and encouragement have given me the confidence to pursue uncharted knowledge. To Jeff, whose insatiable curiosity of the universe inspires me to keep seeking answers.

ACKNOWLEDGMENTS

As a student en route to becoming a scientist in graduate school you are presented with numerous challenges and typically experience frustration, doubt, and failure much sooner than success. The support, guidance, and friendship of many have assisted me along this academic journey.

I thank my mentor Dr. Xin Chen, for her encouragement and helpful scientific advice. Her suggestions improved the quality of this dissertation. Her faith in my abilities has pushed me to become a better writer, communicator, and scientist. I also want to thank Dr. Ben Cheyette and Dr. Dean Sheppard, members of my thesis committee, for their mentorship and critique of my dissertation work. Their enthusiasm for science and problem solving has motivated me throughout graduate school and will continue to do so in my scientific career.

I thank the past and present members of the Chen lab who have provided a supportive work environment. In particular, I would like to thank Coral Ho, Susie Lee, Mohini Patil, Ernest Lam, Jude Dachrut, Ji Zhang, and Michael Xu for their technical assistance, encouragement, calmness, and friendship. Each one of them greatly enriched my graduate school experience.

My greatest gratitude goes to my family; my parents, Pamela and John; my grandparents, Jan, Mary, Kathy, and James; my sister, Claire; my brother, Chris; my best friend, Michelle; and my special someone, Jeff. They have played an instrumental role in my achievements by providing guidance, encouragement, emotional support, and inspiration. This dissertation would not have been possible without them.

CO-AUTHOR ACKNOWLEDGMENTS

The data presented in Chapter 2 were previously published in the Proceedings of the National Academy of Sciences (Kosinski et al., (2007) *Proc Natl Acad Sci U S A* **104**, 15418-23) and is reproduced here in adherence with the PNAS copyright policy.

This work was done in collaboration with co-first author Vivian Li, who performed most of the microarray analysis and validated microarray results by quantitative RT-PCR. The localization of BMP antagonists and *in vitro* studies were performed by Cynthia Kosinski. The manuscript text was primarily written by Cynthia Kosinski.

Epithelial-Mesenchymal Interactions in Intestinal Development

By Cynthia Kosinski

ABSTRACT

Communication between the intestinal epithelium and the underlying mesenchyme is essential in controlling intestinal stem cell (ISC) activity, morphogenesis, differentiation, and homeostasis. These epithelial-mesenchymal interactions involve instructive signaling molecules that belong to multiple signaling families including the Wnt/β-catenin, BMP, and Hedgehog (Hh) pathways. How these pathways coordinate to regulate intestinal development, including ISC self-renewal and differentiation is not completely understood. Potential sources and targets of these signals exist in the microenvironment surrounding ISCs, known as the stem cell niche. Of the niche cells, intestinal subepithelial myofibroblasts (ISEMFs) are considered the main niche cell type since their location at the crypt base positions them closest to ISCs. Herein, we provide evidence that BMP antagonists, including Gremlin 1, Gremlin 2, and Chordin-like 1 are supplied by ISEMFs and smooth muscle cells surrounding the crypt. We show that Gremlin 1 activates Wnt signaling and inhibits the differentiation of intestinal epithelial cells, and thus functions as a stimulating signal that promotes ISC self-renewal.

Working in the converse direction to BMP antagonists are Hh signals, which originate in the intestinal epithelium and target mesenchymal cells, including those comprising the ISC niche. Utilizing *Indian Hedgehog* (*Ihh*) conditional knockout mice, we show that deletion of epithelial Ihh in the small and large intestine disrupts the ISC niche architecture as demonstrated by the loss of the muscularis mucosae, diminished crypt

myofibroblasts, and extracellular matrix breakdown. Gene expression data suggest that Ihh mutants have an overall decrease in BMP signaling, amplified matrix metallopeptidase activity, and deficient extracellular matrix and smooth muscle development. The mesenchymal niche modifications seen in the Ihh mutants are accompanied by striking changes in the intestinal epithelium, including dilated and ectopic crypts, anatomically deranged and mislocated absorptive and secretory cell lineages, and elevated Wnt signaling. Significantly, we detected an increase in the number of ISCs in the Ihh mutants. These results demonstrate that the Ihh regulates ISCs by maintaining the mesenchymal stem cell niche. In total, the work presented in this dissertation describes previously unrecognized paracrine functions of BMP antagonists and Ihh in regulating intestinal development.

TABLE OF CONTENTS

Dedication	iii
Acknowledgments	iv
Abstract of the Dissertation	vi
Table of Contents	viii
List of Figures and Tables	ix
Chapter 1. Introduction	1
Overview	2
Intestinal Development	2
Intestinal Stem Cells	4
Intestinal Stem Cell Niche	7
Wnt Signaling in the Intestine	9
Notch Signaling in the Intestine	12
BMP Signaling in the Intestine	14
Hedgehog Signaling in the Intestine	17
Summary of Thesis	21
Chapter 2. Gene Expression Patterns of Human Colon Tops and Basal Crypts and BMP Antagonists as Intestinal Stem Cell Niche Factors	26
Chapter 3. Indian Hedgehog Regulates Intestinal Stem Cell Fate through Niche Maintenance	68
Chapter 4. Conclusion	132

LIST OF FIGURES AND TABLES

Chapter 1

Figure 1	The Wnt/β-catenin signaling pathway	10
Figure 2	The Notch signaling pathway	13
Figure 3	The BMP signaling pathway	15
Figure 4	The Hedgehog signaling pathway	18

Chapter 2

Figure 1	Hierarchal clustering of genes differentially expressed in colon top and basal crypt as identified by SAM	33
Figure 2	Significant correlation between genes differentially expressed in colon top and basal crypt and Wnt/β-catenin signaling targets	36
Figure 3	Expression and localization of GREM1 and GREM2 by myofibroblast cells and smooth muscle cells at colon crypt	40
Figure 4	Gremlin 1 partially inhibits Caco-2 cell differentiation and activates Wnt/β-catenin signaling in normal intestinal cells	43
Figure 5	Graphical view of human colon intestinal epithelial cell development and stem cell niche maintenance	46
Figure S1	Network analysis for cell cycle and apoptosis genes differentially expressed in colon top and basal crypts by GenMapp from KEGG pathway	59
Figure S2	Differential expression of translation factors and ribosomal proteins in colon bottom versus top crypt compartments by GenMapp	60
Figure S3	Differential gene expression pattern of selected pathways in colon top and basal crypts	61

Figure S4	Genes differentially expressed in colon top and basal crypts and their relationship with Wnt/β-catenin signaling targets	62
Figure S5	Enlarged version of Figure 3E-3G showing colocalization of Gremlin 1 and vimentin at colon crypts	63
Figure S6	Characterization of isolated human colonic myofibroblast 18Co cells	64
Figure S7	Candidate stem/progenitor cell markers in colon crypt gene list illustrated using TreeView	64
Figure S8	Gremlin 1 expression in colon cancer stromal cells revealed by *in situ* hybridization	65
Figure S9	Representative horizontal histological sections of colon top and crypt mucosal compartments	65
Table S1	Quantitative RT-PCR validation of colon bottom/top array expression data	66
Table S2	Primers used for RT-PCR, quantitative RT-PCR, and *in situ* hybridization	67

Chapter 3

Figure 1	Conditional deletion of *Ihh* in mouse intestinal epithelium	76
Figure 2	Loss of ISC niche cells in *Villin-Cre;Ihh$^{flox/flox}$* mice	79
Figure 3	Abnormal intestinal epithelial phenotypes in *Villin-Cre;Ihh$^{flox/flox}$* mice	83
Figure 4	Increased Wnt/β-catenin activity and intestinal stem cell expansion in *Villin-Cre;Ihh$^{flox/flox}$* mice	85
Figure 5	Abnormal intestinal epithelial cell differentiation in *Villin-Cre;Ihh$^{flox/flox}$* mice	87
Figure 6	Normal intestinal development in conditional *Smo* KO Mice	89
Figure 7	Genes differentially expressed in colon tissues from control and *Villin-Cre;Ihh$^{flox/flox}$* mice	92

Figure 8	Disruption of stromal compartment upon Ihh loss	94
Figure S1	Loss of ISC niche cells in *Villin-Cre;Ihh$^{flox/flox}$* mice through postnatal development	109
Figure S2	Loss of ISC niche cells in *Villin-Cre;Ihh$^{flox/flox}$* mice	110
Figure S3	Abnormal intestinal epithelial phenotypes in colon tissue of *Villin-Cre;Ihh$^{flox/flox}$* mice	111
Figure S4	Abnormal activation of Wnt/β-catenin signaling in *Villin-Cre;Ihh$^{flox/flox}$* mice	112
Figure S5	Vacuolation of enterocytes in *Villin-Cre;Ihh$^{flox/flox}$* mice	113
Figure S6	Transmission electron microscopy of microvillar brush border	114
Table S1	Genes differentially expressed in *Villin-Cre;Ihh$^{flox/flox}$* mice versus control mice (full list)	115
Table S2	Primer sequences	131

Chapter 1

Introduction

Overview

The gastrointestinal tract undergoes multiple developmental transitions as it transforms from a simple tube into a functional organ with specialized compartments. The gut epithelium interacts with the underlying mesenchyme to form invaginations referred to as crypts, and protrusions called villi (in the small intestine), or crypt surface (in the colon) (1). Each crypt is comprised of proliferating cells and stem cells, while each villus or crypt surface is comprised of differentiated, functional cells. As the lifespan of a typical gut epithelial cell is 4-5 days, the gut epithelium must continually renew itself. This renewal process is sustained by rapidly cycling intestinal stem cells (ISCs) that receive directive cues from their surrounding microenviroment, known as the stem cell niche. Much progress has been made in identifying signaling pathways involved in intestinal development and homeostasis, including intestinal morphogenesis, intestinal stem cell activity, lineage commitment, terminal differentiation, and cell death. From mouse studies, the Wnt, bone morphogenic protein (BMP), Hedgehog and Notch pathways have all emerged as major contributors to intestinal development and homeostasis (2-4).

Intestinal Development

Intestinal development is a complex process that is guided by epithelial-mesenchymal interactions. The intestinal epithelium originates from an endoderm-derived digestive tube. At early embryonic stages, the tube appears uniform with stratified layers of epithelium. During fetal and neonatal murine development, signals from the surrounding mesoderm-derived mesenchyme transform the digestive tube into a single-layered epithelium with invaginations, known as the crypts of Liberkühn and protrusions called

villi. The entire intestinal morphogenesis process, including the formation of villi and crypts is not fully complete until postnatal day 28 (5). Variations in villi occur along the proximal-distal axis of the gut, with the duodenum featuring long, thin villi and the ileum displaying shorter, thicker villi. During the first week of postnatal life the colon also contains villi, however by weaning age villus structures are replaced by surface epithelium and crypts extend the entire thickness of the epithelium (6). Intestinal epithelial stem cells reside at the crypt base and give rise to a transit-amplifying population. The descendents of these proliferative cells migrate along the crypt-villus axis and differentiate into four epithelial lineages: absorptive, mucin-secreting goblet, peptide hormone-secreting enterendocrine, and antimicrobial-secreting Paneth cells (small intestine only). Most of these differentiated cell types migrate toward the villus tip, where they are shed or undergo apoptosis. The sole exception is Paneth cells, which instead differentiate as they move downward toward the crypt base where they eventually die. Since the average lifespan of intestinal epithelial cells is 3-7 days (with the exception of Paneth cells, which survive approximately 20 days before they are phagocytosed by neighboring cells), the crypt progenitors must continuously divide to sustain the epithelial cell population. Accordingly, the proliferative capacity of dividing progenitors is high, with each crypt generating approximately 200-300 cells per day (2). At this rate of proliferation, enough cells are produced to renew the entire murine intestinal epithelium in 2-5 days.

Intestinal Stem Cells

Intestinal stem cells are characterized by their ability to give rise to all the differentiated cell types of the intestine as well as being able to self-renew. Until recently, the precise location of ISCs was unknown. For at least the past 40 years, it was widely believed that ISCs were positioned four to six cell diameters from the crypt base (the "+4 position stem cell model"). This conclusion stemmed from DNA label-retaining studies in which ISCs were considered to be quiescent and thus label-retaining, while progenitor cells were assumed to be continuously dividing, diluting out the incorporated DNA (7). The +4 position stem cell model gained more momentum when it was discovered that cells in this position were sensitive to radiation, a protective mechanism believed to prevent ISCs from passing on genetically damaged material (8). The fault in these studies, however, is that they failed to directly assess other crucial characteristics of "stemness" in these cells, such as whether +4 cells are capable of generating the four differentiated cell types of the intestinal epithelium.

Recent advances using cell-lineage tracing strategies have identified more definitive ISC markers, nonetheless, debate over the exact location of ISCs remains strong. Dr. Hans Clevers' group recently provided convincing evidence that ISCs are located at the base of the crypt interspersed between Paneth cells, supporting a mostly unrecognized proposal that dates back to 1974 by Bjerknes and Leblond that suggests crypt-base columnar (CBC) cells are ISCs (9-11). The Clevers' group identified Lgr5/Gpr49, a leucine-rich orphan G protein-coupled receptor as a marker that is specifically expressed in CBC cells in the small intestine and in crypt bottom cells in the colon (9). Using this marker, they estimated that each crypt contains approximately four

to six stem cells, which is consistent with previous reports. BrdU labeling experiments revealed that $Lgr5^+$ CBC cells do not behave as quiescent cells as they have an average cycling time of 24 hours. Most importantly, the Clevers' group has shown via genetic marking studies (utilizing tamoxifen injected mice obtained from a Lgr5-EFGFP-IRES-creERT2 × Rosa26-lacZ cross) that $Lgr5^+$ CBC cells produce the four intestinal epithelial cell types in normal ratios. Similarly, $Lgr5^+$ crypt bottom cells in the colon produce enterocytes as well as goblet cells. Furthermore, $Lgr5^+$ CBC cells are retained for at least 12 months and continue to self-renew the epithelium. Thus, by displaying multipotency and longevity, $Lgr5^+$ CBC cells satisfy the requirements that define a stem cell (9).

Notwithstanding these data, fueling ongoing controversy over the location of ISCs are results from a new study by Sangiorgi and Capecchi that uses lineage-tracing experiments of Bmi-1-expressing cells. This study places ISCs above Paneth cells at the +4 position (12). Similar to the $Lgr5^+$ CBC cells, Bmi-1-expressing cells produce all cell types of the intestinal epithelium. Also, Bmi-1-expressing cell numbers persist for 12 months, similarly fulfilling the self-renewal property of stem cells. In comparison to $Lgr5^+$ CBC cells, Bmi-1 expressing cells appear to enter a proliferative state at slower rates, suggesting they are more quiescent. This observation has led to the speculation that two stem cell populations exist: one that represents a slow cycling stem cell surrounded by an inhibitory microenvironment, and one that represents a rapid cycling stem cell that is surrounded by an excitatory microenvironment rich with stimulating signals such as BMP antagonists like Gremlin 1 and Noggin (13). Another significant difference between the $Lgr5^+$ CBC cells and the Bmi-1-expressing cells is that the Bmi-1-expressing cells exist in a descending gradient along the small intestine with the majority of the

labeled cells detected in the duodenum, the proximal region of the small intestine (12). This finding further corroborates the idea that more than one stem cell population exists along the gastrointestinal tract since Bmi-1-expressing cells are largely absent in regions distal to the duodenum.

The availability of Lgr5- and Bmi-1-based genetic systems provides new opportunities to study ISCs. Most recently, the identification of Lgr5-stem cells has led to the discovery of more ISC markers. Analysis of Lgr5 stem cell-enriched genes identified *Achaete scute-like 2* (*Ascl2*) and *Olfactomedin-4* (*Olfm4*) as two specific ISC markers that are excluded from immediate daughter cells (14, 15). The expression of Ascl2 and Olfm4 coincides with expression of Lgr5, uniquely marking CBCs sandwiched between Paneth cells. Several other ISC markers have been proposed including the cholesterol-binding glycoprotein Prominin1, the neural RNA-binding protein Musashi1, and the inactivated form of PTEN (phosphatase and tensin homolog) i.e. phosphorylated PTEN (P-PTEN) (16-18). However, the stem cell specificity of these markers is equivocal as other investigators have found Prominin1, Musashi1 and P-PTEN expression is not solely restricted to ISCs, but rather detected throughout the entire crypt progenitor compartment (19-21). The emergence of Lgr5, Bmi-1, Ascl2, and Olfm4 as validated ISC markers is expected to facilitate the genetic modification of ISCs, the isolation and culture of ISCs, and the visualization of ISCs *in vivo*. These experiments will likely provide further insights into ISC regulatory pathways and function.

Intestinal Stem Cell Niche

Intestinal stem cell behavior is controlled by diffusible factors and physical interactions, imposed by the surrounding microenvironment known as the stem cell niche. Regulating the stem cell's ability to self-renew and remain undifferentiated are essential functions of the niche. The ISC niche encompasses all cellular and non-cellular components that interact with and regulate ISC fate. The proposed ISC niche consists of neighboring epithelial cells, pericryptal intestinal subepithelial myofibroblasts (ISEMFs), enteric neurons, endothelial cells, intraepithelial lymphocytes and the basement membrane (22). It is widely believed that ISEMFs are the most influential mesenchymal niche cell given their close proximity to intestinal epithelial stem cells. ISEMFs possess morphologic and functional properties of both fibroblasts and smooth muscle cells. They express smooth muscle markers such as α-smooth muscle actin and fibroblast markers such as vimentin (23). ISEMFs regulate ISC activity through paracrine signaling of growth factors, cytokines, prostaglandins, and extracellular matrix proteins (24). Factors secreted by these cells include hepatocyte growth factor (Hgf), tissue growth factor-β (Tgf-β), basic fibroblast growth factor (bFGF), and keratinocyte growth factor (Kgf) (25-27). However, many secreted factors important in sustaining the niche remain elusive.

In addition to secreted factors, stem cell fate decisions may also be influenced by physical characteristics of the ISC niche such as those established by the basement membrane (28). The basement membrane of the small intestine and colon is a thin layer of extracellular matrix (ECM) components located at the epithelial-mesenchymal interface. It is mainly composed of type IV collagen, laminin, and nidogen produced by mesenchymal cells and heparan sulfate proteoglycan produced by epithelial cells (29).

ISCs attach to the basement membrane, anchoring themselves within the niche, where directive self-renewing and differentiating signals reside. Additionally, the physical attachment to the basement membrane allows intestinal epithelial cells to attain their proper shape, which may be necessary for the transcription of self-renewing or differentiation gene programs. ECM protein-cell interactions and signaling are primarily mediated by integrins, transmembrane heterodimeric glycoproteins located on the epithelial basal membrane. Strong expression of the epithelial integrin subunits, β1, α2 and α6 are detected in the crypt epithelium. A recent study reported that the specific deletion of β1 integrin in intestinal epithelial cells leads to an increase in epithelial proliferation (30). Mechanistic studies revealed that the increase in proliferation was anchorage-independent and due to the loss of β1-mediated Hedgehog signaling. Thus, ISCs likely integrate physical cues and secreted protein factors provided by the niche to regulate their function. Much remains to be determined about the ISC niche, including the precise signals that influence ISC behavior, the cellular sources of the signals and how supporting stromal cells, cell adhesion molecules and the extracellular matrix impact ISC decisions. The paucity of definitive ISC markers has long impeded the progress of understanding how the niche regulates ISCs. However, with the identification of the specific ISC markers Lgr5, Olfm4, Ascl2, and Bmi-1, better understanding of the niche, including ISC regulatory signals and the individual functional components, is anticipated. Also, greater insight into how deregulation of the ISC niche contributes to colorectal cancer, colonic polyps and celiac disease may be obtained.

Wnt Signaling in the Intestine

In the intestine, the Wnt signaling pathway performs a critical role in the development and maintenance of crypt progenitor compartments (31). The key playmaker in the signaling cascade is the cytoplasmic protein β-catenin, whose fate is determined by a destruction complex that contains two scaffolding proteins, axin and adenomatous polyposis coli (APC), as well as two kinases, casein kinase I (CKI) and glycogen synthase kinase-3beta (GSK3β). In the absence of Wnt, APC and axin bind β-catenin, allowing CKI and GSK3β to phosphorylate a conserved region of Ser and Thr residues in the N terminus of β-catenin. The resulting phosphorylation leads to the ubiquitination and proteasomal degradation of β-catenin, which is manifested by low levels of cytosolic and nuclear β-catenin. Wnt ligands initiate signaling by binding to a Frizzled receptor (FZD1-8) and a low-density lipoprotein-related protein co-receptor (LRP-5 or LRP-6), which in turn activate Dishevelled. The activation of Dishevelled leads to the inhibition of GSK3β. Consequently, β-catenin accumulates and translocates to the nucleus, where it interacts with TCF-4, a member of the TCF/LEF family to regulate transcription of Wnt target genes in the intestine (Figure 1). Among the genes that are upregulated by a Wnt response are *c-Myc*, which promotes cell proliferation (32), *EphB2* and *EphB3*, which control cell segregation in the crypt (33), *Sox9*, which directs Paneth cell differentiation (34, 35), *Lgr5*, which specifically marks intestinal and colonic stem cells (9) and *Axin2*, which acts as a negative feedback regulator of the Wnt pathway.

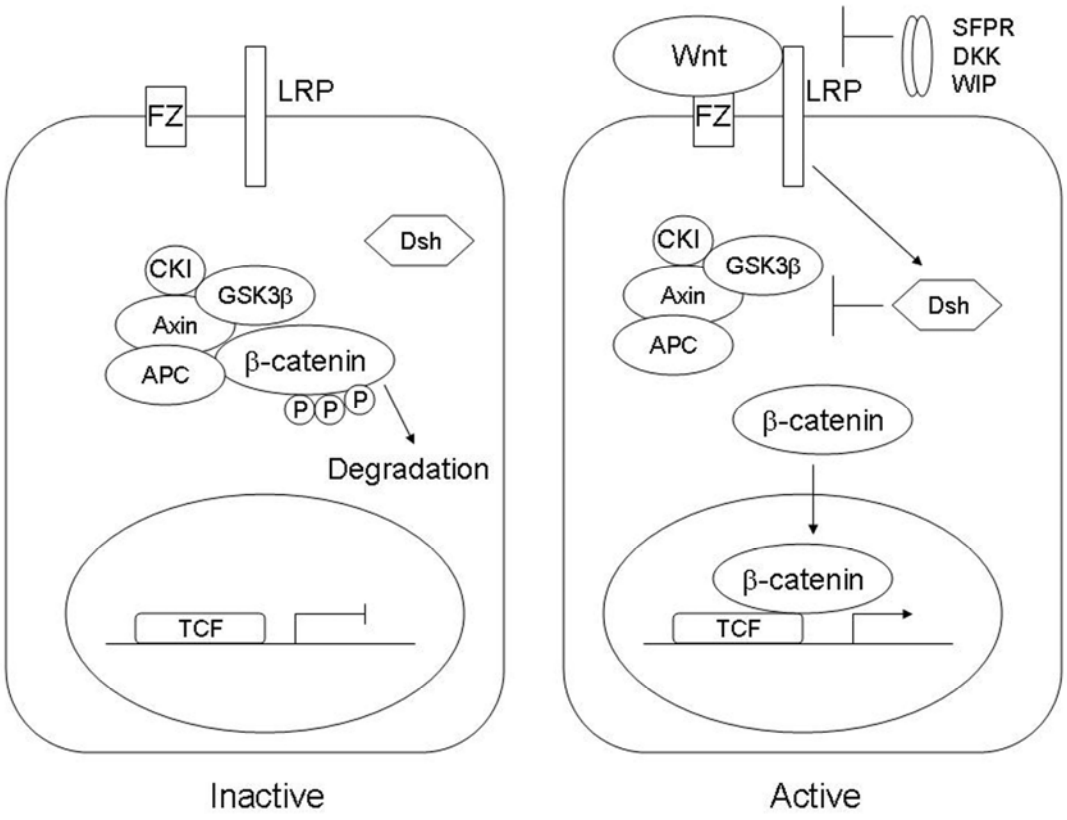

Figure 1. The Wnt/β-catenin signaling pathway. (*Left*) In the absence of Wnt, β-catenin levels are minimized via the β-catenin destruction complex, pictured above as the cluster of APC, Axin, GSK3β and CKI. (*Right*) In the presence of Wnt, the integrity of the β-catenin destruction complex is disrupted, allowing β-catenin to accumulate in the nucleus and activate the transcription of Tcf target genes.

The Wnt pathway has been well studied in the intestine as mutations in the tumor suppressor gene *APC* lead to familial adenomatous polyposis (FAP), a hereditary cancer syndrome. In normal intestine, Wnt signals are involved in the maintenance, proliferation, and fate of intestinal stem cells (36). Nuclear β-catenin, an indicator of active Wnt signaling is detected in proliferative cells comprising the bottom third of the crypt, whereas membrane associated β-catenin is observed above this region along the crypt-villus axis (33). Numerous *in vivo* studies utilizing engineered mice have provided considerable evidence demonstrating Wnt is the key factor that sustains the proliferative

capacity of crypt progenitor cells. Mice containing a deletion of *Tcf-4*, which is the primary transcriptional effector of the Wnt pathway, lack proliferating intestinal epithelial cells after E16.5 as well as a functional stem cell compartment (32, 37). Similarly, transgenic overexpression of *dickkopf homologue 1* (*DKK1*), a specific canonical Wnt inhibitor, results in the absence of proliferating crypts in the murine small intestine, thus indicating that Wnt signaling is required to form and preserve crypts by promoting proliferation (38). Adenoviral expression of DKK1 in adult mice produced conforming results in which the small intestines of treated mice lacked crypts and villi (39). Data are available for the converse studies in which the Wnt pathway is constitutively activated via inactivating mutations in APC or activating mutations in β-catenin. Conditional loss of *APC* in murine intestine results in poorly differentiated intestinal epithelial cells as well as an increase in proliferative cells, a phenotype akin to that seen with early colorectal lesions (40). Wong et al. generated chimeric-transgenic mice expressing constitutively active β-catenin in the small intestine and observed similar increases in the proliferation of crypt cells (41). Besides proliferation, the Wnt signaling pathway also plays a role in cell differentiation, particularly the specification of secretory lineages. *In vivo* studies have demonstrated that when Wnt signaling is inhibited, absorptive cells differentiate normally, but goblet, enterendocrine, and Paneth cells fail to differentiate properly or not at all (37, 38, 42). Thus, the Wnt signaling pathway regulates multiple processes within the intestine, including the proliferation of progenitor cells, the maintenance of progenitor cells in an undifferentiated state (except Paneth cells), and the bestowal of a secretory cell fate to cells committed to terminal differentiation.

Notch Signaling in the Intestine

The Notch signaling pathway is important in regulating key cellular differentiation processes during embryonic development and adult life. Molecular cloning of *Notch* determined that the gene encodes a transmembrane protein which functions as a receptor for ligands (Delta and Jagged) presented on the cell surface of neighboring cells. In mammals, four Notch receptors (Notch 1, Notch 2, Notch 3, and Notch 4) and five Notch ligands have been identified.

Notch is activated when it binds to its ligand on a neighboring cell. The binding triggers a cascade of proteolytic cleavages. The first cleavage is mediated by ADAM protease, an α-secretase, also known as tumor necrosis factor α converting enzyme or TACE. This reaction releases the Notch extracellular region (Notch-EC), and facilitates the next cleavage mediated by γ-secretase at the Notch transmembrane domain. This liberates the intracellular domain of Notch (Notch-IC). Notch-IC subsequently translocates into the nucleus, where it interacts with the transcription factor, CSL (also known as RBP-J in mice) and recruits coactivators (CoA) to form an active transcriptional complex (Figure 2). The transcriptional targets of Notch include the basic helix-loop-helix (bHLH) transcriptional factor hairy/enhancer of split (Hes) family (Hes1 and Hes5).

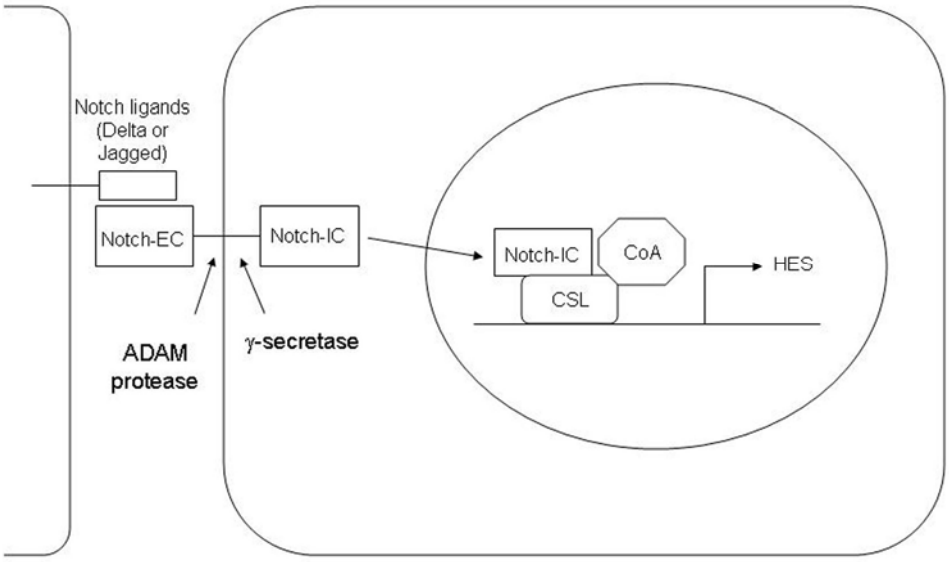

Figure 2. The Notch signaling pathway. Notch signaling is initiated between adjacent cells upon the engagement of Notch receptors with Notch ligands (Delta or Jagged), resulting in two successive proteolytic cleavages of the receptor by ADAM protease and γ-secretase. The cleaved Notch receptor (Notch-IC) translocates into the nucleus, where it interacts with the transcription factor CSL to induce Hes expression.

The identification of Notch pathway components in the intestine provided the first indication that Notch signaling may play a role in gut development and homeostasis (43). It was found that the expression of all Notch receptors and ligands can be detected during various stages of intestinal development. In many cases, these genes are expressed in both proliferative and differentiated intestinal epithelial cells. Subsequent genetic and biochemical experiments have demonstrated that Notch signaling is critical in controlling multiple cell lineages, especially goblet cell differentiation in the intestine. For example, in the zebrafish *DeltaD* mutant, there is an increase of secretory cells and a loss of absorptive cells (44). In mice, there is a massive conversion of cryptic cells into goblet cells after conditional deletion of CSL/RBP-J, the downstream transcription factor of the Notch pathway (42). Consistently, when Hes1 is deleted, there is an increased number of

mucosecreting and enteroendocrine cells at the expense of absorptive cells (45). In converse experiments, Fre et al. overexpressed constitutively active Notch 1 in all cells of the murine intestinal epithelium (46). It was found that these mice had a complete depletion of goblet cells in their intestinal tract. Additionally, there was a marked reduction of enteroendocrine cells as well as Paneth cells. Similar results were reported by Stanger et al (47). In addition, the studies by Stanger et al. also suggest that there are different phenotypes depending on when ectopic Notch signaling is activated: ectopic Notch signaling in embryonic foregut leads to reversible defects in villus morphogenesis and loss of intestinal progenitor cells, whereas ectopic Notch signaling in adult gut leads to a bias against secretory cell fate. Altogether these studies demonstrate that Notch signaling regulates intestinal cell fate determination by controlling the balance between secretory and absorptive cells.

BMP Signaling in the Intestine

Bone morphogenetic proteins (BMPs) are growth factors belonging to the TGF-β superfamily and are implicated in multiple processes including development, morphogenesis, differentiation, proliferation, and apoptosis (48, 49). As shown in Figure 3, BMPs function by uniting their type I (IA, IB, or ALK2) and type II (II, Activin receptor IIA or IIB) serine-threonine kinase receptors. The type I receptor is phosphorylated by the type II receptor, which results in the activation of receptor regulated SMAD-1, SMAD-5, or SMAD-8. The receptor-activated SMAD forms a heterodimeric complex with the common mediator SMAD-4 and translocates the signal to the nucleus, where it drives the transcription of BMP target genes. BMP signaling is

tightly regulated both intracellularly by inhibitory SMADs (SMAD-6 and SMAD-7) as well as extracellularly by BMP antagonists such as Noggin, Gremlin 1, and Chordin.

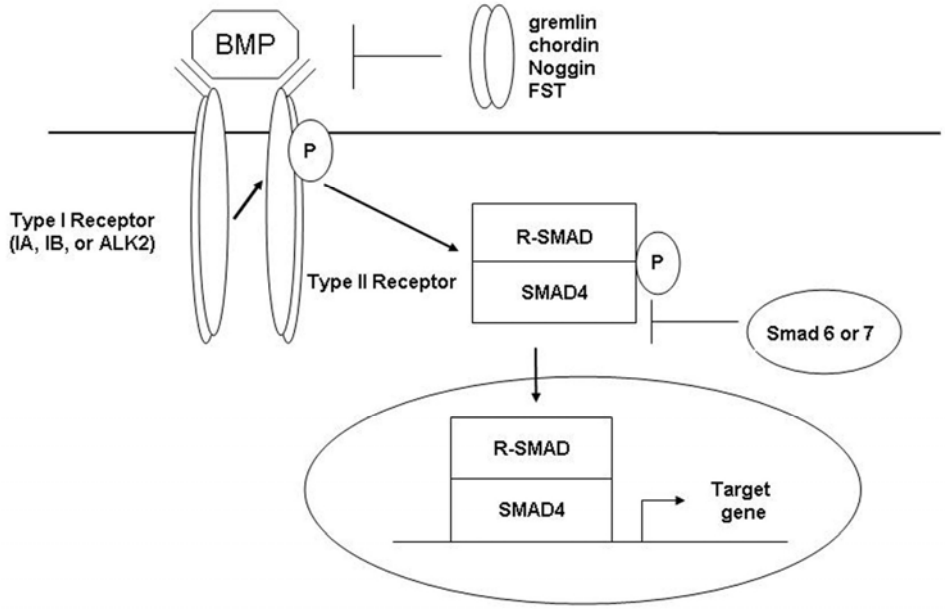

Figure 3. The BMP signaling pathway. BMP signaling is initiated when BMP ligands bind to the complex of BMP type I receptor and BMP type II receptor, leading to the phosphorylation of SMAD1, 5, or 8 (R-SMAD). Phosphorylated SMAD1, 5, or 8 forms a complex with SMAD4 and translocates into the nucleus to activate transcription.

In the intestine, BMP-2 and BMP-4 are highly expressed in the intervillus mesenchyme near the villus tips and display an expression gradient that decreases downward toward the crypt (18, 50-52). The BMP receptor BMPR1A and phosphorylated SMADs, indicators of active BMP signaling, have been detected along the villus epithelial surface (18). Additionally, stromal cells surrounding the crypt base express the BMP antagonists Noggin and Gremlin 1 (18, 53). Altogether, the expression pattern of BMP signaling components supports a role for BMPs in repressing epithelial proliferation and promoting epithelial differentiation. Accordingly, the overexpression of

the BMP antagonist Noggin in mice results in rampant proliferation in stem/progenitor compartments, increased crypt numbers and a Juvenile Polyposis phenotype manifested by hamartomatous polyps (51). Furthermore, *de novo* crypt formation, expansive cell proliferation, increased crypt fission, and polyp formation were all observed upon conditional deletion of BMPR1A using an interferon-inducible promoter. These results indicate that BMPs act to restrict crypt size and formation (18). Moreover, the BMP signaling pathway is implicated in hindering ISC self-renewal by inhibiting the Wnt pathway, appearing to balance stem cell self-renewal versus differentiation (18). The mechanism behind this control involves PTEN, which becomes phosphorylated and inactivated when BMP signaling is inhibited, allowing Phosphatidylinosital-3 kinase (PI3K) via Akt to promote β-catenin nuclear localization and activity. Hence, stem cell activation is dependent on both Wnt signaling and the ability to override the BMP signal.

Interestingly, the intestinal epithelial specific conditional deletion of *BMPR1A* resulted in moderate proliferative defects with no ectopic crypts or polyp development in the intestine as was seen in conditional *BMPR1A* knockout mice generated using the interferon-inducible *Mx1-Cre* line (54). In the epithelial specific *BMPR1A* mutant mice, defects in all 3 secretory cell types were reported. Specifically, these mice displayed diminished numbers of enteroendocrine cells, decreased expression of terminal differentiation markers for enteroendocrine, Paneth, and goblet cells and reduced secretory granule content in Paneth and goblet cells. These results suggest that BMP signaling to the intestinal epithelium plays an important role in the differentiation of the secretory lineages, while BMP signaling within the mesenchymal compartment plays an important role in crypt formation and restricting proliferation to the crypt zone. Thus,

loss of mesenchymal BMP signaling leads to aberrant epithelial proliferation and intestinal polyposis.

Hedgehog Signaling in the Intestine

The Hedgehog (Hh) signaling pathway is a critical regulatory cascade involved in intestinal morphogenesis (55). In mammals, three Hh ligands have been identified: Sonic hedgehog (Shh), Indian hedgehog (Ihh) and Desert hedgehog (Dhh). The Hh signaling components include the receptors, Patched (Ptch), a 12-span transmembrane protein and Smoothened (Smo), a 7-span transmembrane protein as well as members of the Gli family of zinc-finger transcription factors (Gli1, Gli2 and Gli3). In the absence of Hh ligands, the Ptch receptor inhibits Smo activity, and as a result full-length Gli proteins (Gli2/3) are phosphorylated by protein kinase A (PKA), Gli2 is degraded, and Gli3 is cleaved to produce the truncated repressor form of Gli (Gli3R). In this form, Gli lacks the transcriptional activation domain (Gli2) and represses Hh target genes. When Hh binds to Ptch, it releases Smo from Ptch-mediated suppression. This triggers the stabilization and nuclear translocation of Gli transcription factors (Figure 4). Gli subsequently activates downstream targets including *Gli1* and *Ptch*. As with most evolutionarily conserved signaling pathways, the Hh pathway is tightly regulated by negative feedback signals. For example, Hh activation induces the expression of hedgehog interacting protein 1 (Hhip1), a cell surface protein that binds to and sequesters hedgehog ligands. Additionally, Hh also induces the expression of Ptch, the inhibitory receptor, in order to limit activation of the pathway.

All 3 Hh ligands are expressed in the gastrointestinal tract. Ihh and Shh are exclusively expressed in epithelial cells, while Dhh expression is confined to Schwann cells, peripheral nerves and endothelial cells in the gut (56). Hh-responsive cells as indicated by the expression of the Hh target genes Ptch and Gli are located within the mesenchyme (57, 58). In particular, Hh-responsive cells include pericryptal myofibroblasts, muscularis mucosae cells, and villus core cells in the small intestine and pericryptal myofibroblasts and muscularis mucosae cells in the colon (58). These data provide strong descriptive evidence that Hh signaling in the small intestine and colon acts in a paracrine direction, moving from the epithelium to the mesenchyme.

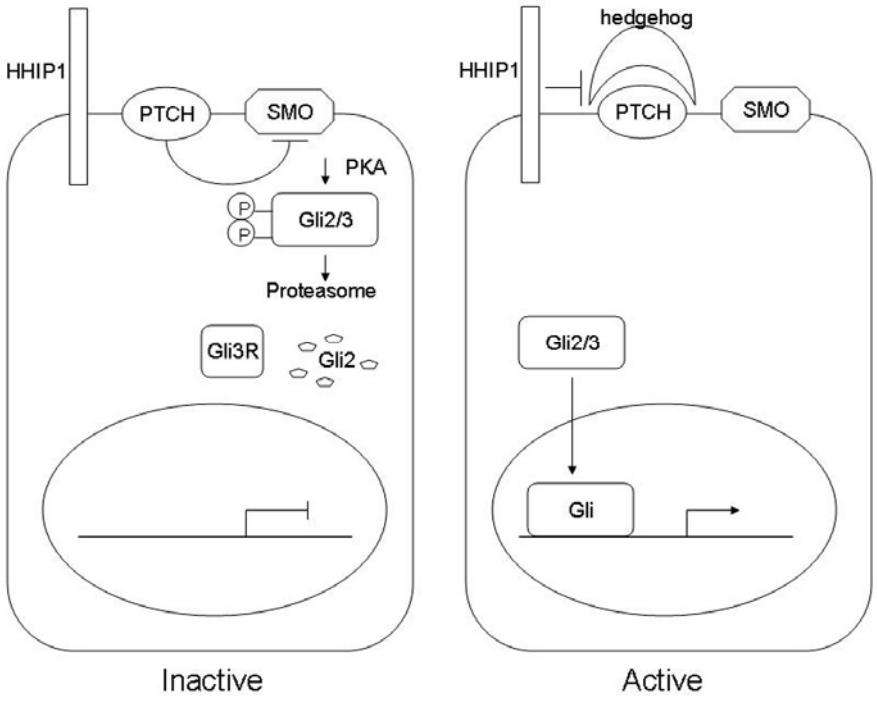

Figure 4. The Hedgehog signaling pathway. (*Left*) In the absence of Hh ligand, Ptch blocks Smo, resulting in the post-translation processing of Gli transcription factors into the repressive form. (*Right*) Engagement of Hh with the Ptch receptor activates Smo, leading to accumulation of full-length Gli2 and Gli3 and the transcription of Hh target genes.

Not surprisingly, *Ihh*- and *Shh*-null mice display marked gastrointestinal abnormalities during late embryonic development including attenuated smooth muscle layers and intestinal malrotation (57). The two mutant mice also display individual phenotypes, likely reflecting the fact that *Ihh* and *Shh* are expressed in distinct domains along the gastrointestinal tract. $Shh^{-/-}$ mice display intestinal transformation of the stomach as observed by the expression of the intestinal enterocyte marker alkaline phosphatase in the stomach epithelium. Other phenotypes detected in $Shh^{-/-}$ mice include lengthening of duodenal villi and overgrowth of the stomach epithelium. While the developmental defects of $Shh^{-/-}$ mice localize primarily to the proximal region of the gastrointestinal tract, where Shh expression peaks, developmental defects in $Ihh^{-/-}$ mice localize to the distal small intestine and colon, where Ihh expression abounds (57, 58). $Ihh^{-/-}$ mice exhibit reduced proliferation in the ISC compartment, villi that are hypoplastic and reduced in numbers, and Hirschsprung's disease-like enlarged colons.

As *Ihh*- and *Shh*-null mice die at birth, the role of Hh signaling in the neonatal and adult gastrointestinal tract has been explored through the use of various mouse models, including transgenic rodents, anti-Hh antibody-treated mice and chemically-treated mice using cyclopamine, an antagonist of Hh signaling. Madison et al. used the intestinal-epithelial specific villin promoter to overexpress the Hedgehog interacting protein (Hhip), a negative regulator of Hh signaling, to block all Hh signals (59). Defective villus formation, increased proliferation, aberrant crypt structures and mislocalized ISEMFs were all observed in *villin-Hhip* mice, suggesting Hh signals pattern the crypt-villus axis through their interactions with ISEMFs. The *villin-Hhip* mice also showed abnormal differentiation of the absorptive lineage as determined by the lack of expression

of brush border markers and poorly developed microvilli. This phenotype resembled the phenotype described in mice injected with an anti-Hh antibody in which the mice displayed immature microvillus architecture and reduced density of microvilli (60). Failure of enterocyte differentiation was also observed in the colon of cyclopamine-treated rats (61). The colonic enterocytes had altered distribution of the brush-border protein villin and acquired expression of the goblet cell marker intestinal trefoil factor. Taken together, these findings suggest Hh signals indirectly regulate enterocyte differentiation via an unknown factor found in mesenchymal Hh-responsive cells.

Von Dop et al. studied the role of Hh signaling in the colon of adult mice by inactivating the Hh receptor Ptch. In these mice, the Hh pathway is constitutively active since the repressive constraint on Smo is removed (62). The Ptch1 mutant mice showed diminished numbers of epithelial precursor cells, inhibition of Wnt signaling, increased BMP signaling, and the accumulation of myofibroblasts in the lamina propria. These results are consistent with the notion that Hh signals to the mesenchyme, where they regulate secondary signals that influence epithelial behavior. More specifically, this study concluded that Hh signals induce mesenchymal BMPs to negatively regulate precursor cell proliferation. In another recent study, the overexpression of Ihh under the villin promoter resulted in the expansion of villus core smooth muscle (58). Although the reported phenotype described for this mouse model is limited, it does provide additional confirmation that Hh signals regulate mesenchymal cells.

Summary of Thesis

In this thesis, I investigated the interplay between ISCs and their mesenchymal niche, examining signals that emanate from the niche and influence ISC behavior as well as signals that originate from the intestinal epithelium and act on the mesenchymal niche. We performed gene expression analysis comparing human colon top and crypt compartments and identified genes that are key in ISC maintenance as well as signaling pathways critical in the transition of stem/progenitor cells to differentiated colonic epithelial cells (Chapter 2). Of the crypt genes identified, several were localized to the ISC niche including the BMP antagonist Gremlin 1 (*GREM1*) (Chapter 2). We then conducted *in vitro* experiments on intestinal epithelial cells to determine whether Gremlin 1 influences epithelial differentiation and/or proliferation (Chapter 2). Next, we examined epithelial-to-mesenchymal interactions that occur in the opposite direction, focusing on Indian hedgehog, an epithelially expressed morphogenetic protein known to target mesenchymal cells that comprise the proposed ISC niche (Chapter 3). To investigate how Hh signals affect the ISC niche, we generated intestine specific Indian hedgehog knockout mice (*Villin-Cre;Ihh*$^{flox/flox}$) (Chapter 3). The phenotype of these mice was defined using gene expression profiling, gross anatomical changes and microscopic anatomy as determined through immunohistochemistry, electron microscopy and quantitative RT-PCR (Chapter 3). To determine if the mesenchymal niche changes following Ihh loss affect the ISC population, we performed *in situ* hybridization for the specific ISC marker *Olfm4* (Chapter 3). Finally, we determined whether the phenotypes observed in *Villin-Cre;Ihh*$^{flox/flox}$ mice are strictly due to paracrine Ihh signaling by

generating mice with the deletion of *Smo*, the receptor that mediates Hh signaling, in intestinal epithelial cells (Chapter 3).

References

1. de Santa Barbara, P., van den Brink, G. R. & Roberts, D. J. (2003) *Cell Mol Life Sci* **60,** 1322-32.
2. Sancho, E., Batlle, E. & Clevers, H. (2004) *Annu Rev Cell Dev Biol* **20,** 695-723.
3. Radtke, F., Clevers, H. & Riccio, O. (2006) *Curr Mol Med* **6,** 275-89.
4. Brabletz, S., Schmalhofer, O. & Brabletz, T. (2009) *J Pathol* **217,** 307-17.
5. Calvert, R. & Pothier, P. (1990) *Anat Rec* **227,** 199-206.
6. Lacy, E. R. & Colony, P. C. (1985) *Gastroenterology* **89,** 138-50.
7. Potten, C. S., Kovacs, L. & Hamilton, E. (1974) *Cell Tissue Kinet* **7,** 271-83.
8. Potten, C. S. (1977) *Nature* **269,** 518-21.
9. Barker, N., van Es, J. H., Kuipers, J., Kujala, P., van den Born, M., Cozijnsen, M., Haegebarth, A., Korving, J., Begthel, H., Peters, P. J. & Clevers, H. (2007) *Nature* **449,** 1003-7.
10. Bjerknes, M. & Cheng, H. (1981) *Am J Anat* **160,** 51-63.
11. Bjerknes, M. & Cheng, H. (1981) *Am J Anat* **160,** 77-91.
12. Sangiorgi, E. & Capecchi, M. R. (2008) *Nat Genet* **40,** 915-20.
13. Scoville, D. H., Sato, T., He, X. C. & Li, L. (2008) *Gastroenterology* **134,** 849-64.
14. van der Flier, L. G., van Gijn, M. E., Hatzis, P., Kujala, P., Haegebarth, A., Stange, D. E., Begthel, H., van den Born, M., Guryev, V., Oving, I., van Es, J. H., Barker, N., Peters, P. J., van de Wetering, M. & Clevers, H. (2009) *Cell* **136,** 903-12.
15. van der Flier, L. G., Haegebarth, A., Stange, D. E., van de Wetering, M. & Clevers, H. (2009) *Gastroenterology* **137,** 15-7.
16. Zhu, L., Gibson, P., Currle, D. S., Tong, Y., Richardson, R. J., Bayazitov, I. T., Poppleton, H., Zakharenko, S., Ellison, D. W. & Gilbertson, R. J. (2009) *Nature* **457,** 603-7.
17. Potten, C. S., Booth, C., Tudor, G. L., Booth, D., Brady, G., Hurley, P., Ashton, G., Clarke, R., Sakakibara, S. & Okano, H. (2003) *Differentiation* **71,** 28-41.
18. He, X. C., Zhang, J., Tong, W. G., Tawfik, O., Ross, J., Scoville, D. H., Tian, Q., Zeng, X., He, X., Wiedemann, L. M., Mishina, Y. & Li, L. (2004) *Nat Genet* **36,** 1117-21.
19. Snippert, H. J., van Es, J. H., van den Born, M., Begthel, H., Stange, D. E., Barker, N. & Clevers, H. (2009) *Gastroenterology* **136,** 2187-2194 e1.
20. Gregorieff, A., Pinto, D., Begthel, H., Destree, O., Kielman, M. & Clevers, H. (2005) *Gastroenterology* **129,** 626-38.
21. Bjerknes, M. & Cheng, H. (2005) *Nat Genet* **37,** 1016-7; author reply 1017-8.
22. Walker, M. R., Patel, K. K. & Stappenbeck, T. S. (2009) *J Pathol* **217,** 169-80.
23. Powell, D. W., Mifflin, R. C., Valentich, J. D., Crowe, S. E., Saada, J. I. & West, A. B. (1999) *Am J Physiol* **277,** C183-201.
24. Powell, D. W., Adegboyega, P. A., Di Mari, J. F. & Mifflin, R. C. (2005) *Am J Physiol Gastrointest Liver Physiol* **289,** G2-7.
25. Kinoshita, Y., Nakata, H., Hassan, S., Asahara, M., Kawanami, C., Matsushima, Y., Naribayashi-Inomoto, Y., Ping, C. Y., Min, D., Nakamura, A. & et al. (1995) *Gastroenterology* **109,** 1068-77.

26. Babyatsky, M. W., Rossiter, G. & Podolsky, D. K. (1996) *Gastroenterology* **110,** 975-84.
27. Dignass, A. U., Tsunekawa, S. & Podolsky, D. K. (1994) *Gastroenterology* **106,** 1254-62.
28. Jones, D. L. & Wagers, A. J. (2008) *Nat Rev Mol Cell Biol* **9,** 11-21.
29. Simon-Assmann, P., Simo, P., Bouziges, F., Haffen, K. & Kedinger, M. (1990) *Digestion* **46 Suppl 2,** 12-21.
30. Jones, R. G., Li, X., Gray, P. D., Kuang, J., Clayton, F., Samowitz, W. S., Madison, B. B., Gumucio, D. L. & Kuwada, S. K. (2006) *J Cell Biol* **175,** 505-14.
31. Gregorieff, A. & Clevers, H. (2005) *Genes Dev* **19,** 877-90.
32. van de Wetering, M., Sancho, E., Verweij, C., de Lau, W., Oving, I., Hurlstone, A., van der Horn, K., Batlle, E., Coudreuse, D., Haramis, A. P., Tjon-Pon-Fong, M., Moerer, P., van den Born, M., Soete, G., Pals, S., Eilers, M., Medema, R. & Clevers, H. (2002) *Cell* **111,** 241-50.
33. Batlle, E., Henderson, J. T., Beghtel, H., van de Born, M. M. W., Sancho, E., Huls, G., Pawson, T. & Clevers, H. (2002) *Cell* **111,** 251-263.
34. Blache, P., van de Wetering, M., Duluc, I., Domon, C., Berta, P., Freund, J. N., Clevers, H. & Jay, P. (2004) *J Cell Biol* **166,** 37-47.
35. Mori-Akiyama, Y., van den Born, M., van Es, J. H., Hamilton, S. R., Adams, H. P., Zhang, J., Clevers, H. & de Crombrugghe, B. (2007) *Gastroenterology* **133,** 539-46.
36. Clevers, H. (2006) *Cell* **127,** 469-80.
37. Korinek, V., Barker, N., Moerer, P., van Donselaar, E., Huls, G., Peters, P. J. & Clevers, H. (1998) *Nat Genet* **19,** 379-83.
38. Pinto, D., Gregorieff, A., Begthel, H. & Clevers, H. (2003) *Genes Dev* **17,** 1709-13.
39. Kuhnert, F., Davis, C. R., Wang, H. T., Chu, P., Lee, M., Yuan, J., Nusse, R. & Kuo, C. J. (2004) *Proc Natl Acad Sci U S A* **101,** 266-71.
40. Sansom, O. J., Reed, K. R., Hayes, A. J., Ireland, H., Brinkmann, H., Newton, I. P., Batlle, E., Simon-Assmann, P., Clevers, H., Nathke, I. S., Clarke, A. R. & Winton, D. J. (2004) *Genes Dev* **18,** 1385-90.
41. Wong, M. H., Rubinfeld, B. & Gordon, J. I. (1998) *J Cell Biol* **141,** 765-77.
42. van Es, J. H., van Gijn, M. E., Riccio, O., van den Born, M., Vooijs, M., Begthel, H., Cozijnsen, M., Robine, S., Winton, D. J., Radtke, F. & Clevers, H. (2005) *Nature* **435,** 959-63.
43. Schroder, N. & Gossler, A. (2002) *Gene Expr Patterns* **2,** 247-50.
44. Crosnier, C., Vargesson, N., Gschmeissner, S., Ariza-McNaughton, L., Morrison, A. & Lewis, J. (2005) *Development* **132,** 1093-104.
45. Jensen, J., Pedersen, E. E., Galante, P., Hald, J., Heller, R. S., Ishibashi, M., Kageyama, R., Guillemot, F., Serup, P. & Madsen, O. D. (2000) *Nat Genet* **24,** 36-44.
46. Fre, S., Huyghe, M., Mourikis, P., Robine, S., Louvard, D. & Artavanis-Tsakonas, S. (2005) *Nature* **435,** 964-8.
47. Stanger, B. Z., Datar, R., Murtaugh, L. C. & Melton, D. A. (2005) *Proc Natl Acad Sci U S A* **102,** 12443-8.
48. Waite, K. A. & Eng, C. (2003) *Nat Rev Genet* **4,** 763-73.

49. Zhang, J. & Li, L. (2005) *Dev Biol* **284,** 1-11.
50. Hardwick, J. C., Van Den Brink, G. R., Bleuming, S. A., Ballester, I., Van Den Brande, J. M., Keller, J. J., Offerhaus, G. J., Van Deventer, S. J. & Peppelenbosch, M. P. (2004) *Gastroenterology* **126,** 111-21.
51. Haramis, A. P., Begthel, H., van den Born, M., van Es, J., Jonkheer, S., Offerhaus, G. J. & Clevers, H. (2004) *Science* **303,** 1684-6.
52. Batts, L. E., Polk, D. B., Dubois, R. N. & Kulessa, H. (2006) *Dev Dyn* **235,** 1563-70.
53. Kosinski, C., Li, V. S., Chan, A. S., Zhang, J., Ho, C., Tsui, W. Y., Chan, T. L., Mifflin, R. C., Powell, D. W., Yuen, S. T., Leung, S. Y. & Chen, X. (2007) *Proc Natl Acad Sci U S A* **104,** 15418-23.
54. Auclair, B. A., Benoit, Y. D., Rivard, N., Mishina, Y. & Perreault, N. (2007) *Gastroenterology* **133,** 887-96.
55. van den Brink, G. R. (2007) *Physiol Rev* **87,** 1343-75.
56. Bitgood, M. J. & McMahon, A. P. (1995) *Dev Biol* **172,** 126-38.
57. Ramalho-Santos, M., Melton, D. A. & McMahon, A. P. (2000) *Development* **127,** 2763-72.
58. Kolterud, A., Grosse, A. S., Zacharias, W. J., Walton, K. D., Kretovich, K. E., Madison, B. B., Waghray, M., Ferris, J. E., Hu, C., Merchant, J. L., Dlugosz, A. A., Kottmann, A. H. & Gumucio, D. L. (2009) *Gastroenterology* **137,** 618-28.
59. Madison, B. B., Braunstein, K., Kuizon, E., Portman, K., Qiao, X. T. & Gumucio, D. L. (2005) *Development* **132,** 279-89.
60. Wang, L. C., Nassir, F., Liu, Z. Y., Ling, L., Kuo, F., Crowell, T., Olson, D., Davidson, N. O. & Burkly, L. C. (2002) *Gastroenterology* **122,** 469-82.
61. van den Brink, G. R., Bleuming, S. A., Hardwick, J. C., Schepman, B. L., Offerhaus, G. J., Keller, J. J., Nielsen, C., Gaffield, W., van Deventer, S. J., Roberts, D. J. & Peppelenbosch, M. P. (2004) *Nat Genet* **36,** 277-82.
62. van Dop, W. A., Uhmann, A., Wijgerde, M., Sleddens-Linkels, E., Heijmans, J., Offerhaus, G. J., van den Bergh Weerman, M. A., Boeckxstaens, G. E., Hommes, D. W., Hardwick, J. C., Hahn, H. & van den Brink, G. R. (2009) *Gastroenterology* **136,** 2195-2203 e1-7.

Chapter 2

Gene Expression Patterns of Human Colon Tops and Basal Crypts and BMP Antagonists as Intestinal Stem Cell Niche Factors

Gene Expression Patterns of Human Colon Tops and Basal Crypts and BMP Antagonists as Intestinal Stem Cell Niche Factors

Cynthia Kosinski[*], Vivian SW Li[†], Annie SY Chan[†], Ji Zhang[*‡], Coral Ho[*], Wai Yin Tsui[†], Tsun Leung Chan[†], Randy C. Mifflin[§], Don W. Powell[§], Siu Tsan Yuen[†], Suet Yi Leung[†¶] and Xin Chen[*¶]

[*]Dept. of Biopharmaceutical Sciences, University of California, San Francisco, CA, USA; [†]Dept. of Pathology, The University of Hong Kong, Queen Mary Hospital, Pokfulam, Hong Kong; [‡]Dept. of Surgery, Beijing Cancer Hospital, Beijing, China; and [§] Dept. of Internal Medicine, University of Texas Medical Branch, Galveston, TX , USA.

Summary

Human colon epithelial cell renewal, proliferation, and differentiation are stringently controlled by numerous regulatory pathways. To identify genetic programs of human colonic epithelial cell differentiation *in vivo* as well as candidate marker genes that define colonic epithelial stem/progenitor cells and the stem cell niche, we applied gene expression analysis of normal human colon tops and basal crypts using expression microarrays with 30,000 genes. Nine hundred and sixty-nine cDNA clones were found to be differentially expressed between human colon crypts and tops. Pathway analysis revealed the differential expression of genes involved in cell cycle maintenance and apoptosis, as well as genes in bone morphogenetic protein (BMP), Notch, Wnt, EPH and MYC signaling pathways. BMP antagonists gremlin 1, gremlin 2, and chordin-like 1 were found to be expressed by colon crypts. *In situ* hybridization and RT-PCR confirmed that these BMP antagonists are expressed by intestinal cryptal myofibroblasts and smooth muscle cells at the colon crypt. *In vitro* analysis demonstrated that gremlin 1 partially inhibits Caco-2 cell differentiation upon confluence and activates Wnt signaling in normal rat intestinal epithelial cells. Collectively, the expression data set provides a comprehensive picture of human colonic epithelial cell differentiation. Our study also suggests that BMP antagonists are candidate signaling components that make up the intestinal epithelial stem cell niche.

Introduction

The human adult colonic epithelium undergoes perpetual regeneration fueled by intestinal epithelial stem and progenitor cells located at the colon crypt base. Perturbation of the pathways regulating stem cell renewal contributes significantly to neoplastic transformation. The current basis of our understanding of intestinal stem cells is primarily derived from studying the small intestine, which shares major regulatory pathways in common with the colon. Specifically, several key regulatory signals are involved in intestinal stem cell renewal and differentiation, including the Wnt, bone morphogenetic protein (BMP), and Notch pathways (1-3).

Among these pathways, canonical Wnt signaling plays a major role in maintaining intestinal stem cell fate and progenitor cell proliferation (4). BMP signaling, in contrast, has been reported to inhibit intestinal stem cell activation and promote intestinal differentiation (5). Cell fate decisions in the intestine have been shown to involve Notch signaling, which specifically directs cells toward a secretory lineage in the gut (6). All the evidence suggests there is a close interaction of several key pathways in directing intestinal epithelial stem cell renewal and differentiation. Yet how these different pathways coordinate in the specific anatomical compartment of the intestine remains mostly unknown.

Intestinal epithelial stem cells are supported by underlying myofibroblasts known as intestinal subepithelial myofibroblast (ISEMF), which are in close proximity to the smooth muscle cells of the muscularis mucosae layer. These cells at the base of intestinal crypts may contribute to the stem cell niche and act as regulators of intestinal stem cell self-renewal and differentiation.

Several genomic studies have been applied to study mouse intestinal epithelial stem cells and their differentiation program by using either expression array technology or cDNA library sequencing (7-9). These gene expression analyses have provided valuable information and candidate markers for mouse gastrointestinal stem/progenitor cells, as well as revealing the differentiation program of these cells. However, no information regarding the stem cell niche environment, specifically for the supporting cells, is known because previous experiments used microdissected or isolated epithelial cells. Furthermore, no data are available with regards to the human intestine, especially for the human colon. Data on the proliferation program governing the stem/progenitor cell compartment and the differentiation program of colon epithelial cells are of particular importance because colon cancer is one of the most common cancer types, whereas small intestinal cancer is exceedingly rare in humans.

In this article, we characterized the gene expression profiles of human colon by comparing the gene expression pattern between the top and the basal crypt compartments. We identified a comprehensive list of differentially expressed genes encompassing major pathways regulating intestinal epithelial stem cell renewal. Among these pathways, we identified elements that contribute to the stem cell niche, which were then validated by cellular localization and *in vitro* functional studies. Our data set provides a comprehensive picture of the human colonic epithelial cell differentiation program and helps identify elements that contribute to the maintenance of the intestinal stem cell niche.

Results

Gene Expression Signatures of Human Colon Top and Bottom Crypt Compartments

Using cDNA microarrays containing 44,500 cDNA clones, representing approximately 30,000 unique genes, we generated gene expression profiles from nine paired horizontally dissected human colon top versus bottom crypt tissue compartments. We next applied significance analysis of microarrays (SAM) to the array data set and identified 969 cDNA clones, representing approximately 736 unique genes that are differentially expressed in colon tops versus bottom crypts, with a false discovery rate of <0.1%. Among these genes, 367 cDNA clones (299 unique genes) were highly expressed in colon bottom crypts; and 602 cDNA clones (437 unique genes) were expressed in colon crypt tops and surface (the complete gene data set is available for download from http://www.pnas.org/content/suppl/2007/09/05/0707210104.DC1/07210Table1.xls).

Careful examination of the genes that are highly expressed at colon basal crypts revealed that, apart from previously well known genes such as the c-myc and the EphB family (*EPHB2*, *EPHB3* and *EPHB4*), two major clusters exists (Cluster I and II in Figure 1). Cluster I includes many genes involved in cell proliferation and cell cycle regulation, as well as candidate oncogenes (e.g., *CDC20*, *Cyclin B2*, *PTTG1* and *FYN*). These genes are cell cycle-regulated and are highly expressed in tumor cells, compared with normal tissues in a variety of tumor types (10). As such, these genes are most likely to be expressed by proliferating crypt progenitor cells. Cluster II includes many genes that encode secretory proteins and genes involved in cell matrix or matrix modeling (e.g., Fibronectin, *TIMP3*, *ADAMTS1* and *TAGLIN*). Some of these genes (including

Fibronectin and *TAGLIN*) have been found to be expressed by myofibroblasts as well as smooth muscle cells (11, 12). Therefore, we suspect that genes in this cluster most likely represent genes which are expressed by crypt stromal cells. Strikingly, there are three BMP antagonists expressed in this cluster: gremlin 1 (*GREM1*), gremlin 2 (*GREM2*) and chordin-like 1 (*CHRDL1*), whose expression and role in the normal human colon are mostly unknown. The genes expressed in the colon top include genes that inhibit cell proliferation (*p21* and *MAD*), cell adhesion molecules (*CDH1* and *TJP3*), and genes encoding functional proteins of gut epithelial cells (membrane transporters *ABCB1*, *ABCG2* or enzymes like *CA4*). Together the data support that our microarray analysis accurately captures the global gene expression patterns of colon tops versus basal crypts.

To further characterize the functional significance of genes expressed in colon basal crypts and tops, we performed Gene Ontology (GO) term analysis and identified GO terms, which are enriched in each gene list with a cutoff *P* value of < 0.05 (GO term summary of the colon top and bottom crypt compartments is available for download from http://www.pnas.org/content/suppl/2007/09/05/0707210104.DC1/07210Table2.xls). GO term analysis facilitates the interpretation of data by providing biological, physiological, and functional descriptions of gene products. The GO terms that are enriched and unique in the basal crypt gene list include "M phase," "cell cycle," "protein biosynthesis," "macromolecular biosynthesis," and "DNA replication". These terms are clearly related to the cell proliferation and cell renewal at basal crypts. In contrast, GO terms that are enriched and unique in the colon top gene list include "cell communication," "digestion," "establishment of localization," "transport," "ion transport," etc. These GO terms are

consistent with the expression of genes required for digestive function and transport in mature intestinal epithelial cells.

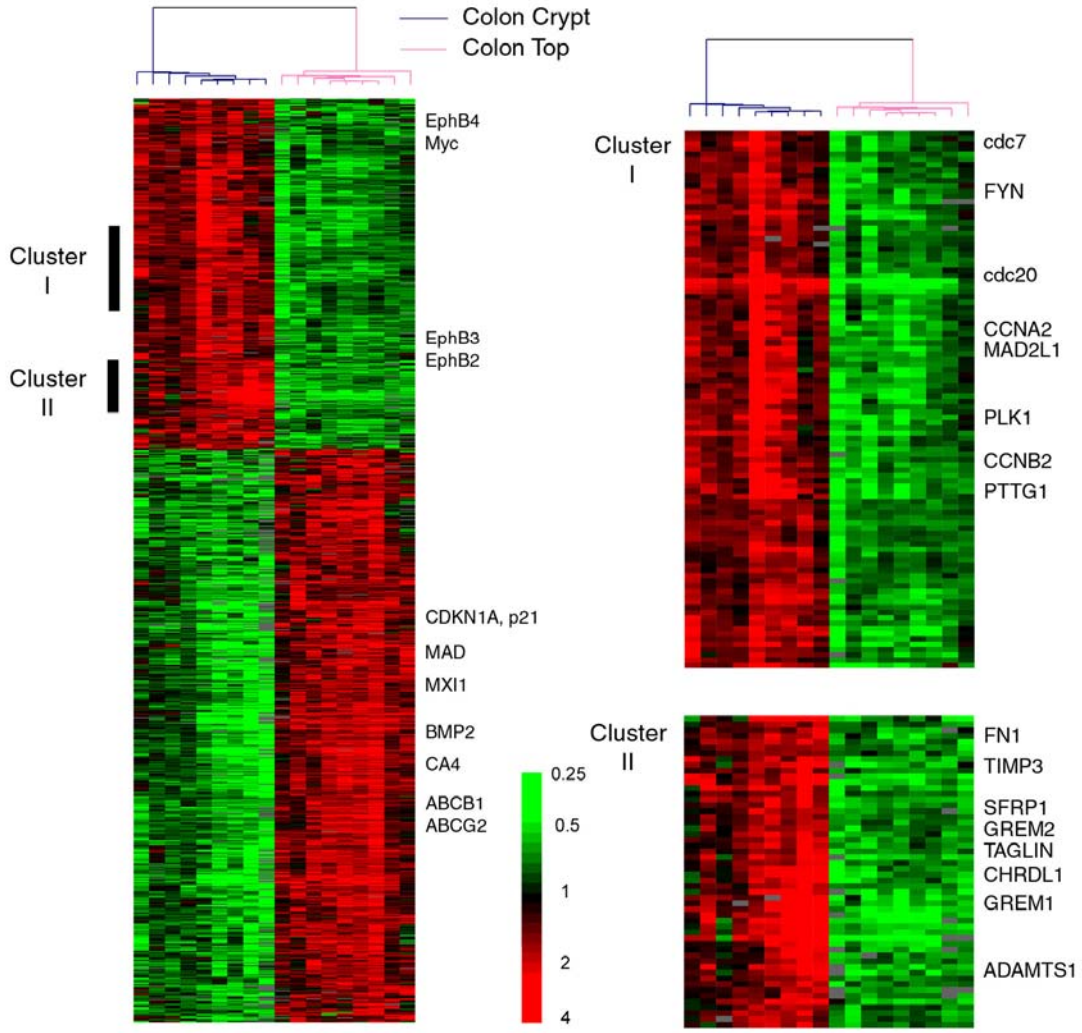

Figure 1. Hierarchical clustering of genes differentially expressed in colon top and basal crypt as identified by significance analysis of microarrays (SAM). Cluster I is enriched in genes associated with cell proliferation, and cluster II is enriched in genes expressed in pericryptal mesenchymal cells.

Expression Profiling in Different Molecular Pathways

To gain a broader picture of gene expression changes and to elucidate the molecular and biological pathways involved in colon crypt maturation, we examined the global expression profile data set by using paired *t*-test. Of the 25,132 cDNA clones, 6,087 were found to be significantly altered between the two compartments with the cutoff value at $P < 0.01$ (approximate false discovery rate of 4%). Genes differentially expressed in bottom crypt compartment compared to top crypt compartment are available for download from http://www.pnas.org/content/suppl/2007/09/05/0707210104.DC1/07210Table3.xls. These 6,087 transcripts were then visualized by using GenMapp software to examine their relationship in various biological pathways. Expression data of genes in key signal transduction pathways regulating stem cell renewal also were extracted by using a threshold of $P < 0.05$ in paired *t*-test.

Cell Cycle and Apoptosis

A significant increased gene expression signature enriched in the cell cycle pathway was observed in bottom crypts, consistent with the findings that proliferative activity is located within this compartment (Figure S1A). In particular, 85% of the differentially expressed genes within this pathway were significantly up-regulated in the bottom compartments. By contrast, inhibitors of cell cycle, including *CDKN1A* and *CDKN2A*, were down-regulated in the bottom compartment. Genes involved in RNA and protein processing, including ribosomal proteins and translation factors, also were up-regulated in the bottom crypts (Figure S2). We next examined genes involved in the apoptosis pathway and noted that most of these genes, including *TNF*, its receptor *TNFRSF1B*,

CRADD, *CASP10*, and *BAK1,* are significantly down-regulated in the colon bottoms (Figure S1B). Our array data are consistent with the occurrence of cell maturation and elimination of epithelial cells through apoptosis at the colon top compartment.

We next examined the expression of an essential group of genes that control cell growth: the Myc/Mad/Max network (Figure S3A). As expected, oncogenic *MYC* was highly expressed in the proliferative bottom crypt, whereas its dimerization partner *MAX* and its antagonist *MAD* were restricted to the upper crypt. In addition, the *MXI1* gene that functions to antagonize *MYC* by competing for *MAX*, also was highly expressed at colon tops. Our findings suggest that proliferation is prohibited in the upper mature colon compartment by expression of multiple *MYC* antagonists.

Wnt Signaling Pathway

To verify the key contribution of the Wnt signaling pathway in controlling colon crypt development, we correlated the 969 cDNA clones that were differentially expressed as identified by SAM with the previously published Wnt target gene data set obtained by using inducible dnTCF-4 in CRC cell lines by van de Watering et al. (13). Interestingly, we observed an exceedingly high concordance of expression between the two data sets (Pearson correlation coefficient, -0.661; $P < 0.001$) (Figure 2). Genes highly expressed in colon tops are mostly induced by interruption of Wnt signaling through dnTCF4 (e.g., *p21*, *BMP2*, *MAD* and *CDH18*), whereas genes highly expressed in colon crypts are mostly repressed by dnTCF4 (e.g., *MYC*, *CDCA7*, *EPHB2* and *EPHB3*) (Figure S4). These results provide direct evidence that Wnt/β-catenin signaling pathways are a major determinant of gene expression patterns along the colon crypt axis.

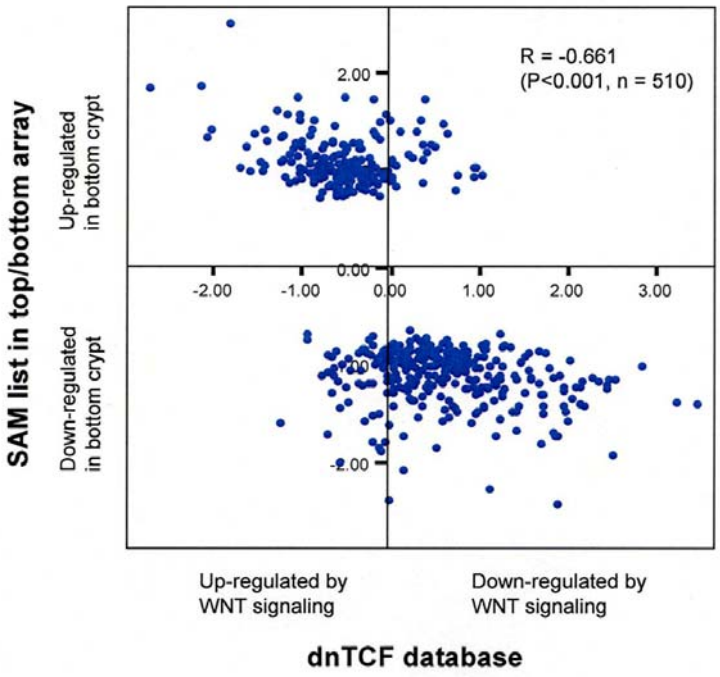

Figure 2. Significant correlation between genes differentially expressed in colon top and basal crypt and Wnt/β-catenin signaling targets. Microarray data of inducible expression of dnTCF4 in Ls174 cells were retrieved from van de Wetering et al. (13), and overlapping clones with colon top-bottom crypt gene list as identified by SAM were selected and calculated for correlation. The x axis measures mean gene expression change (log2) 23 h after dnTCF4 induction, and the y axis measures mean fold change (log2) of bottom versus top colon crypt compartments.

BMP Signaling Pathway

We noted differential expression of multiple BMP components along the colon crypt axis (Figure S3B). *BMP1*, *BMP2, BMP5* and *BMP7, SMAD7*, and *BMPR2* were highly expressed in colon tops, whereas BMP antagonists *CHRDL1*, *GREM1*, and *GREM2* were enriched in basal colon crypts. This observation suggests that BMP signaling is activated in the upper crypt, whereas secretory inhibitors *CHRDL1*, *GREM1*, and *GREM2* located at the bottom antagonize BMP signaling in the intestinal epithelial stem cell niche.

NOTCH Signaling Pathway

It is known that the transmembrane NOTCH receptor is cleaved upon activation by its ligand (Delta/JAG), releasing the intracellular domain of Notch (NICD). NICD then migrates to the nucleus and activates the transcriptional regulator RBPSUH/RBP-Jk by binding to it. We observed an expression profile consistent with the activation of NOTCH signaling in the bottom crypt where *NOTCH1*, *NOTCH2* and *NOTCH3*, *RBPSUH* and *TLE2* were highly expressed at the basal crypt and the NOTCH ligand *JAG1* was expressed at the top (Figure S3C).

The EPH Family

We noted a distinct expression gradient of multiple members of the EPHA and EPHB family of tyrosine kinase receptors as well as their ligands in the colon crypt axis (Figure S3D). Expression of EPHB receptors and their ligands are implicated in maintaining the correct positioning as well as driving proliferation of the progenitor compartment in the crypt-villus axis of the mouse intestine (14, 15). Consistent with the published data on the EPHB families, we noted expression of *EPHB1*, *EPHB2*, *EPHB3*, *EPHB4* and *EPHB6* in the crypt base, whereas the ligand *EFNB2* was expressed at colon tops. Interestingly, we also noted differential expression of the EPHA receptor family in the colon crypt axis, with high expression of *EPHA1*, *EPHA4*, *EPHA7* at the crypt base and high expression of *EPHA2* and *EPHA5*, and the ligand *EFNA1* in colon tops. Our results call for further study of the role of the EPHA family in controlling colon crypt maturation and its possible involvement in the oncogenic process.

Quantitative RT-PCR Validation of Differentially Expressed Genes

To verify our bottom-top array data, several genes belonging to different key pathways were selected for validation by using quantitative RT-PCR in four pairs of samples, including *MXI1* (Myc/Mad/Max family); *APC* and *SFRP1* (WNT signaling), *GREM1*, *GREM2*, and *CHRDL1* (BMP signaling); *JAG1* (Notch pathway); *EFNA1* (Eph family); *DUSP5* (MAPK pathway); and *GPC4* (candidate stem cell marker). All of the selected genes were confirmed to be differentially expressed between colon bottom-top compartments by quantitative RT-PCR (Supplemental Table 1).

BMP Antagonists are Expressed by Subepithelial Myofibroblasts and Smooth Muscle Cells at Colon Crypts

One of the most intriguing observations is the distribution of BMP signaling pathway molecules along the colon crypt axis, including BMP ligands and receptor and signaling molecules. In the colon top, *BMP1*, *BMP2*, *BMP5* and *BMP7*, *SMAD7*, and *BMPR2* are highly expressed, whereas the basal crypt exhibits high expression of three BMP antagonists, *GREM1*, *GREM2*, and *CHRDL1* (Figure 1 and Figure S3B). The latter information, which was previously unknown, suggests the unusual requirement to block BMP signaling at the colon basal crypt region. Furthermore, we discovered that the three BMP antagonists are part of a cocluster of genes that are enriched for those putatively expressed by intestinal crypt stromal cells, such as the fibronectin gene (Figure 1), which prompted us to suspect that these BMP antagonists also may be expressed by stromal cells.

To investigate the cellular origin of BMP antagonists, we performed *in situ* hybridization for *GREM1* and *GREM2* on human colon tissues. *In situ* hybridization revealed strong expression of *GREM1* and *GREM2* in the mesenchymal cells in the basal part of the lamina propria and muscularis mucosae of the colon (Figure 3A and 3B), whereas sense probes showed no staining (data not shown). Expression corresponded to cells on serial sections that stained for fibronectin (Figure 3C) and α-smooth muscle actin (α-SMA) (Figure 3D), markers expressed in both myofibroblasts and smooth muscle cells. Transcripts of *GREM1* and *GREM2* were not detected in epithelial cells, mesenchymal cells in the top part of the lamina propria and submucosa, or smooth muscle cells in the muscularis propria (data not shown).

In the colon, it has been shown that myofibroblasts are vimentin-positive, whereas smooth muscle cells are vimentin-negative (16). Although expression of *GREM1* and *GREM2* in α-smooth muscle actin-positive smooth muscle cells of the muscularis mucosae is unequivocal, specific expression of *GREM1* and *GREM2* by cryptal myofibroblasts remained unclear because of their inconspicuous morphology. Thus, we performed coimmunofluorescence with vimentin to further define the cellular origin. Consistently, we observed no *GREM1* signal in colon tops. In addition, we found *GREM1* mRNA (Figure 3E) and vimentin staining (Figure 3F) colocalized (Figure 3G, white arrows; also see Figure S5 for the enlarged version of the coimmunostaining) in certain mesenchymal cells surrounding the basal crypts, suggesting that gremlin 1 is also secreted by myofibroblasts.

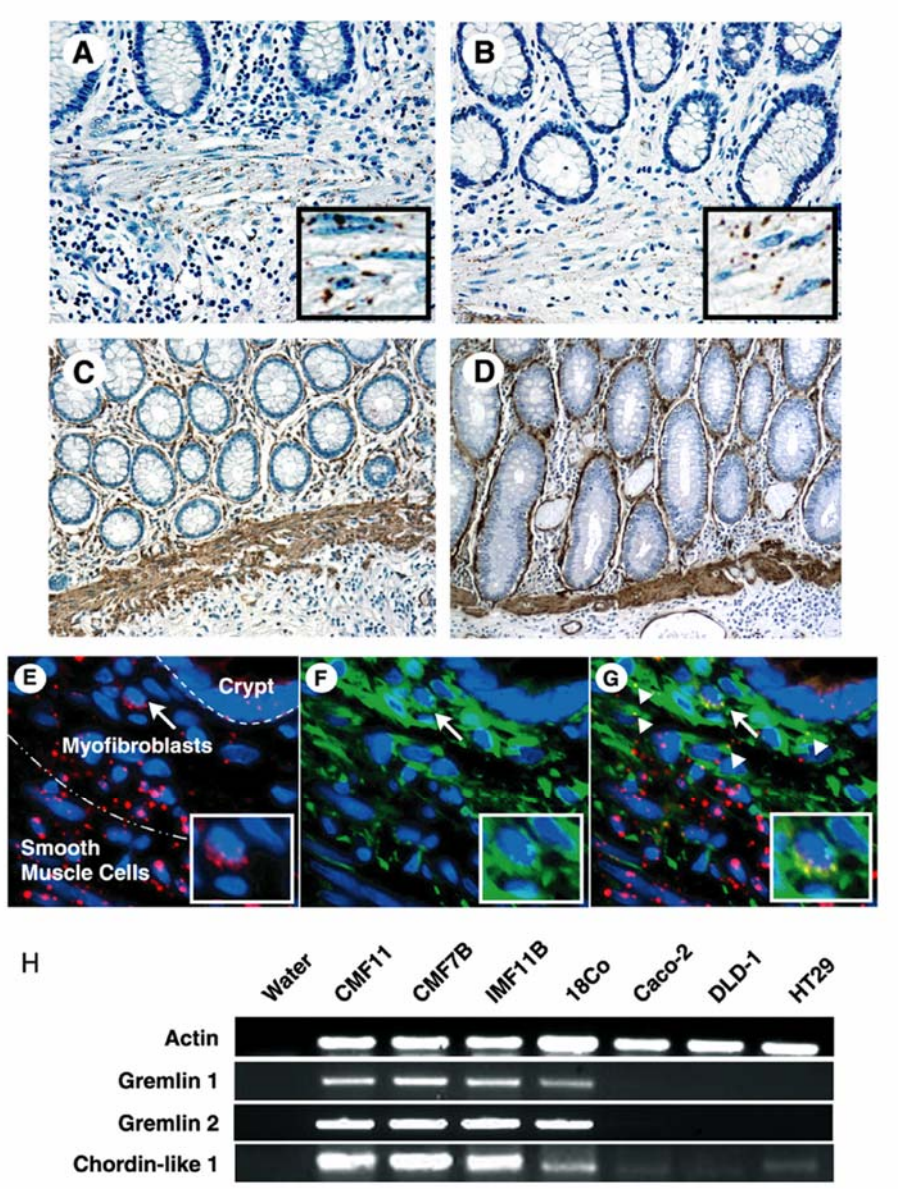

Figure 3. Expression and localization of *GREM1* and *GREM2* by myofibroblast cells and smooth muscle cells at colon crypt. (A and B): In situ hybridization (ISH) for *GREM1* (A) and *GREM2* (B). Dark brown dots indicate positive staining; (C and D): Immunohistochemical staining of fibronectin (C) and α-smooth muscle actin (D) as markers for intestinal myofibroblasts as well as smooth muscle cells. Dark brown staining indicates positive staining. (E, F) Double labeling for *GREM1* mRNA (red, E) and myofibroblast marker vimentin (green, F) at colon basal crypt region. (G) Combined image showing co-expression of *GREM1* and vimentin (yellow dots indicated by white arrows) at scattered pericryptal mesenchymal cells corresponding to myofibroblasts. See Figure S5 for the enlarged version of fluorescent ISH/immunostaining. (H) RT-PCR analysis of BMP antagonists expression in four intestinal myofibroblast isolates (CMF11, CMF7B, IMF11B and 18Co) as well as three colon cancer cell lines (Caco-2, DLD-1, HT29).

To further validate our findings, we isolated primary colonic myofibroblasts from histologically normal human colonic tissue and assayed for gene expression by RT-PCR. The myofibroblast features of isolated cell lines were confirmed by immunofluorescent staining for fibronectin, vimentin, and α-smooth muscle actin (Figure S6). The mRNA for BMP antagonists *GREM1*, *GREM2*, and *CHRDL1* were detected in human colonic and ileal myofibroblasts, but never or weakly in colon tumor epithelial cells (Figure 3H).

Taken together, the data demonstrate that gremlin 1, gremlin 2, and chordin-like 1 in the gastrointestinal tract likely originate from myofibroblasts and smooth muscle cells, both located at the crypt base in proximity to the stem cell niche. Thus, we hypothesized that, through inhibiting BMP signaling locally, these BMP antagonists may function to maintain Wnt signaling and inhibit differentiation at the crypt base.

Gremlin 1 Partially Inhibits Caco-2 Cell Differentiation

To determine whether gremlin 1 interferes with differentiation in intestinal epithelial cells, Caco-2 cells were treated with recombinant gremlin 1 and gene expression of intestinal differentiation markers was assayed by quantitative RT-PCR. Caco-2 cells have been shown to spontaneously differentiate into an enterocyte phenotype in 21 days upon reaching confluence and form a polarized monolayer resembling the intestine (17). In a microarray study of Caco-2 cell differentiation, it was found that expression levels of mature differentiation marker genes reach a plateau at 4 to 7 days postconfluence, and the expression levels do not significantly go up during the rest of the 21 days in culture (Saaf A et al., personal communication). We have further validated these results by quantitative RT-PCR (data not shown). Therefore, we chose 7 days postconfluence to

study the effect of gremlin 1 on Caco-2 cell differentiation. We assayed the expression of two genes: *p21/CDKN1A*, a marker for cell cycle inhibition; and *ANPEP*, a brush border enzyme. We found that 7 days of gremlin 1 treatment consistently decreased *p21* gene expression by 20-30% in Caco-2 cells compared to control cells (Figure 4A). Similarly, 7 days of gremlin 1 treatment consistently decreased *ANPEP* gene expression by 40-50% in Caco-2 cells compared to control cells (Figure 4A). These findings suggest that gremlin 1 partially inhibits intestinal differentiation, and thus gremlin 1 may play a crucial role in inhibiting differentiation near the crypt base.

Gremlin 1 Activates Wnt Signaling in Intestinal Cells

In a previous study, overexpressing the BMP antagonist noggin in the intestine promoted Wnt activity and the development of ectopic crypts (18). Consistent with the hypothesis that BMP antagonists may activate Wnt signaling, we noticed that, in Caco-2 cell differentiation assays, gremlin 1 is able to transiently induce expression of the known Wnt target gene *AXIN2* (19, 20) in Caco-2 cells at 4 h (Figure 4A). To test our hypothesis that gremlin 1 assists in maintaining Wnt signaling in normal intestine, we treated two normal rat intestinal epithelial cell lines, IEC-6 and IEC-18, with gremlin 1 for 48 h and examined the expression of *AXIN2*. Quantitative RT-PCR analysis revealed that the expression of *AXIN2* was significantly up-regulated by gremlin 1 treatment in both tested cell lines (Figure 4B). We next examined whether gremlin 1 affects β-catenin activity by assaying the subcellular localization of β-catenin in IEC-18 cells. We found that, in untreated IEC-18 cells, none of the cells displayed nuclear β-catenin staining. After incubating with gremlin 1, nuclear β-catenin was observed in a small number of

IEC-18 cells (Figure 4 C and D). All these data support that gremlin 1 is able to activate Wnt signaling in intestinal epithelial cells.

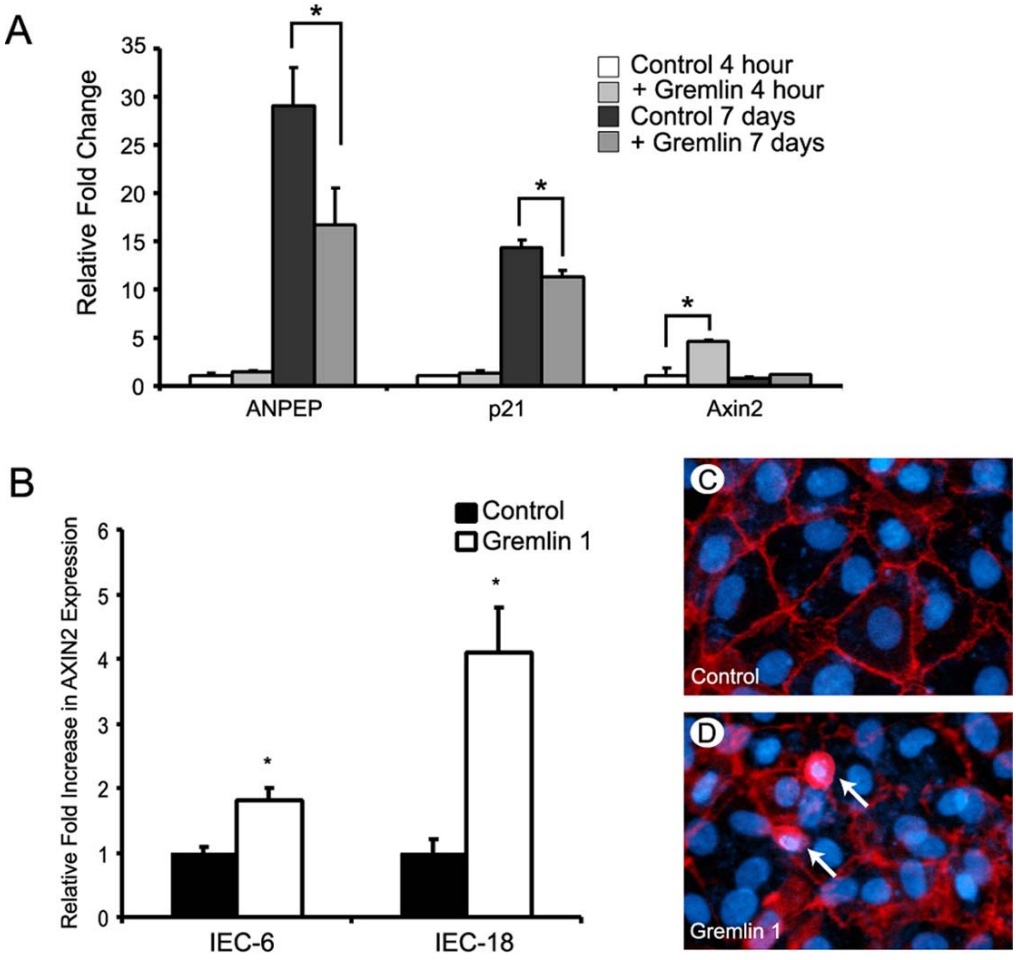

Figure 4. Gremlin 1 partially inhibits Caco-2 cell differentiation and activates Wnt/β-catenin signaling in normal intestinal cells. (A) Quantitative RT-PCR analysis revealed a statistically significant decrease in expression of intestinal epithelial differentiation markers *ANPEP* and *p21* at day 7 when Caco-2 cells were cultured in growth media supplemented with gremlin 1. The analysis detected a significant up-regulation of the *AXIN2* transcript in Caco-2 cells following a 4 hour treatment with gremlin 1 (*, $P < 0.05$). (B) Quantitative RT-PCR analysis demonstrated a statistically significant increase in *AXIN2* expression in normal rat intestinal cells IEC-6 and IEC-18 after 48 hours of treatment with gremlin 1 (*, $P < 0.01$). (C and D) Gremlin 1 induces nuclear/cytoplasm localization of β-catenin in IEC-18 cells.

In summary, our data support that the BMP antagonists gremlin 1, gremlin 2, and chordin-like 1 are expressed by colon crypt myofibroblasts and smooth muscle cells and contribute to the stem cell niche by activating Wnt signaling and inhibiting differentiation of basal crypt epithelial cells.

Discussion

In this manuscript, we provide a comprehensive genomic analysis of genes differentially expressed at human colon top and basal crypt compartments. Our results reveal alteration in a diverse spectrum of genes reflecting not only a difference in cell proliferation versus differentiation/apoptosis along the colon crypt axis but also changes in various components of key signaling pathways regulating colon stem cell renewal. Although many similarities were noted in comparison with an expression profiling database derived from mouse small intestine (8), our data extend the findings to human and provide unique information about the colon, including elements highly relevant to colon carcinogenesis. Specifically, our data captured information not only from the epithelial cells, but also the supporting tissue microenvironment, which may contribute critical elements for creating and maintaining the stem cell niche.

The identification of genes highly expressed in colon crypts provides us a unique opportunity to search for markers of intestinal stem/progenitor cells. We compared the crypt gene list with genes that are highly expressed in human ES and embryonic carcinoma (EC) cells (21) and identified 31 genes, including *GAB1*, *PTTG1*, *EBAF*, *GPC4*, and *MYBL,* which are highly expressed in ES and EC cells as well as in colon crypts (complete list of mutually expressed genes available for download from

http://www.pnas.org/content/suppl/2007/09/05/0707210104.DC1/07210Table5.xls and Figure S7). These genes mutually expressed in basal crypts and ES and EC cells represent potential markers for intestinal stem or progenitor cells. Some potential cell surface proteins (e.g., GPC4) might be useful markers for the purification of intestinal stem/progenitor cells. One has to be cautious, however, because some of these genes may simply represent proliferating cell signatures in ES, EC and crypt progenitor cells. Further studies to address the cellular localization of these genes in the intestinal compartment and their function in intestinal stem/progenitor cell differentiation will improve our understanding of intestinal stem/progenitor cells.

Although we observed gene expression profiles reflecting activated Wnt signaling in colon crypts (Figure 2), the exact mechanism leading to Wnt activation remains unclear. We have observed differential expression of several members involved in transduction or regulation of Wnt signaling along the colon crypt axis. Specifically, *APC*, *WNT5B* and *TCF4* were localized at the crypt top, whereas *AXIN2*, *DKK3*, *TCF3*, *SFRP1*, *SFRP2*, *FZD2*, *FZD3*, *FZD7* and *FZDB* were all restricted to the bottom. Many of these observed differential expression patterns were consistent with an expression study based on *in situ* hybridization in mouse intestine (22). The reason for the expression of several Wnt secretory inhibitors in the colon crypt base is unclear. It may suggest either a negative-feedback regulation or the need to fine tune Wnt activity through an intricate balance of positive and negative regulators in this specific anatomical location.

Altogether, based on our expression profiling data, we generated a model depicting the components and signaling molecules featured in this study and their differential expression along the colon crypt axis (Figure 5), including activated Wnt and

Notch signaling at the crypts and BMP signaling at the tops. The differential distribution of Eph receptors and their ligands, as well as MYC and MYC antagonists, helps maintain crypt polarity through regulating cell positioning and cell proliferation.

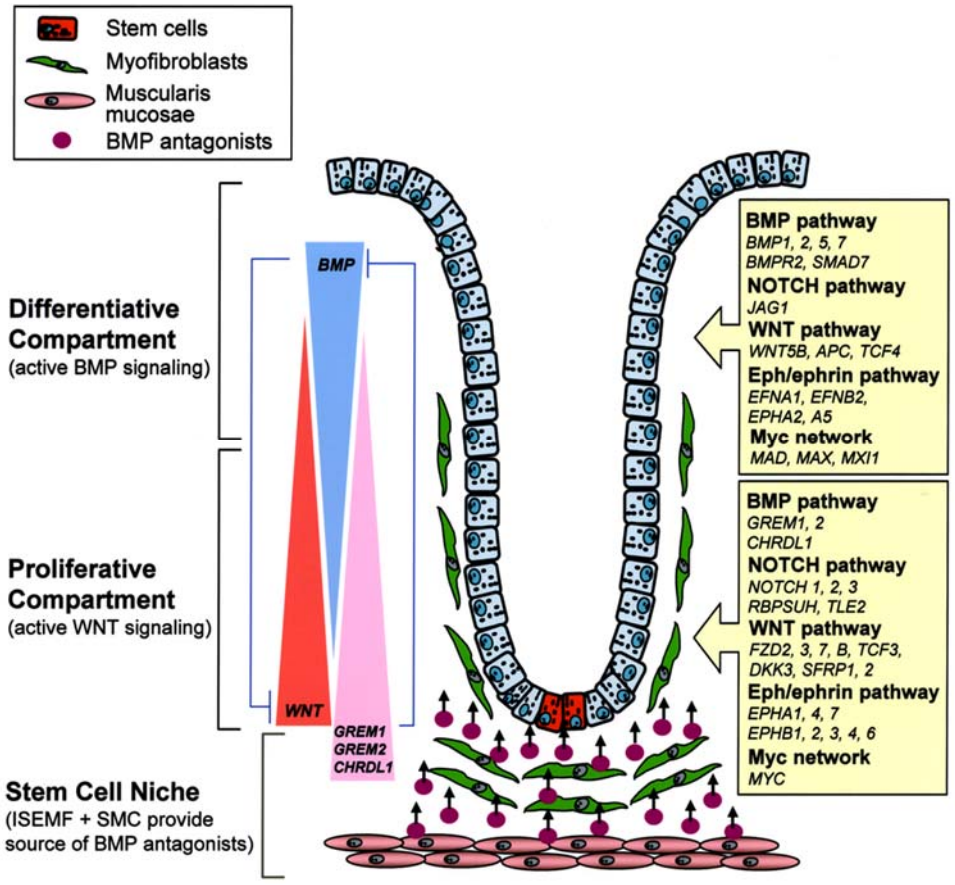

Figure 5. Graphical view of human colon intestinal epithelial cell development and stem cell niche maintenance. Only genes with significant differential expression in paired *t*-test ($P < 0.05$) are listed. ISEMF, intestinal subepithelial myofibroblast; SMC, smooth muscle cell.

The discovery of genes localized to the colonic stem cell niche provides further understanding of the signaling pathways important in this region. However, the detailed mechanisms of how the different signaling pathways coordinate to create this niche remains largely unknown. It has been hypothesized that Wnt signaling is required but not

sufficient for intestinal stem cell activation and self-renewal. A second signal to antagonize BMP is required so as to release its inhibitory effect on nuclear translocation of β-catenin. In mouse intestine, transient expression of the BMP antagonist noggin has been observed in pericryptal mesenchymal cells and intestinal epithelial stem cells, which may contribute to this required second signal (23). Although a cDNA clone corresponding to noggin was not present in our array, we found expression of three different BMP antagonists, including *GREM1*, *GREM2*, and *CHRDL1*, in colon basal crypts by pericryptal mesenchymal cells. Moreover, we found a similar effect of gremlin 1 in promoting nuclear translocation of β-catenin and activating Wnt signaling. These findings led us to propose a model of how BMPs and their antagonists, including gremlin 1, contribute to create the colonic epithelial stem cell niche through modulation of Wnt activity (Figure 5). In this model, BMPs act to restrict stem cell expansion and are expressed at colon tops with a decreasing gradient towards the crypt. BMP antagonists, including gremlin 1, expressed by ISEMFs and smooth muscle cells in turn create an opposite gradient to antagonize BMPs, thus maintaining Wnt activity at the crypt base. This gradient then creates an environment that promotes stem cell self-renewal and expansion at the crypt base region. Indeed, the expression of multiple BMP antagonists by ISEMFs and smooth muscle cells has provided an optimal anatomical setup for the creation and maintenance of the stem cell niche in the basal crypt region of the colon.

Both BMPs and their antagonists play essential roles in stem cell biology, although their functions may vary in different stem cell systems (24). In a recent study, *GREM1* was reported to be expressed in stromal cells of basal cell carcinoma (BCC) of the skin, and gremlin 1 was shown to inhibit differentiation and promote proliferation in

basal cell carcinoma cells *in vitro* (25). Expression of *GREM1* also was noted in stromal cells in diverse types of human cancer, including colon cancer. Consistently, we observed *GREM1* expression by stromal cells in a subset of human colon cancer samples (Figure S8). The staining of *GREM1* in tumor stromal cells tends to be stronger than that in normal myofibroblast and smooth muscle cells at the colon crypt. The data suggest that *GREM1* expression is up-regulated during the development of a subset of colon tumors, and thus BMP antagonists may represent important stem cell niche factors in both normal and neoplastic conditions. It would be of great interest to further investigate and clarify the role of BMP antagonists in the colon cancer stem cell niche. Such studies may provide new opportunities for therapeutic strategy through the modulation of BMP activity.

Materials and Methods

Tissue Samples and RNA extraction

Colectomy specimens were received fresh from the operating theater immediately upon resection. The study included 11 patients who underwent colectomy for either adenocarcinoma, or localized non-neoplastic conditions. Morphologically normal colon mucosae distant from pathological lesions were dissected free from the underlying submucosa and muscularis propria. The dissected mucosae were laid completely flat on a metal surface and frozen in liquid nitrogen. A small 5-mm square of flat mucosa was cut out and embedded in embedding medium for frozen sectioning. Ten microgram-thick serial horizontal were cut such that the early sections contained the top compartment, whereas the deeper sections contained the basal crypt compartment. H&E slides were

prepared from each 100-μm interval, and the intervening sections were collected into separate tubes containing Trizol (Invitrogen, Carlsbad, CA) reagent. For each case, tissue from the superficial crypt compartment and tissue from the basal crypt compartment were selected based on the consecutive H&E sections and submitted for RNA extraction. Tissue from the mid-crypt region was kept for future use and not studied. Expression profiling was performed in nine pairs of patient samples. Spare-paired RNA from two patients, and paired RNA extracted from two independent patients were used for validation studies by quantitative RT-PCR. This study was approved by the Ethics Committee of the University of Hong Kong and Internal Review Board of University of California, San Francisco.

RNA amplification, microarray procedure

cDNA clones representing about 30,000 unique genes were obtained from Stanford Functional Genomics Facility. Total RNA isolated from nine pairs of colon top and crypt compartments, together with universal human reference RNA (Strategene, La Jolla, CA) was amplified using MessageAmp kit (Ambion, Austin, TX). Amplified RNAs were converted to aminoallyl-modified cDNA and coupled to hydroxysuccinimidyl esters of Cy3 or Cy5 (Amersham-Pharmacia, Piscataway, NJ) and hybridized to microarrays as described (26). The array was then scanned with a GenePix 4000B microarray scanner (Axon Instruments, Union City, CA). Primary data collection and analysis were carried out using GenePix Pro 3.0 (Axon Instruments). Areas of the array with obvious blemishes were manually flagged and excluded from subsequent analysis. The raw data were deposited into Stanford Microarray Database (SMD) (27), http://smd.stanford.edu.

The raw data also were submitted to Gene Expression Omnibus (http://www.ncbi.nlm.nih.gov/projects/geo, accession no. GSE6894).

Microarray Analysis

For initial data analysis, all nonflagged array elements for which the fluorescent intensity in either channel was >2.5 times the local background were considered well measured. Genes for which <75% of measurements were available across all the samples were excluded from further analysis. This resulted in 25,132 cDNA clones that were downloaded from Stanford Microarray Database. For SAM analysis, data were mean centered, and genes with >1.5-fold variation in four arrays were selected. Missing data were estimated using 10 nearest neighbor KNN imputing algorithm. Paired SAM was performed with 512 permutations (28). A total of 969 cDNA clones with significant differential expression between bottom-top compartments was identified. The GO term finder program was used to analyze the list of differentially expressed genes for enrichment of specific functional groups (29).

To gain a broader picture for the differential gene expression, a paired *t* test was performed using the whole data set independently to identify genes that were significantly altered ($P < 0.01$, n = 18) between each pair of samples. A total of 6,087 cDNA clones satisfying the previous criteria was then extracted. For graphical display, the 6,087 significant cDNA clones identified were imported into GenMapp software (30) to illustrate the expression difference between bottom-top crypt compartments among different pathways.

Genes with differential expression as identified by SAM were arranged by hierarchical clustering using the average linkage clustering method and visualized by using TreeView. Data regarding the global gene expression level changes after interruption of Wnt signaling in colon cancer cells through inducible dnTCF4 (13) were retrieved from http://smd.stanford.edu/cgi-bin/publication/viewPublication.pl?pub_no=191; and genes highly expressed in human ES and EC cells (31) were downloaded from http://microarray-pubs.stanford.edu/es_cells_2/ for comparison with our data set.

Real-Time Quantitative RT-PCR

Quantitative RT-PCR was performed to validate microarray data as well as to study gene expression variation in Caco-2 and rat intestinal epithelial cells (IEC-6 and IEC-18) treated with 0.5 μg/ml recombinant mouse gremlin 1 (R&D Systems, Minneapolis, MN). The procedure was carried as described (32). In brief, total RNA was subjected to DNase I digestion to remove any genomic DNA contamination. Two-step reverse transcription was carried out using MultiScribe™ Reverse Transcriptase (Applied Biosystems, Foster City, CA). Human or rat GAPDH was used as the normalization control in subsequent quantitative analysis. For confirmation of microarray data in this study, the following primers and probe were used: GAPDH-F: CCTTCATTGACCTCAACTACAT; GAPDH-R: GAAGATGGTGATGGGATTTC; and GAPDH-probe: CAAGCTTCCCGTTCTCAGCC. Other primers and probe reagents were purchased from TaqMan Gene Expression Assay (Applied Biosystems). For the gene expression study in cells, SYBR Green Master Mix (Applied Biosystems) was used together with the

primer pairs listed in Supplemental Table 2. Quantification was performed using the ABI Prism 7700 sequence detection system (Applied Biosystems) according to the relative standard method. Calibration curves were generated for each transcript and validated by using linear regression analysis ($r^2 \geq 0.99$). Transcript quantification was performed in triplicate for every sample and reported relative to GAPDH.

Cell Culture

Caco-2, DLD-1, HT 29, IEC-6 and IEC-18 cells were obtained from American Type Culture Collection (ATCC, Manassas, VA). Caco-2, DLD-1, IEC-6 and IEC-18 cells were cultured in Dulbecco's modified Eagle's medium (DMEM) with 4.5 g/L glucose and L-glutamine. HT 29 cells were cultured in RPMI-1640 with 2.0 g/L glucose and L-glutamine. The media was supplemented with 10% fetal bovine serum (5% for IEC-18 cells), penicillin (50 units/ml), and streptomycin (50 μg/ml). Transferrin (0.01 mg/ml) was added to media for Caco-2 cells. An intestinal subepithelial myofibroblast cell line, 18Co, was purchased from ATCC (33). Primary intestinal myofibroblast cultures were established from histologically normal margins of surgically resected colonic (CMF) or ileal (IMF) tissue by using the outgrowth method described by Mahida *et al*. (34). The myofibroblast phenotype was verified by immunohistochemistry and flow cytometry as described (35, 36). The primary myofibroblasts were cultured in MEM Eagle's with Earle's BSS Medium that was supplemented with 10% NuSerum, 200 μM L-glutamine, penicillin (50 units/ml), and streptomycin (50 μg/ml).

In situ hybridization and Immunohistochemistry

In situ hybridization was performed using digoxigenin-labeled probes as previously described (37). Human (gremlin 1) *GREM1* and human (gremlin 2) *GREM2* riboprobes were used in this study and generated by appending the T7 promoter sequence to the respective 5' end of antisense and sense primers (Supplemental Table 2). For immunohistochemistry, paraffin tissue sections were dewaxed with xylene and hydrated in graded alcohols. Antigen retrival was performed by boiling slides for 10 min in sodium-citrate buffer (10mM, pH 6.0). Following antigen retrival, the slides were treated with primary monoclonal antibodies directed against either α-smooth muscle actin (αSMA) (DAKO, Carpinteria, CA; 1:50 dilution) or fibronectin (NeoMarkers, Fremont, CA; 1:1000 dilution). The slides were incubated with biotinylated goat anti-mouse antibody, followed by ABC immunodetection (VECTASTAIN elite ABC reagent, Vector Laboratories, Burlingame, CA) using DAB to reveal antibody binding.

Double staining using *in situ* hybridization and immunofluorescence

In situ hybridization was performed using human *GREM1* riboprobe as described in the previous section. Double staining by using immunofluorescence and *in situ* hybridization was carried out as described previously (38). To detect the secondary streptavidin complex, streptavidin-specific Alexa Fluor 594 (Invitrogen) was used. After mRNA detection, the slides were incubated overnight with primary antibody vimentin (Neomarkers, 1:1000 dilution). The antibody binding was detected by incubating the sections with FITC goat anti-mouse secondary antibody. The slides were mounted with

Vectashield containing DAPI (Vector Laboratories). Images were captured with the Zeiss upright Axioscope2 Plus fluorescence microscope.

RT-PCR

Total RNA was extracted from CMF11, CMF7B, IMF11B, 18Co, DLD-1, Caco-2, and HT 29 cells using TRIzol reagent (Invitrogen). For each reaction, 1 μg of RNA was reversed transcribed to cDNA. PCR amplification was carried out as described (39). The primer sequences are listed in Supplemental Table 2.

Immunofluorescence

IEC-18 cells cultured on chambered slides and treated with 0.5 μg/ml recombinant mouse gremlin 1 (R&D Systems) for 0 or 24 h were fixed with 4% paraformaldehyde at room temperature for 20 min. Cells were permeabilized with 0.1% Triton X-100 in PBS for 15 min. After blocking with PBS containing 0.5% goat serum for 30 min, the cells were incubated with primary antibodies against vimentin (Neomarkers, 1:800 dilution), fibronectin (Neomarkers, 1:1000 dilution), or α-smooth muscle actin (αSMA) (Dako, 1:50 dilution). The primary antibody binding was detected with goat anti-mouse antibody conjugated to Alexa 568 (Invitrogen). The slides were mounted with Vectashield mounting medium containing DAPI (Vector Laboratories). Images were acquired using the Zeiss upright Axioscope2 Plus fluorescence microscope.

Acknowledgments

We thank the Stanford Functional Genomic Facility and Stanford Microarray Database for support on microarray experiments and Chris Haqq, Julie Sneddon, Patrick Brown, and Linheng Li for experimental advice. This work was supported in part by National Institutes of Health Grants R21DK-069309 (to X.C.) and R01DK-055783 (to D.W.P.), Research Grants Council of the Hong Kong Special Administrative Region Grant HKU7524/06M (to S.Y.L., S.T.Y., T.L.C., and X.C.), and a California Institute for Regenerative Medicine stem cell fellowship (to C.K.).

References

1. Rubin, D. C. (2007) *Curr Opin Gastroenterol* **23**, 111-4.
2. Crosnier, C., Stamataki, D. & Lewis, J. (2006) *Nat Rev Genet* **7**, 349-59.
3. Leedham, S. J., Brittan, M., McDonald, S. A. & Wright, N. A. (2005) *J Cell Mol Med* **9**, 11-24.
4. Clevers, H. (2006) *Cell* **127**, 469-80.
5. He, X. C., Zhang, J. & Li, L. (2005) *Ann N Y Acad Sci* **1049**, 28-38.
6. van Es, J. H. & Clevers, H. (2005) *Trends Mol Med* **11**, 496-502.
7. Stappenbeck, T. S., Mills, J. C. & Gordon, J. I. (2003) *Proc Natl Acad Sci U S A* **100**, 1004-9.
8. Mariadason, J. M., Nicholas, C., L'Italien, K. E., Zhuang, M., Smartt, H. J., Heerdt, B. G., Yang, W., Corner, G. A., Wilson, A. J., Klampfer, L., Arango, D. & Augenlicht, L. H. (2005) *Gastroenterology* **128**, 1081-8.
9. Giannakis, M., Stappenbeck, T. S., Mills, J. C., Leip, D. G., Lovett, M., Clifton, S. W., Ippolito, J. E., Glasscock, J. I., Arumugam, M., Brent, M. R. & Gordon, J. I. (2006) *J Biol Chem* **281**, 11292-300.
10. Whitfield, M. L., George, L. K., Grant, G. D. & Perou, C. M. (2006) *Nat Rev Cancer* **6**, 99-106.
11. Pourreyron, C., Dumortier, J., Ratineau, C., Nejjari, M., Beatrix, O., Jacquier, M. F., Remy, L., Chayvialle, J. A. & Scoazec, J. Y. (2003) *Int J Cancer* **104**, 28-35.
12. Lawson, D., Harrison, M. & Shapland, C. (1997) *Cell Motil Cytoskeleton* **38**, 250-7.
13. van de Wetering, M., Sancho, E., Verweij, C., de Lau, W., Oving, I., Hurlstone, A., van der Horn, K., Batlle, E., Coudreuse, D., Haramis, A. P., Tjon-Pon-Fong, M., Moerer, P., van den Born, M., Soete, G., Pals, S., Eilers, M., Medema, R. & Clevers, H. (2002) *Cell* **111**, 241-50.
14. Batlle, E., Henderson, J. T., Beghtel, H., van de Born, M. M. W., Sancho, E., Huls, G., Pawson, T. & Clevers, H. (2002) *Cell* **111**, 251-263.
15. Holmberg, J., Genander, M., Halford, M. M., Anneren, C., Sondell, M., Chumley, M. J., Silvany, R. E., Henkemeyer, M. & Frisen, J. (2006) *Cell* **125**, 1151-63.
16. Adegboyega, P. A., Mifflin, R. C., DiMari, J. F., Saada, J. I. & Powell, D. W. (2002) *Arch Pathol Lab Med* **126**, 829-36.
17. Chantret, I., Barbat, A., Dussaulx, E., Brattain, M. G. & Zweibaum, A. (1988) *Cancer Res* **48**, 1936-42.
18. Haramis, A. P., Begthel, H., van den Born, M., van Es, J., Jonkheer, S., Offerhaus, G. J. & Clevers, H. (2004) *Science* **303**, 1684-6.
19. Leung, J. Y., Kolligs, F. T., Wu, R., Zhai, Y., Kuick, R., Hanash, S., Cho, K. R. & Fearon, E. R. (2002) *J Biol Chem* **277**, 21657-65.
20. Jho, E. H., Zhang, T., Domon, C., Joo, C. K., Freund, J. N. & Costantini, F. (2002) *Mol Cell Biol* **22**, 1172-83.
21. Sperger, J. M., Chen, X., Draper, J. S., Antosiewicz, J. E., Chon, C. H., Jones, S. B., Brooks, J. D., Andrews, P. W., Brown, P. O. & Thomson, J. A. (2003) *Proc Natl Acad Sci U S A* **100**, 13350-5.

22. Gregorieff, A., Pinto, D., Begthel, H., Destree, O., Kielman, M. & Clevers, H. (2005) *Gastroenterology* **129**, 626-38.
23. He, X. C., Zhang, J., Tong, W. G., Tawfik, O., Ross, J., Scoville, D. H., Tian, Q., Zeng, X., He, X., Wiedemann, L. M., Mishina, Y. & Li, L. (2004) *Nat Genet* **36**, 1117-21.
24. Zhang, J. & Li, L. (2005) *Dev Biol* **284**, 1-11.
25. Sneddon, J. B., Zhen, H. H., Montgomery, K., van de Rijn, M., Tward, A. D., West, R., Gladstone, H., Chang, H. Y., Morganroth, G. S., Oro, A. E. & Brown, P. O. (2006) *Proc Natl Acad Sci U S A* **103**, 14842-7.
26. Haqq, C., Nosrati, M., Sudilovsky, D., Crothers, J., Khodabakhsh, D., Pulliam, B. L., Federman, S., Miller, J. R., 3rd, Allen, R. E., Singer, M. I., Leong, S. P., Ljung, B. M., Sagebiel, R. W. & Kashani-Sabet, M. (2005) *Proc Natl Acad Sci U S A* **102**, 6092-7.
27. Sherlock, G., Hernandez-Boussard, T., Kasarskis, A., Binkley, G., Matese, J. C., Dwight, S. S., Kaloper, M., Weng, S., Jin, H., Ball, C. A., Eisen, M. B., Spellman, P. T., Brown, P. O., Botstein, D. & Cherry, J. M. (2001) *Nucleic Acids Res* **29**, 152-5.
28. Tusher, V. G., Tibshirani, R. & Chu, G. (2001) *Proc Natl Acad Sci U S A* **98**, 5116-21.
29. Boyle, E. I., Weng, S., Gollub, J., Jin, H., Botstein, D., Cherry, J. M. & Sherlock, G. (2004) *Bioinformatics* **20**, 3710-5.
30. Dahlquist, K. D., Salomonis, N., Vranizan, K., Lawlor, S. C. & Conklin, B. R. (2002) *Nat Genet* **31**, 19-20.
31. Sperger, J. M., Chen, X., Draper, J. S., Antosiewicz, J. E., Chon, C. H., Jones, S. B., Brooks, J. D., Andrews, P. W., Brown, P. O. & Thomson, J. A. (2003) *Proc Natl Acad Sci U S A* **100**, 13350-5.
32. Leung, S. Y., Chen, X., Chu, K. M., Yuen, S. T., Mathy, J., Ji, J., Chan, A. S., Li, R., Law, S., Troyanskaya, O. G., Tu, I. P., Wong, J., So, S., Botstein, D. & Brown, P. O. (2002) *Proc Natl Acad Sci U S A* **99**, 16203-8.
33. Valentich, J. D., Popov, V., Saada, J. I. & Powell, D. W. (1997) *Am J Physiol* **272**, C1513-24.
34. Mahida, Y. R., Galvin, A. M., Gray, T., Makh, S., McAlindon, M. E., Sewell, H. F. & Podolsky, D. K. (1997) *Clin Exp Immunol* **109**, 377-86.
35. Saada, J. I., Pinchuk, I. V., Barrera, C. A., Adegboyega, P. A., Suarez, G., Mifflin, R. C., Di Mari, J. F., Reyes, V. E. & Powell, D. W. (2006) *J Immunol* **177**, 5968-79.
36. Shao, J., Sheng, G. G., Mifflin, R. C., Powell, D. W. & Sheng, H. (2006) *Cancer Res* **66**, 846-55.
37. Leung, S. Y., Yuen, S. T., Chu, K. M., Mathy, J. A., Li, R., Chan, A. S., Law, S., Wong, J., Chen, X. & So, S. (2004) *Gastroenterology* **127**, 457-69.
38. West, R. B., Rubin, B. P., Miller, M. A., Subramanian, S., Kaygusuz, G., Montgomery, K., Zhu, S., Marinelli, R. J., De Luca, A., Downs-Kelly, E., Goldblum, J. R., Corless, C. L., Brown, P. O., Gilks, C. B., Nielsen, T. O., Huntsman, D. & van de Rijn, M. (2006) *Proc Natl Acad Sci U S A* **103**, 690-5

39. Obermeier, F., Hausmann, M., Kellermeier, S., Kiessling, S., Strauch, U. G., Duitman, E., Bulfone-Paus, S., Herfarth, H., Bock, J., Dunger, N., Stoeck, M., Scholmerich, J., Falk, W. & Rogler, G. (2006) *Eur J Immunol* **36**, 2691-9.

Supplementary Information

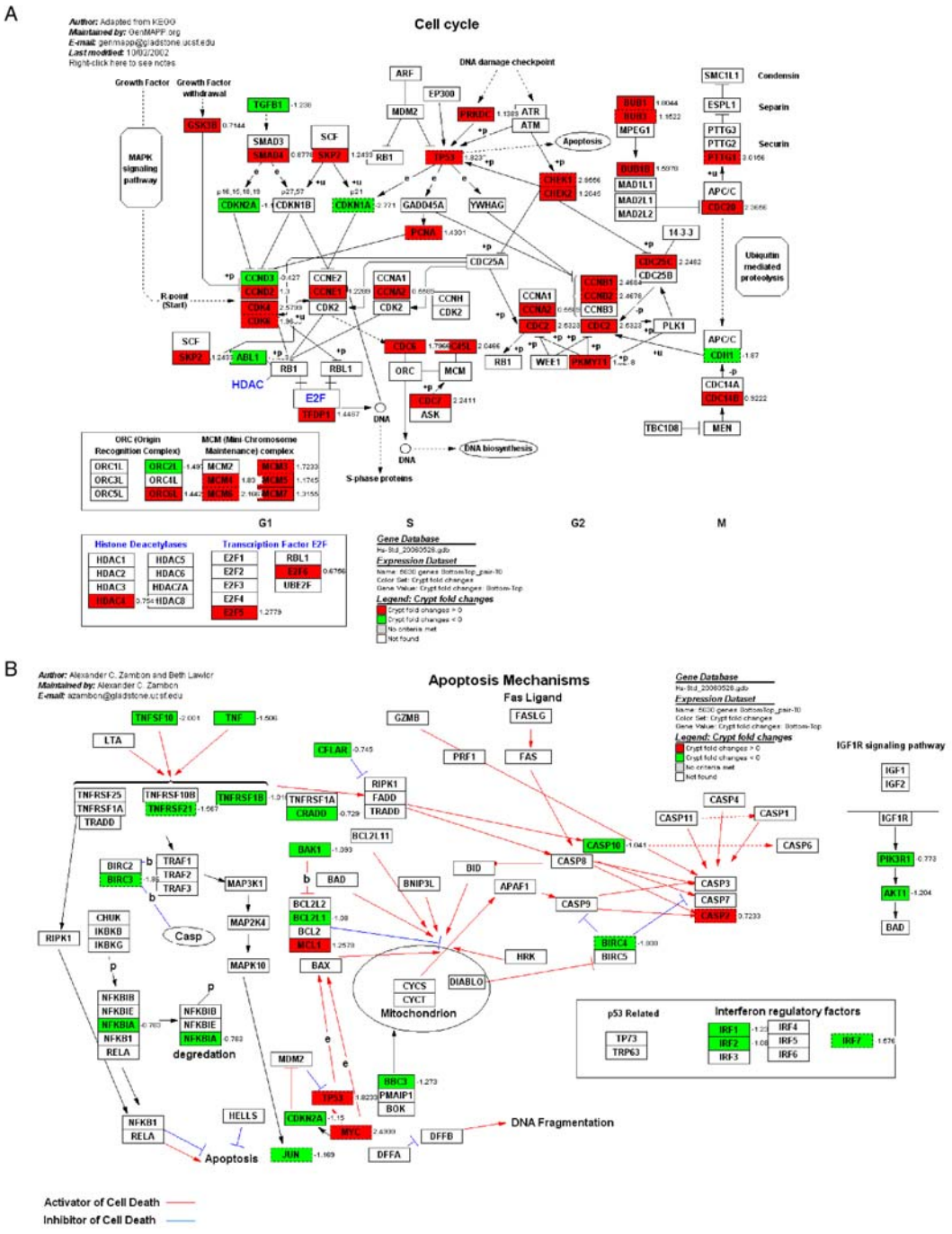

Figure S1. Network analysis for cell cycle (*A*) and apoptosis (*B*) genes differentially expressed in colon top and basal crypts by GenMapp from KEGG pathway. Highlighted genes are those significantly altered in paired *t*-test ($P < 0.01$), where red represents genes overexpressed in bottom crypt and green represents down-regulated genes.

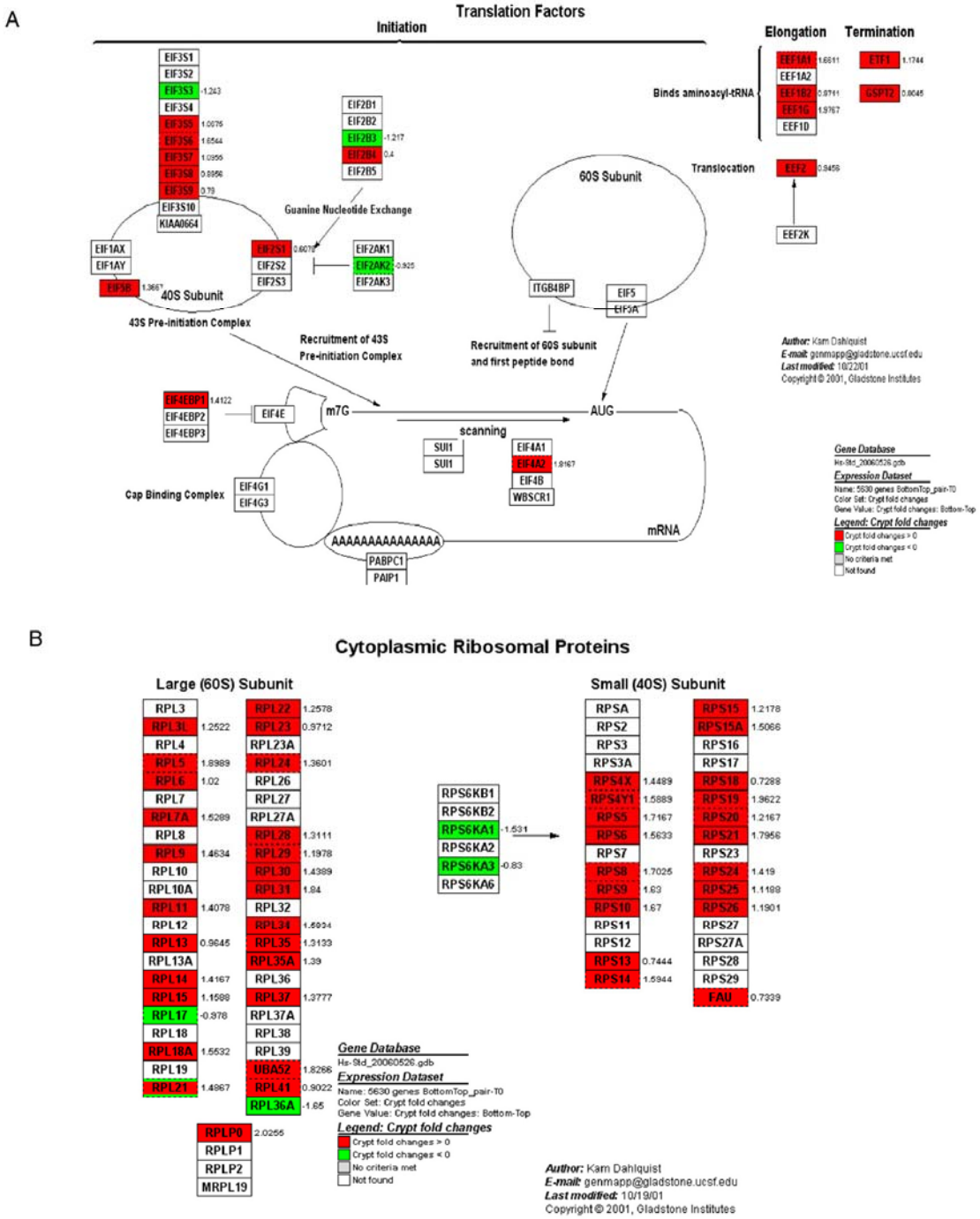

Figure S2. Differential expression of translation factors and ribosomal proteins in colon bottom versus top crypt compartments by GenMapp. Highlighted genes are those significantly altered in paired *t*-test ($P < 0.01$), where red color represents genes overexpressed in bottom crypt and green color represents downregulated genes. (A) 16 out of 19 translation factors (84%) and (B) 43 out of 48 ribosomal proteins (90%) are overexpressed in bottom crypt.

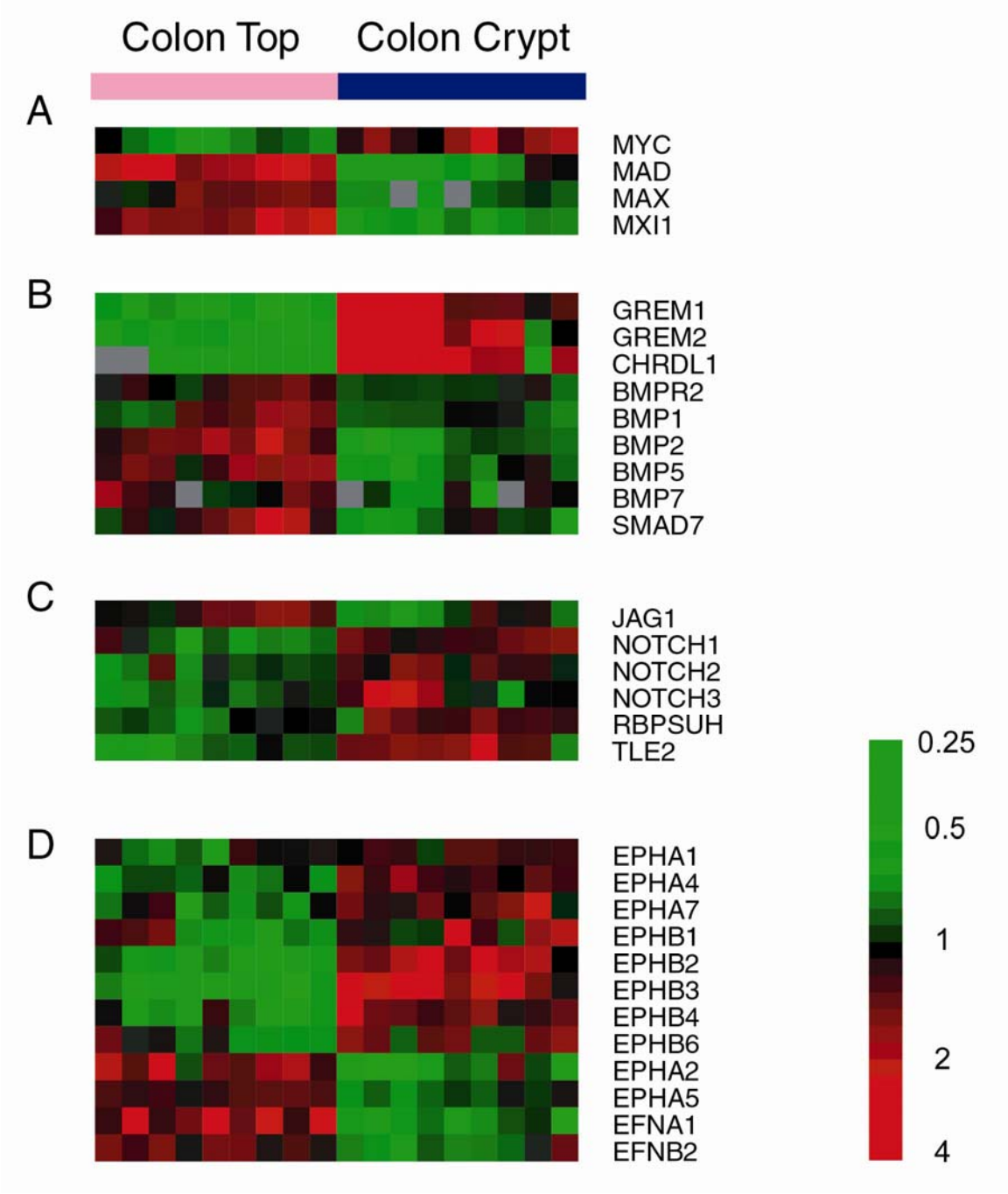

Figure S3. Differential gene expression pattern of selected pathways in colon top and basal crypts. (A) Myc/Max/Mad network. (B) BMP pathway. (C) NOTCH pathway. (D) Eph/ephrin pathway. All the genes listed were significant in paired *t*-test ($P < 0.05$).

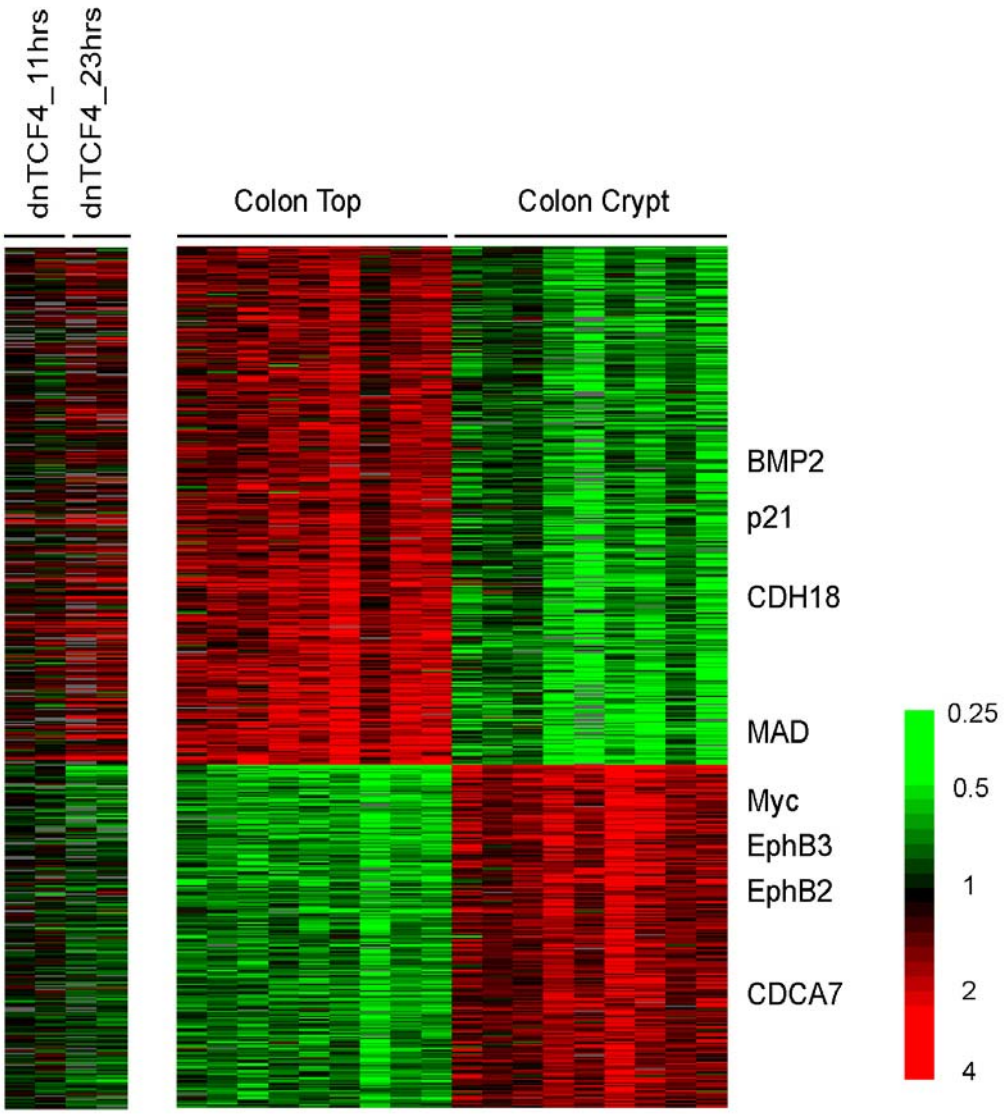

Figure S4. Genes differentially expressed in colon top and basal crypt and their relationship with Wnt/β-catenin signaling targets. Microarray data of inducible expression of dnTCF4 in Ls174 cells were retrieved from van de Wetering et al.(13), and overlapping clones with colon top/bottom crypt gene list as identified by SAM were selected. Common genes in both data sets were displayed by using TreeView.

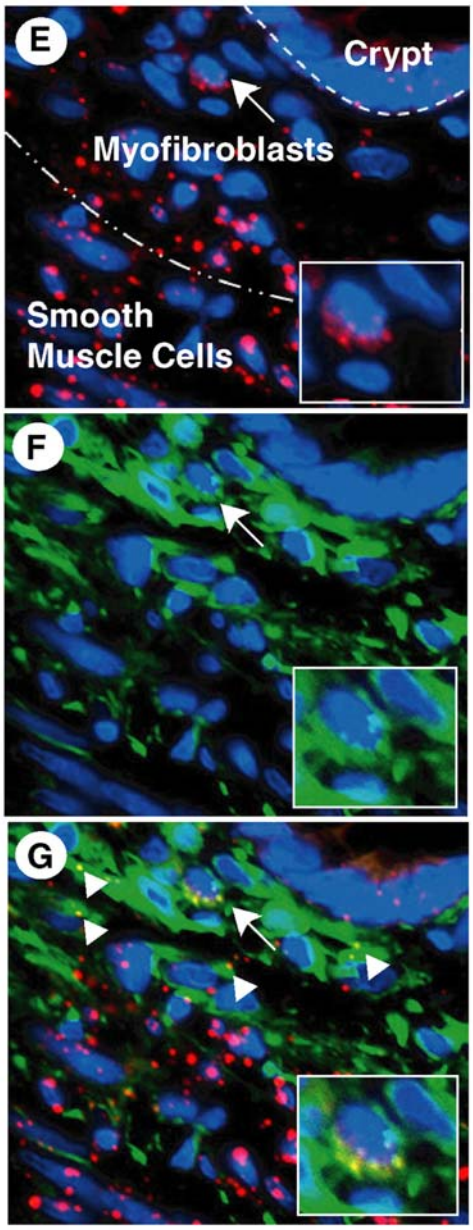

Figure S5. Enlarged version of Figure 3E-3G showing the colocalization (white arrows) of gremlin 1 (red dots) and myofibroblast marker vimentin (green staining) at colon crypts.

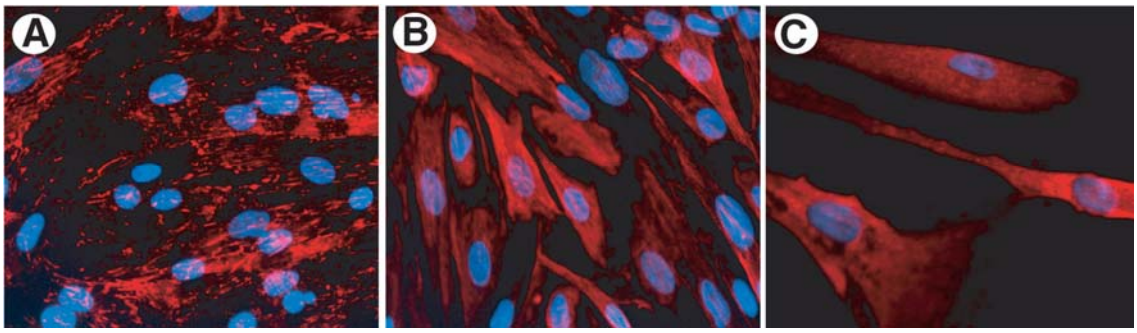

Figure S6. Characterization of isolated human colonic myofibroblast 18Co cells by immunofluorescent staining of fibronectin (*A*), vimentin (*B*), and α-smooth muscle actin (*C*).

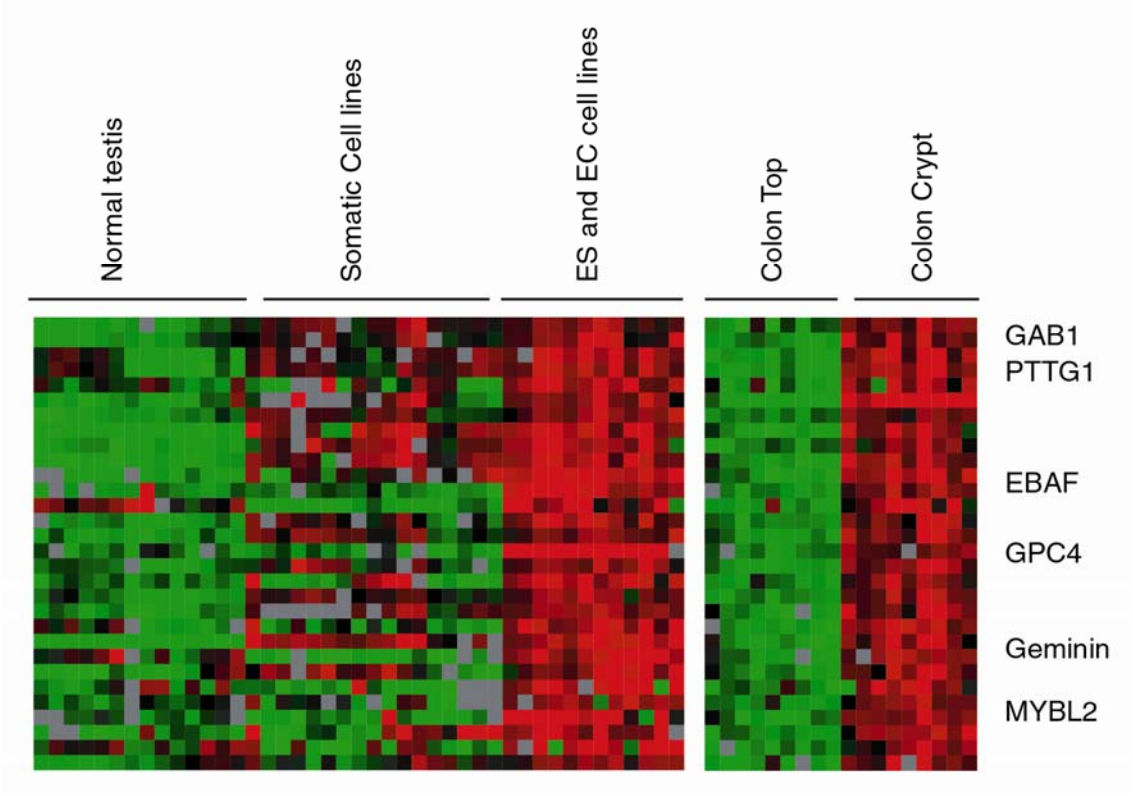

Figure S7. Candidate stem/progenitor cell markers in colon crypt gene list illustrated by using TreeView. Specifically, 895 genes reported to be highly expressed in human ES and EC cells by Sperger et al. (21) were compared to 367 clones highly expressed in colon crypts. Thirty-one genes in common between these two data sets were noted. The complete list of genes is available for download from http://www.pnas.org/content/suppl/2007/09/05/0707210104.DC1/07210Table5.xls.

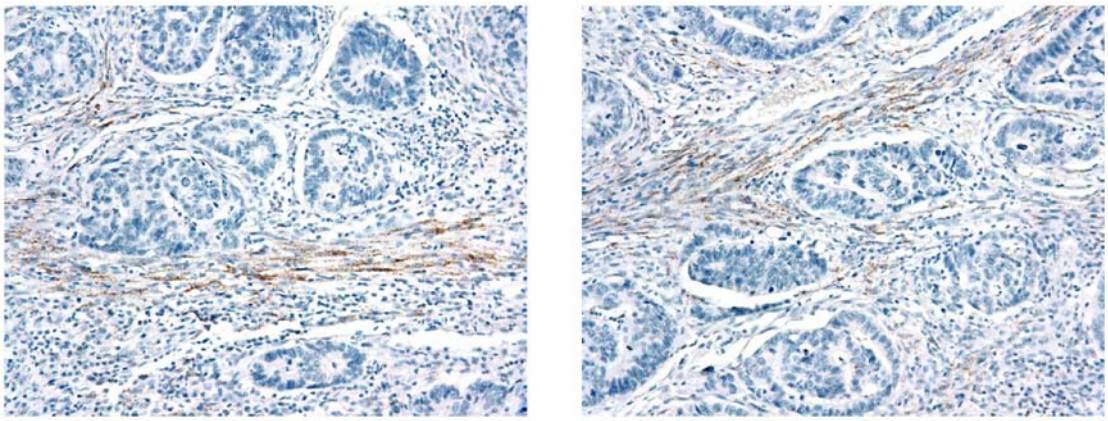

Figure S8. Gremlin 1 expression in colon cancer stromal cells revealed by *in situ* hybridization. Dark brown dots indicate positive staining.

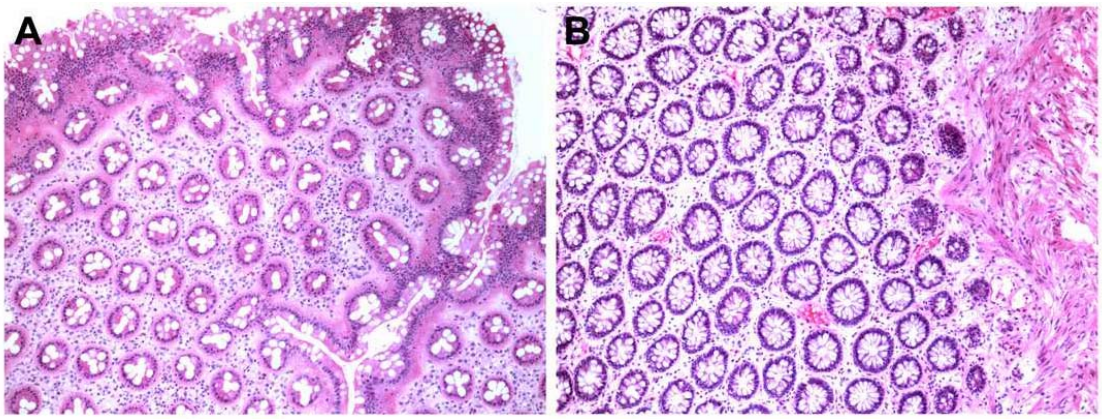

Figure S9. Representative horizontal histological sections of colon top (*A*) and crypt (*B*) mucosal compartments submitted for RNA extraction.

Table S1. Quantitative RT-PCR validation of colon bottom/top crypt array expression data.

Genes	Bottom/top array fold change (log2)	Paired *t*-test *p*-value (array)	Expressed at colon Position	Bottom/top qRT-PCR fold change (log2)	Paired *t*-test *p*-value (qRT-PCR)
APC	-0.94	0.012	Top	-1.021	0.002
SFRP1	2.265	<0.001	Bottom	2.788	0.017
MXI1	-2.553	<0.001	Top	-3.200	0.002
JAG1	-1.042	0.004	Top	-0.951	0.026
DUSP5	-2.450	<0.001	Top	-2.336	0.002
EFNA1	-2.400	<0.001	Top	-2.874	0.002
CHRDL1	5.317	<0.001	Bottom	6.646	0.004
GREM1	3.043	<0.001	Bottom	7.536	< 0.001
GREM2	3.960	<0.001	Bottom	6.068	0.001
GPC4	1.682	<0.001	Bottom	0.928	0.002

Table S2. Primers used for RT-PCR, quantitative RT-PCR, and *in situ* hybridization.

Table S2A: Primers used for RT-PCR analysis

Human Primers	Forward Sequence (5' -3')	Reverse Sequence (5' -3')
Gremlin 1	GTCACACTCAACTGCCCTGA	GGTGAGGTGGGTTTCTGGTA
Gremlin 2	CCTCAATCCTGGTCTTTGGA	TGGATCAACCATGTGCAGTT
Chordin-like1	CCACCTCAGGTAGAGGTCCA	GTGCATGGCGTGAATAATTG
Chordin	TGTGAGAAGGTGCAGTGTCC	AAGAGCCTTCGGCTTCTTTC
FST	GTTTTCTGTCCAGGCAGCTC	AGCTTCCTTCATGGCACACT
TWSG1	TCCCCTTCTTCATGAGCATC	AGCCAAATTTGAAGGCAAAA
Actin	TCACAATGTGGCCGAGGACTTTGA	GCACGAAGGCTCATCATTCAAA

Table S2B: *In situ* hybridization probes

Human Primers	Forward Sequence (5' -3')	Reverse Sequence (5' -3')
Gremlin 1	AACAGTCGCACCATCATCAA	CGATGGATATGC
Gremlin 2	TGTGGGGACTTAGCTTCCTG	TCCACCAAATGC

Table S2C: Primers used for qRT-PCR

Human Primers	Forward Sequence (5' -3')	Reverse Sequence (5' -3')
ANPEP	CCACCTTGGACCAAAGTAAAGC	TCTCAGCGTCACCTGGTAGGA
p21	TGGAGACTCTCAGGGTCGAAA	GGCGTTTGGAGTGGTAGAAATC
Axin-2	TGCTCTGTTTTGTCTTAAAGGTCTGA	ACAGATCATCCCATCCAACACA
GAPDH	GAAGGTGAAGGTCGGAGTC	GAAGATGGTGATGGGATTTC

Rat Primers	Forward Sequence (5' -3')	Reverse Sequence (5' -3')
Axin-2	TGCCAAAACGGAATACGAAAG	TGCACTGGACATCCCTCCTT
GAPDH	TGCCAAGTATGATGACATCAAGAAG	TAGCCCAGGATGCCCTTTAGT

Chapter 3

Indian Hedgehog Regulates Intestinal Stem Cell Fate through Niche Maintenance

INDIAN HEDGEHOG REGULATES INTESTINAL STEM CELL FATE THROUGH NICHE MAINTENANCE

Cynthia Kosinski[1], Daniel E. Stange[2], Chuanrui Xu[1], Annie SY Chan[3], Coral Ho[1], Randy C. Mifflin[4], Don Powell[4], Hans Clevers[2], Suet Yi Leung[3], and Xin Chen[1]

[1]Department of Bioengineering and Therapeutic Sciences, University of California, San Francisco, CA, USA;

[2]Hubrecht Institute, KNAW & University Medical Center Utrecht, Utrecht, The Netherlands;

[3]Department of Pathology; University of Hong Kong, Queen Mary Hospital, Pokfulam, Hong Kong;

[4]Department of Internal Medicine, University of Texas Medical Branch, Galveston, TX, USA.

Summary

The intestinal stem cell (ISC) niche supports and regulates ISCs through both physical interactions and diffusible factors. However, how the niche influences ISC regulation remains elusive. Here, we examined the role of Indian hedgehog (Ihh) in niche organization and how perturbation of niche components affects ISC fate. We find that deleting intestinal epithelial Ihh leads to disrupted niche architecture as manifested by the loss of the muscularis mucosae, extracellular matrix deterioration, and reduced crypt myofibroblasts. Moreover, deregulation of the niche leads to an expansion of ISCs. Mechanistic studies reveal inhibiting Hh deregulates BMP signaling, up-regulates MMPs, and disrupts extracellular matrix proteins, fostering a pro-growth environment for ISCs. We show that the muscularis mucosae is a novel component of the ISC niche, which acts with myofibroblasts to restrict crypt size and prevent abnormal stimulation of ISCs. Thus, Ihh functions as a critical regulator of ISC self-renewal by maintaining the ISC niche.

Introduction

In the adult intestine, gut epithelial cells undergo repeated progenitor cell proliferation, terminal differentiation and cell death, a process that requires intestinal epithelial stem cells (ISCs) to engage in a continuous dialogue with neighboring epithelial and mesenchymal cells (1, 2). The ISC is located at or near the base of the crypt. The debate on the exact location of ISCs has been reignited by two recent genetic lineage tracing studies in which Lgr5 and Bmi1 emerged as candidate ISC markers (3, 4). Lgr5 and Bmi1-labeled cells both possess the quality of "stemness" as demonstrated by their longevity and multipotency; however, Lgr5-labeled cells were found at the base of the crypt interspersed between Paneth cells while Bmi1-labeled cells were primarily found at the +4 position. Since the discovery of Lgr5 intestinal stem cells, additional ISC markers have been identified based on the gene signature of Lgr5 stem cells, including Achaete Scute-Like 2 (Ascl2) and Olfactomedin-4 (Olfm4) (5, 6). Other ISCs markers have been proposed including the cholesterol-binding glycoprotein Prominin1 and the neural RNA-binding protein Musashi1 (7, 8). However, subsequent studies have challenged the specificity of these markers as they found Prominin1 and Musashi1 are broadly expressed in intestinal crypts, marking transit-amplifying cells as well as ISCs (9, 10).

The continuous shedding of intestinal epithelial cells into the gut lumen requires ISCs to self-renew daily. The regenerative capacity of ISCs is directed by structural and biochemical cues received from the ISC niche (11). The niche is a complex structure that modulates intestinal homeostasis by maintaining a fine balance between stem cell self-renewal and downstream differentiation. The different cell types believed to contribute to the ISC niche include neighboring epithelial cells, pericryptal intestinal subepithelial

myofibroblasts (ISEMFs), smooth muscle cells (SMCs), endothelial cells, immune cells, and the basement membrane. The most influential components of the ISC niche are considered pericryptal ISEMFs due to their close proximity to ISCs (12, 13). These mesenchymal niche cells secrete various factors that favor or restrict ISC self-renewal including cytokines, growth factors, and matrix proteins. Among them are BMP antagonists, such as Noggin and Gremlin 1, which act with Wnt signals to maintain an environment permissive for ISC self-renewal (14, 15). Indeed, recent *in vitro* culture of intestinal epithelium incorporated either myofibroblasts or extracellular signals that are believed to be produced by myofibroblasts such as BMP antagonists into the culture system (16, 17). Yet how ISEMFs are regulated within the ISC niche, their precise role in fostering ISC self-renewal and proliferation, and whether they are the only major contributors of the mesenchymal ISC niche remains unclear.

The Hedgehog (Hh) signaling pathway plays a critical role during gut development (18). Evidence that Hh signals may target intestinal mesenchymal cells including those forming the niche has emerged from studies that characterized the expression pattern of Hh signaling components (19, 20). Expression of the Hh ligands, Sonic Hedgehog (Shh) and Indian Hedgehog (Ihh) has been detected exclusively in the intestinal epithelium, while expression of Hh target genes, Patched (Ptch-1), and Gli1 has been observed in the mesenchyme. Expression of the other Hh ligand, Desert Hedgehog (Dhh), does not overlap with epithelially expressed Shh or Ihh and is limited to Schwann cells, peripheral nerves, and endothelial cells in the gut (21). A detailed analysis of the gut expression pattern of Hh components in early postnatal mice revealed Hh-responsive cells (Gli1-positive cells) within the small intestinal villus core, muscularis mucosae and

pericryptal myofibroblasts (20). In the colon, a similar pattern was detected with Hh-responsive cells in the muscularis mucosae and in regions surrounding the crypts. These data suggest Hh signaling in the intestine predominantly functions in a paracrine direction, from the epithelium to the mesenchyme.

The importance of Hh signaling in intestinal development has been demonstrated by studies using knockout and transgenic mice. Both Shh- and Ihh-null mice display marked gastrointestinal abnormalities including attenuated smooth muscle layers and intestinal malrotation (19). Interestingly, the gut phenotype seen in *Ihh*$^{-/-}$ mice is more dramatic compared to that observed in *Shh*$^{-/-}$ mice. *Ihh*$^{-/-}$ mice exhibit hypoplastic villi, diminished proliferation in the ISC compartment, and Hirschsprung's disease-associated enlarged colons. On the other hand, *Shh*$^{-/-}$ mice display intestinal transformation of the stomach as well as overgrown stomach epithelium and duodenal villi. The distinct differences observed between the knockouts are consistent with the Hh ligand expression profile along the gastrointestinal tract in which Shh expression concentrates in the stomach, while Ihh expression peaks in the small intestine (20). These data suggest Ihh is the primary functional Hh in the intestine as well as the colon. However, our understanding of Ihh's role in intestinal development is limited as *Ihh*$^{-/-}$ mice die prenatally before gut differentiation is complete. Mice overexpressing the Hedgehog interacting protein (Hhip), a negative regulator of Hh signaling, demonstrated that inhibiting all Hh ligands in the gut leads to the mislocalization of ISEMFs and expansion of immature SMCs (22). Furthermore, these mice showed increased cell proliferation and aberrant crypt-like structures, as well as enhanced Wnt activity. In converse experiments, enhanced Hh signaling due to the conditional deletion of *Ptch1* resulted in accrual of

colonic myofibroblasts and colonic crypt hypoplasia (23). Similarly, overexpression of *Ihh* in the intestinal epithelium led to the expansion of SMCs in the villus cores of adult mice (20).

Despite the recent advances, the exact role of Ihh in ISC regulation and gut development still remains unclear. Here we examined the function of Ihh in the postnatal gastrointestinal tract by generating intestinal epithelial conditional *Ihh* knockout mice. We show that the ISC niche critically depends on Ihh signaling. In the absence of intestinal Ihh, mice display a loss of the muscularis mucosae, a disorganized and compromised extracellular matrix (ECM), and reduced crypt myofibroblasts. Furthermore, alterations in the ISC niche are accompanied by abnormal epithelial phenotypes, including an increase in ISCs and intestinal epithelial progenitors, deranged and mislocated absorptive and secretory cell lineages, dilated and misplaced intestinal crypts and increased Wnt signaling, eventually leading to adenomatous epithelium with dysplastic changes. We also demonstrate that blocking Hh signals in ISEMFs up-regulates matrix metallopeptidases (MMPs), providing a favorable environment for intestinal stem/progenitor expansion. We conclude that Ihh prevents abnormal ISC activation and differentiation by maintaining the ISC niche. This study also provides, for the first time, a possible functional role for muscularis mucosae cells as key components of the ISC niche.

Results

Generation of *Ihh* Conditional Knockout Mice

A partial description of Ihh's role in intestinal development has been provided by a study of $Ihh^{-/-}$ mice (19). However, these mice die at birth, a time when intestinal morphogenesis is still ongoing. Late embryogenesis marks the onset of many transformations including villus formation and cytodifferentiation, and while these processes begin during late embryonic stages they are still being modified after birth. Additionally, the intervillus epithelium undergoes a prominent transition around postnatal day (P) 7 when crypt development commences. Postnatally, mesenchymal ISC niche cells partake in instructive crosstalk with crypt epithelial cells to control cell proliferation, differentiation, and apoptosis. Thus, to examine the full role of Ihh in intestinal development including the critical postnatal period when crypt structures are established and the ISC niche is engaged, we generated a conditional *Ihh*-deficient mouse line. We bred $Ihh^{flox/flox}$ mice to *Villin-Cre* mice, which express Cre in the epithelial cells of the small and large intestine from E12.5 onward (24). This cross generated *Villin-Cre;*$Ihh^{flox/flox}$ mice that had intestinal *Ihh* gene expression levels that were 4% of control mice, confirming that the *Villin-Cre*-mediated recombination of the Ihh^{flox} allele was successful. The gene expression level of *Ptch1* and *Gli1*, two direct transcriptional targets of Hh signals were 19% and 9% of the control mice, respectively (Figure 1A). These results suggest that Ihh is the key Hh molecule in mediating Hh signaling in intestinal tissues, and Shh or Dhh cannot replace its function. The absence of Ihh at the protein level was confirmed in *Villin-Cre;*$Ihh^{flox/flox}$ mice using Ihh immunohistochemistry (Figure 1B).

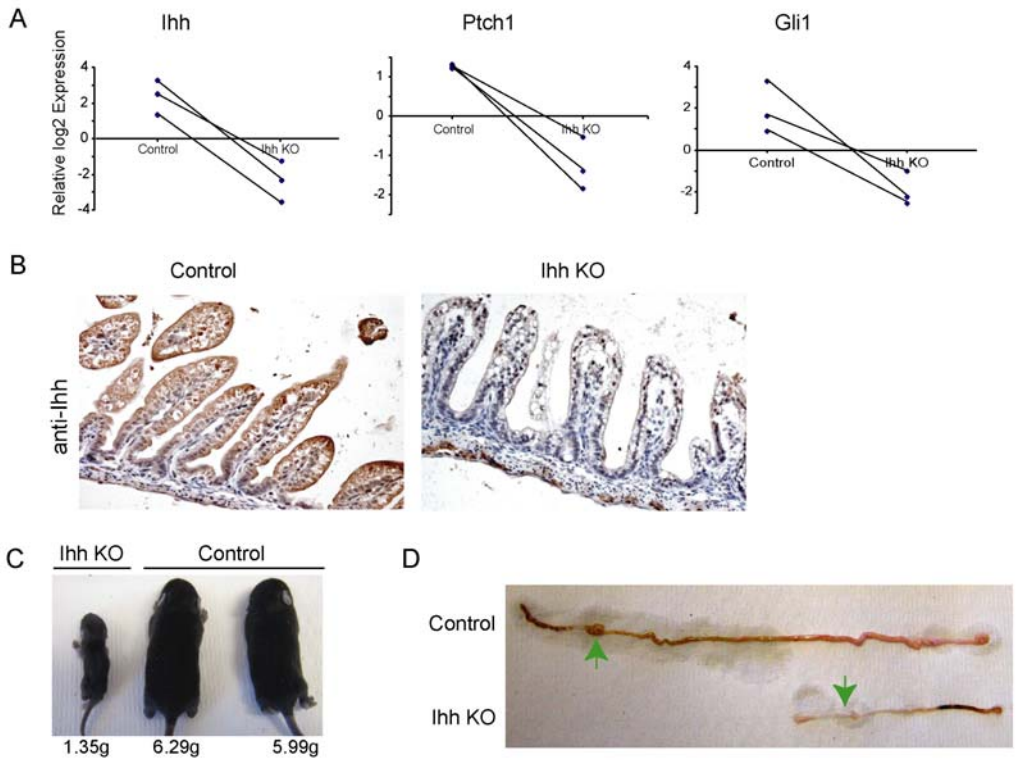

Figure 1. Conditional Deletion of *Ihh* in Mouse Intestinal Epithelium. (A) quantitative RT-PCR of P7-P9 jejunum for *Ihh*, *Ptch* and *Gli1* mRNA in control and *Villin-Cre;Ihh*$^{flox/flox}$ mice. Lines represent the average of three *Villin-Cre;Ihh*$^{flox/flox}$ litters normalized to GAPDH. The mutants had significant decreases in *Ihh*, *Ptch*, and *Gli1* expression levels compared to control; (B) Immunohistochemical staining of Ihh shows expression of Ihh in epithelial cells along the crypt-villus axis in control mice that is abrogated in *Villin-Cre;Ihh*$^{flox/flox}$ mice; (C) Image of P9 mice from control (right two) and *Villin-Cre;Ihh*$^{flox/flox}$ mice (left one). The weight of each mouse is indicated at the bottom; (D) Gross images of gastrointestinal tracts resected from control (upper) and *Villin-Cre;Ihh*$^{flox/flox}$ mice (lower). The arrow indicates the cecum.

Villin-Cre;Ihh$^{flox/flox}$ mice were born alive and similar in size to their control littermates. However, at P3 it was apparent that the mutant mice were not thriving; the mice were noticeably smaller than their control littermates. The majority of *Villin-Cre;Ihh*$^{flox/flox}$ mice died between P7 and P10, although some managed to survive as long as P30. The early lethality of *Villin-Cre;Ihh*$^{flox/flox}$ mice is likely caused by malnourishment as the mutants weighed approximately one-third of their age-matched

control littermates at the time of death (Figure 1C). The presence of milk in the stomach indicates, however, that the mutant mice did not die from a failure to eat.

The length of the small intestine of *Villin-Cre;Ihh$^{flox/flox}$* mice was markedly shorter than their control littermates (Figure 1D). The diameter of the small and large intestine was slightly smaller in the mutant mice. Plausibly, the reduced body size of the *Villin-Cre;Ihh$^{flox/flox}$* mice may have led to this phenotype; however, stunted control mice that weighed less than half of their normal-sized control littermates had only marginal decreases in intestinal lengths (unpublished data). Also in contrast to control littermates, yellow liquid stool or no stool was observed in the colon of *Villin-Cre;Ihh$^{flox/flox}$* mice, suggesting these mice are not sufficiently absorbing or digesting their milk.

Loss of Intestinal and Colonic Niche Cells in *Villin-Cre;Ihh$^{flox/flox}$* Mice

It has previously been reported that Ihh signals in a paracrine direction, moving from its origin in intestinal epithelial cells towards Hh signaling effectors in mesenchymal cells (20). Since mesenchymal cells are the key Hh target cells we hypothesized their composition and ultimately the ISC niche would be altered in *Villin-Cre;Ihh$^{flox/flox}$* mice. We investigated the myofibroblast and smooth muscle changes by α-smooth muscle actin (α-SMA) immunostaining. The most striking and consistent change observed in the *Villin-Cre;Ihh$^{flox/flox}$* mice was the loss of a horizontal layer of α-SMA positive cells at the crypt base in the small intestine and colon that corresponds to the muscularis mucosae (red arrows) (Figure 2A, 2B, 2E and 2F; Figure S1A and S1B). The complete loss of muscularis mucosae cells was observed soon after birth and persisted throughout development (Figure S1A and 1B). Since the cellular components of the muscularis

mucosae in mice have not been well-characterized, we performed a double-labeling experiment for α-SMA and desmin. Myofibroblasts can be distinguished from fibroblasts by their expression of α-SMA, and separated from SMCs by their lack of desmin expression, a smooth muscle marker. The staining results revealed that in control mice, the cells comprising the thin layer below the small intestinal crypt expressed α-SMA (green), but not desmin (red), indicating the muscularis mucosae layer absent from the small intestine of *Villin-Cre;Ihh*$^{flox/flox}$ mice is composed of myofibroblasts (Figure 2C and 2D; Figure S2). In the control colon, α-SMA and desmin co-expressed (yellow) along the muscularis mucosae underneath colonic crypts, demonstrating the missing muscularis mucosae layer in the colon of *Villin-Cre;Ihh*$^{flox/flox}$ mice is composed of SMCs (Figure 2G and 2H; Figure S2).

Since ISEMFs, especially pericryptic myofibroblasts have traditionally been considered the key components of the ISC niche, we examined the composition of these cells in mutant mice. In the colon, we consistently observed diminished numbers of pericryptal myofibroblasts at the crypt base (Figure 2E and 2F; Figure S1A). In the small intestine, loss of pericryptal myofibroblasts was more variable, while the concentration of myofibroblasts in the lamina propria was generally reduced (Figure 2A and 2C; Figure S1B). At sites where superimposed inflammation occurred, we observed an expansion of the villus core with an accumulation of myofibroblasts at the villus core tip (data not shown). In summary, our data indicate that deletion of Ihh results in the disappearance of the muscularis mucosae and fewer ISEMFs surrounding the intestinal and colonic crypt base, disrupting the composition of the ISC niche.

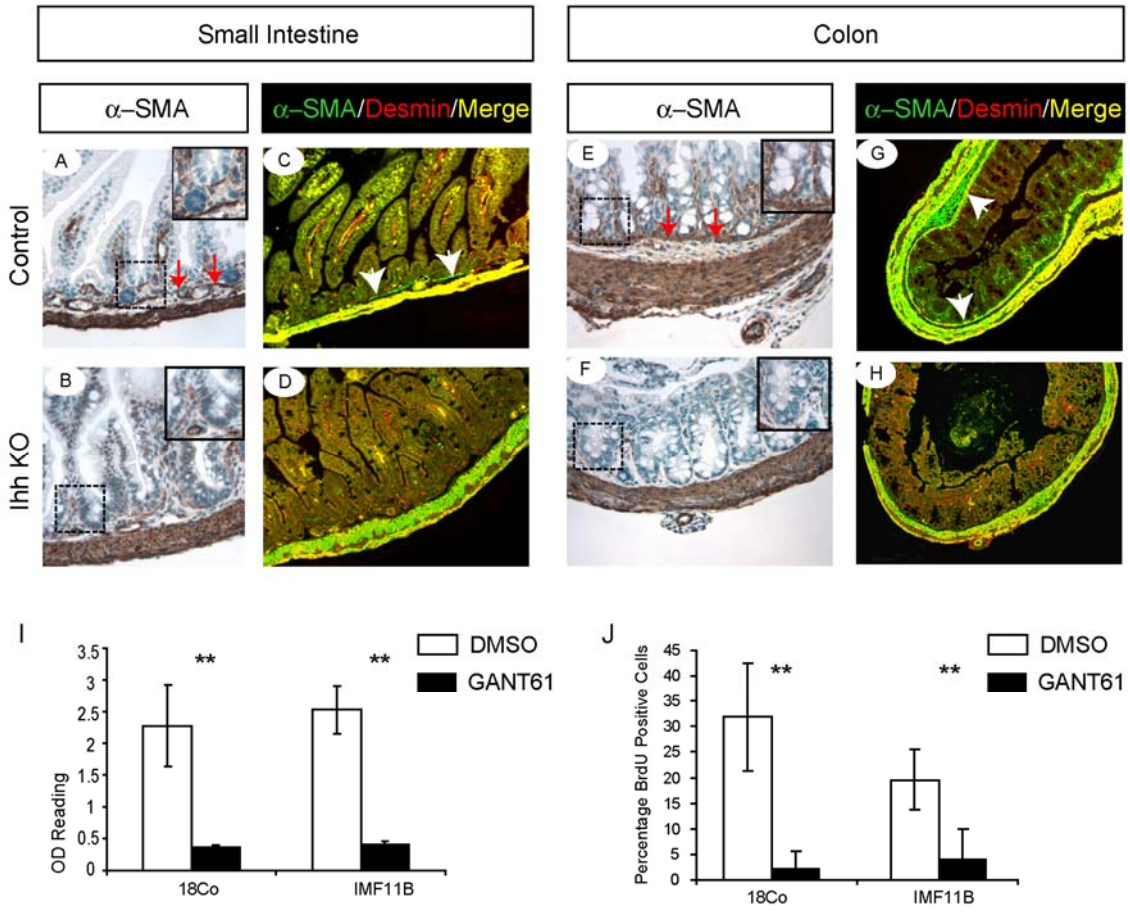

Figure 2. Loss of ISC Niche Cells in *Villin-Cre;Ihh$^{flox/flox}$* Mice. (A, B, E and F): Immunostaining of stromal marker α-SMA (brown) in small intestine (A-B) and colon (E-F) in control (A and E) and mutant mice (B and F). In control, the muscularis mucosae (A and E, arrows) is located subjacent to crypts in the small intestine and colon, whereas in the mutant mice (B and F) no muscularis mucosae is evident. Pericryptic myofibroblasts are shown in detail in small intestine (A, B, inset) and colon (E, F, inset); (C, D, G and H): Double immunofluorescent staining of α-SMA (green) and desmin (red) to distinguish ISEMFs and SMCs in the small intestine (C and D) and colon (G and H) in control (C and G) and mutant mice (D and H). The muscularis mucosae in the small intestine (white arrows) predominantly expresses α-SMA (green), revealing the composition of this layer is mainly ISEMFs. In the colon, the muscularis mucosae expresses both α-SMA and desmin (G, white arrows), indicating the composition of this layer is mainly SMCs. See Figure S2 for individual color channels; (I-J) Inhibition of Hh signaling by GANT61 inhibits ISEMF cell proliferation. (I) Decreased cell growth of ISEMF cell lines (18Co and IMF11B) after GANT61 treatment as determined by the WST-1 assay; (J) Decreased cell proliferation of ISEMFs following GANT61 treatment as detected by BrdU labeling; **, $P < 0.001$.

The diminished ISEMFs observed in *Villin-Cre;Ihh*$^{flox/flox}$ mice suggested that Ihh loss might impair ISEMF proliferation. To test this hypothesis, we examined cell growth in the presence of GANT61, a small-molecule antagonist of GLI1-mediated transcription (25). The cell viability of two human ISEMF primary isolates (18Co and IMF11B) after GANT61 treatment was significantly decreased, suggesting Hh signaling is critical for ISEMF expansion (Figure 2I). Additionally, BrdU labeling provided evidence that loss of Hh impedes ISEMF proliferation (Figure 2J). Analysis of activated caspase 3/7 to measure for apoptosis revealed no differences between DMSO-treated ISEMFs and GANT61-treated ISEMFs (data not shown). Thus, these *in vitro* results provide additional support that reduced levels of Hh signals suppress ISEMF proliferation.

Morphological Alterations in the Intestine of *Villin-Cre;Ihh*$^{flox/flox}$ Mice

As we detected marked differences in the structure of the ISC niche between control and mutant mice, we sought to determine whether these differences were accompanied by changes in the intestinal epithelium. Histological examination revealed striking contrasts between the small intestines of *Villin-Cre;Ihh*$^{flox/flox}$ mice and their control littermates (Figure 3A-3C). Elimination of Ihh resulted in crypts that appeared wider, loosely organized, and crowded with nuclei. Additionally, the mutant mice displayed distorted villus architecture in which villi appear dilated with an expanded intravillus stroma (Figure 3C). Villus branching accompanied by aberrant crypt-like structures was also detected in the small intestine of *Villin-Cre;Ihh*$^{flox/flox}$ mice (Figure 3B). The ectopic crypts contained cells that were positive for the proliferation marker Ki67 (Figure 3E). Furthermore, proliferating cells in the mutant mice greatly outnumbered those in control

littermates with their distribution extending beyond the normal confines of the crypt (Figure 3D-3F). A similar crypt phenotype was noted in the colon of *Villin-Cre;Ihh*$^{flox/flox}$ mice in which crypts were dilated with frequent branching and had disturbed orientation and a high degree of proliferation (Figure S3). Thus, in the absence of Ihh the normal patterning of intestinal epithelial cell proliferation is disrupted, resulting in the intercalation of proliferative cells among differentiated villus cells in the small intestine and differentiated cells at the top of colonic crypts.

Interestingly, older mice (P19-P30) that we analyzed revealed epithelial and morphological changes that are consistent with the initial stages of small intestinal and colorectal cancer. Crypt fission is a process in which new crypts are produced and is believed to occur in response to stem cells doubling in number. Elevated rates of crypt fission indicate high proliferative activity and are associated with higher risks of colon cancer. While crypt fission normally occurs in neonatal mice, we observed a much higher incidence of crypt fission in *Villin-Cre;Ihh*$^{flox/flox}$ colons compared to control, revealing major proliferation abnormalities (Figure S3). In P30 *Villin-Cre;Ihh*$^{flox/flox}$ jejunum, we observed marked elongation of crypts with florid proliferation (Figure 3G). Additionally, in some areas, we saw a loss of epithelial maturation, characterized by the absence of villus architecture and proliferative crypt cells reaching the luminal surface (Figure 3G). This was accompanied by the onset of dysplastic changes, giving the morphological appearance of an early tubular adenoma (Figure 3H). In P30 *Villin-Cre;Ihh*$^{flox/flox}$ colon, a small adenoma with mild dysplasia was detected in the midst of disorganized and disoriented crypts (Figure 3I and 3J). These observations suggest that loss of Ihh

expression induces florid proliferative events that promote neoplastic transformation in the small intestine and colon.

It is known that a small amount of mosaic Cre expression exists in the colon of Villin-Cre transgenic mice. In cases in which *Villin-Cre;Ihh*$^{flox/flox}$ mice survived beyond P15, we noticed normal crypt structures adjacent to dilated crypts in the colon (Figure 3K). Interestingly, beneath the normal crypt structures α-SMA staining detected an intact muscularis mucosae, whereas below neighboring dilated crypts, no α-SMA staining was detected, revealing an absence of muscularis mucosae (Figure 3L). Futhermore, Ki67 positive cells were restricted to crypt bottoms in regions where the muscularis mucosae was present; however, in the absence of the muscularis mucosae, differentiated cells occupied crypt bottoms and proliferative cells were found at crypt bottoms and tops (Figure 3M). These results suggest the muscularis mucosae influences crypt epithelial fate and it is a key component of the ISC niche.

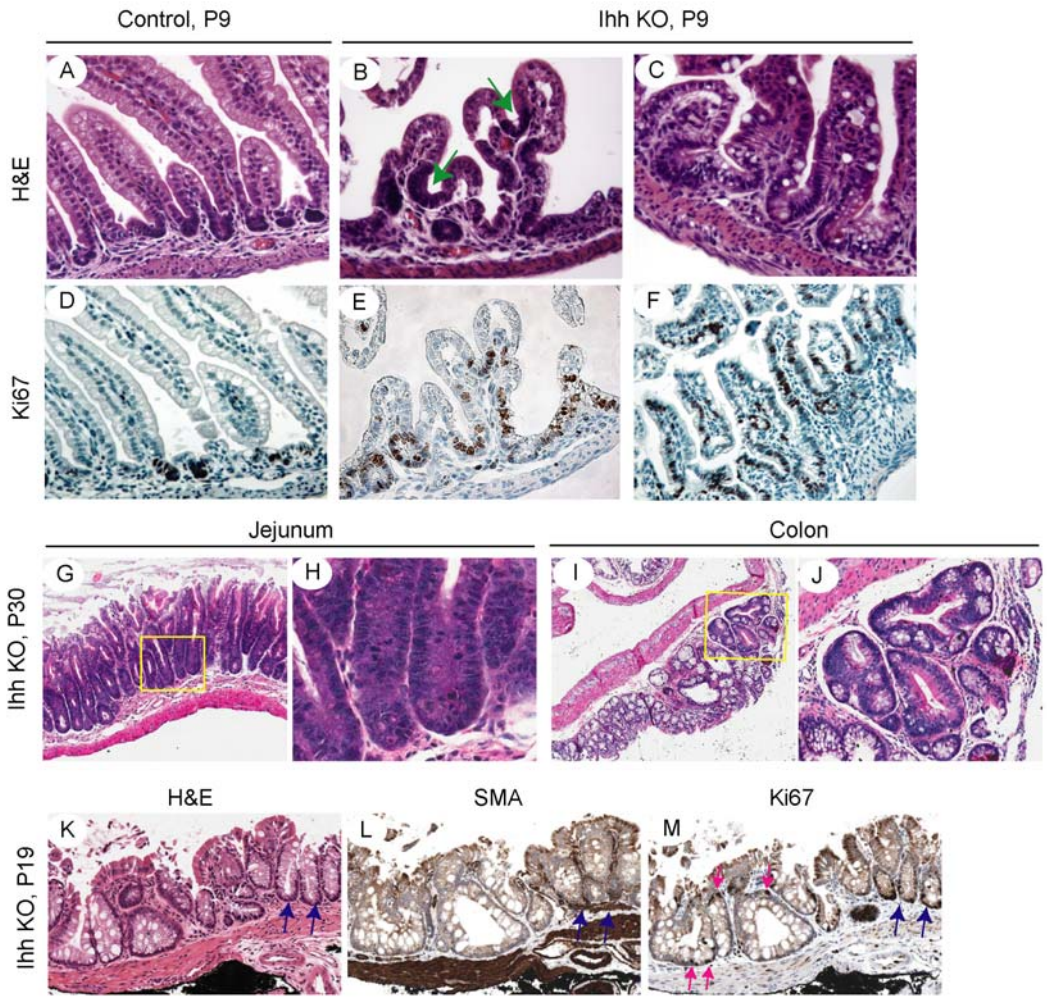

Figure 3. Abnormal intestinal epithelial phenotypes in *Villin-Cre;Ihh*$^{flox/flox}$ mice. (A-C): H&E staining of small intestine tissues from control (A) and *Villin-Cre;Ihh*$^{flox/flox}$ mice (B and C). Note the sprouting villi and ectopic crypt formation in *Villin-Cre;Ihh*$^{flox/flox}$ mice (arrows) in (B). In addition, dilated crypts are frequently observed in these mutant mice (C); (D-F): Ki67 staining showing cell proliferation is restricted to the intervillus base in control (D). In *Villin-Cre;Ihh*$^{flox/flox}$ mice, there is an expansion of Ki67 positive cells (E, F) and the ectopic crypts show high levels of Ki67 staining (E); (G) H&E staining of jejunum from P30 *Villin-Cre;Ihh*$^{flox/flox}$ mice shows early adenomatous foci with marked elongation of crypts and a loss of differentiation towards the surface; (H) High power view of the crypt base lesion shows dysplastic changes and frequent mitosis. (I) In the P30 *Villin-Cre;Ihh*$^{flox/flox}$ mice colon, accumulation of dilated and disoriented crypts leads to a localized elevated lesion in the mucosa, with evolution into a tubular adenoma with mild dysplasia (J); (K-M) Relationship between dilated crypts in colon of *Villin-Cre;Ihh*$^{flox/flox}$ mice and loss of muscularis mucosae cells subjacent to crypts. Blue arrows indicate areas with normal crypt morphology (K) above muscularis mucosae cells (L). Typical Ki67 staining pattern is observed in morphologically normal crypts (blue arrows) while Ki67 is expressed at both bottoms and tops of dilated crypts (red arrows) (M).

Loss of Intestinal Epithelial Ihh Signaling Activates Wnt/β-catenin and Expands the ISC Population

Given that we observed several manifestations in the *Villin-Cre;Ihh*$^{flox/flox}$ mice that were comparable to those seen in mice with increased Wnt signaling, including enhanced epithelial cell proliferation, branched villi, and enlarged crypts, we sought to analyze whether mutant mice displayed increased Wnt activity (26, 27). Typically, the expression of Wnt/β-catenin target genes (e.g., Cd44, Sox9, EphB2) is restricted to the crypt proliferative compartment (Figure 4A and 4B; Figure S4A and S4C). However, in mutant mice Cd44, Sox9, and EphB2 expression was highly expressed throughout the crypt and along the villus in the small intestine as well as along the entire crypt length in the colon (Figure 4C and 4D; Figure S4B and S4D). Furthermore, staining for β-catenin in mutant mice showed increased intensity of staining in crypts extending up the villi, with presence of cytoplasmic and some nuclear staining, providing additional evidence that the mutant mice have increased Wnt activity (Figure S4E and S4F).

We next addressed whether the loss of Ihh affected the ISC population by performing *in situ* hybridization for *Olfm4*, a marker for small intestinal stem cells (6). *Villin-Cre;Ihh*$^{flox/flox}$ mice showed an increase in expression of *Olfm4* as well as an increase in the number of *Olfm4*+ cells per crypt compared to control mice (Figure 4E and 4F). A previous study of *Ihh*$^{-/-}$ mice suggested that a complete loss of Ihh diminishes the number of ISCs; however, this study lacked a definitive ISC marker and based its findings solely on a cell proliferation marker (19). Thus, by utilizing a specific ISC marker, we provide compelling evidence that deactivation of Ihh leads to an increase in ISCs.

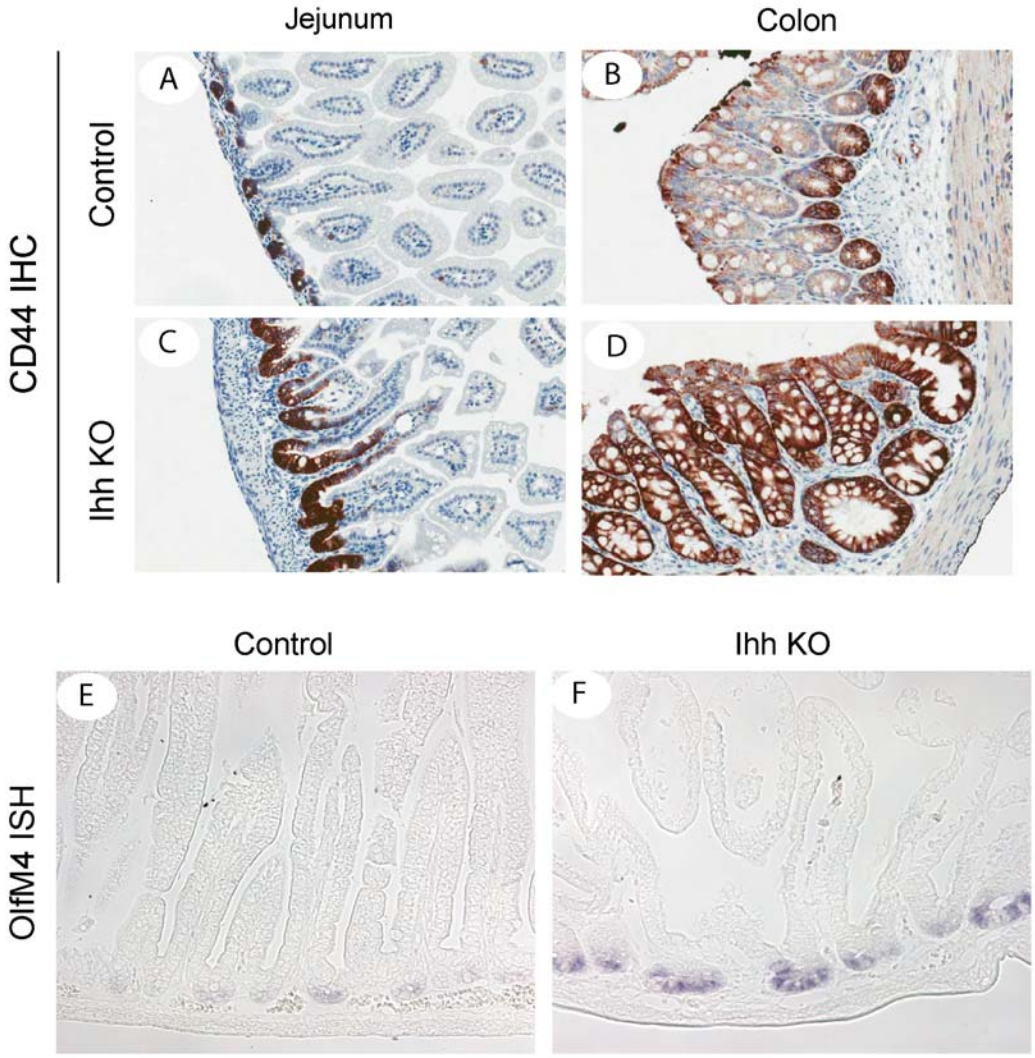

Figure 4. Increased Wnt/β-catenin activity and intestinal stem cell expansion in *Villin-Cre;Ihh*$^{flox/flox}$ mice. (A-D) Immunostaining of Wnt target gene CD44 in control jejunum (A) and colon (B) and mutant jejunum (C) and colon (D); (E-F) In situ hybridization of the small intestine for *Olfm4* in control (G) and mutant mice (H). The expression pattern of *Olfm4* reveals an increase in intestinal stem cell number and expression level in mutant mice (H), relative to control (G).

Altered Differentiation of the Absorptive and Secretory Cell Lineages in *Villin-Cre;Ihh*$^{flox/flox}$ Mice

Villin-Cre;Ihh$^{flox/flox}$ mice display a strong increase in epithelial proliferation, suggesting these mice fail to properly regulate proliferation and/or differentiation. To determine

whether the expansion of epithelial proliferation occurred to the detriment of intestinal epithelial differentiation, we examined the differentiation pattern of the 4 different intestinal cell types (enterocytes, goblet, enteroendocrine, and Paneth cells) in *Villin-Cre;Ihh*$^{flox/flox}$ mice. In the small intestine of mutant mice, histological examination revealed a failure of enterocyte maturation as manifested by vacuolated epithelial cells lining the villus (Figure S5A and S5B). The morphology of these vacuolated cells are consistent with those previously described as enterocyte precursors (28) and reminiscent of the phenotype described in mice injected with an anti-Hh antibody that show poor lipid transport (29). Immunostaining results showed that vast regions along the villi were absent for the absorptive enterocyte marker fatty acid binding protein (Fabp) (Figure 5A and 5B). Immunostaining of serial sections demonstrated that Ki67 is expressed by Fabp-negative villus epithelial cells, indicating deletion of Ihh leads to a loss of polarity in which proliferating cells are no longer restricted to the crypt but are infiltrating the differentiation compartment (Figure 5C). Furthermore, villin staining in the mutant mice revealed discontinuous and sporadic expression of the brush border protein (Figures 5D and 5E). Electron microscopy studies showed that microvilli were less dense in mutant mice compared to control mice (Figure S6A and S6B). In contrast to the enterocyte lineage, we observed an increase in all small intestinal secretory lineage cells, including Paneth, goblet and enterendocrine cells in *Villin-Cre;Ihh*$^{flox/flox}$ mice (Figure 5F-5K). Similar arrest in enterocyte differentiation was also seen in colon samples of *Villin-Cre;Ihh*$^{flox/flox}$ mice, resulting in vacuolated cells that line the top and surface of the colonic mucosa (Figure S5C and S5D). Immature microvilli resembling those found in undifferentiated crypt cells were also detected near the top of colonic crypts in the mutant

mice (Figure S6C and S6D). Additionally, there was a marked increase in goblet cell differentiation, especially at crypt bases (data not shown). Altogether, our studies suggest an expansion of the secretory cell lineages at the expense of the enterocyte differentiation program in *Villin-Cre;Ihh*$^{flox/flox}$ mice.

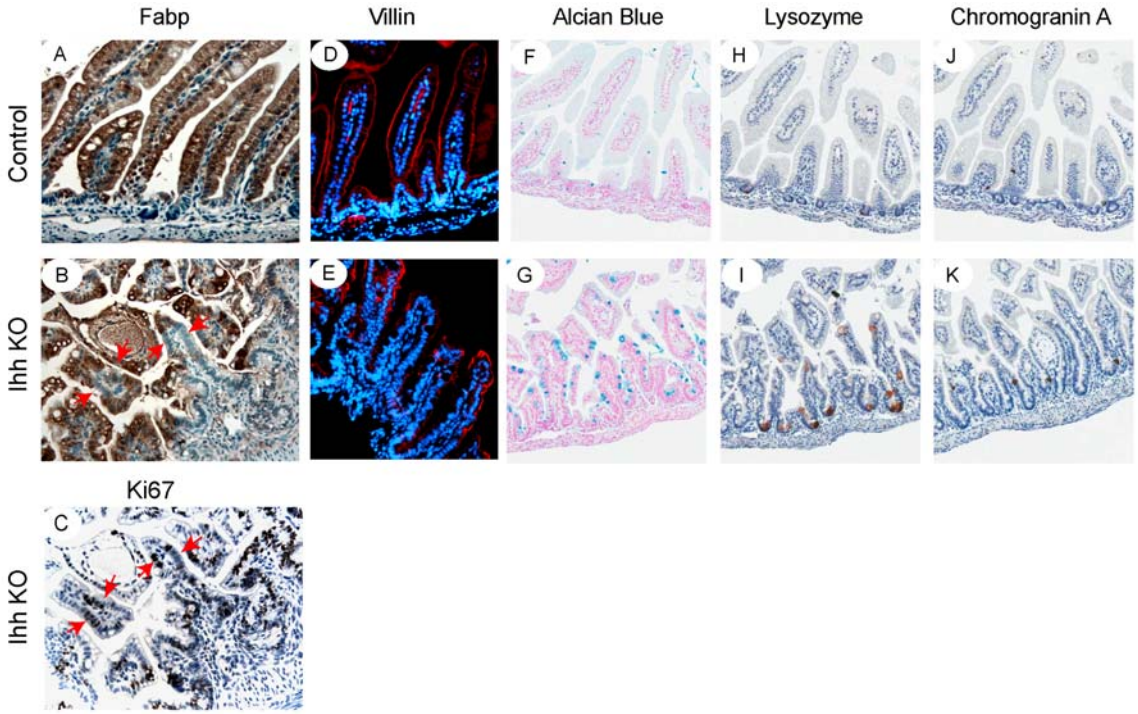

Figure 5. Abnormal Intestinal Epithelial Cell Differentiation in *Villin-Cre;Ihh*$^{flox/flox}$ Mice. (A-B) Immunostaining of enterocyte marker Fabp in control (A) and *Villin-Cre;Ihh*$^{flox/flox}$ mice (B). Fabp staining is missing from some regions along the villus epithelium in mutant mice (red arrows); (C) Ki67 staining of a consecutive section to (B) shows that the regions lacking Fabp staining are positive for Ki67 (red arrows); (D-E) Immunofluorescent staining of enterocyte brush border marker villin in control (D) and *Villin-Cre;Ihh*$^{flox/flox}$ mice (E). Again, various regions with missing villin staining can be seen in the mutant mice; (F-G): Increased goblet cells detected by Alcian blue staining in *Villin-Cre;Ihh*$^{flox/flox}$ mice; (H) In P9 control mice, lysozyme staining for Paneth cells is barely detectable in crypts since Paneth cells typically do not physically mature until P14. (I) In P9 *Villin-Cre;Ihh*$^{flox/flox}$ mice, prominent lysozyme staining is seen at crypt bases, indicating the Paneth cell differentiation program occurs sooner and is stronger; (J-K) Chromogranin A staining reveals more enterochromaffin cells in *Villin-Cre;Ihh*$^{flox/flox}$ intestine (K) compared to control (J).

Paracrine Ihh Signaling Responsible for *Villin-Cre;Ihh*$^{flox/flox}$ Phenotype

While some studies suggest Hh signals in an autocrine direction, acting directly on intestinal epithelial cells (30, 31), more recent reports support the idea that Hh signals predominantly in a paracrine fashion in the intestine (20, 32). To exclude the possibility that the phenotypes we observed in conditional *Ihh* knockout mice were due to autocrine Hh signaling, we deleted the required hedgehog receptor *Smoothened* (*Smo*) in intestinal epithelial cells by crossing *Villin-Cre* mice with *Smo*$^{flox/flox}$ mice to generate *Villin-Cre;Smo*$^{flox/flox}$ mice. We found that *Villin-Cre;Smo*$^{flox/flox}$ mice were born at the expected Mendelian frequency. Unlike *Villin-Cre;Ihh*$^{flox/flox}$ mice, these *Villin-Cre;Smo*$^{flox/flox}$ mice were healthy with no gross abnormalities up to 15 months of age. Microscopic examination revealed normal intestinal and colonic architecture (Figure 6A). All four epithelial cell lineages were well developed, and normal Wnt signaling was observed (Figure 6B). The results provide strong evidence that autocrine Hh signaling is not required for intestinal epithelial cell proliferation and differentiation, and Hh signaling functions strictly in a paracrine manner during gut morphogenesis.

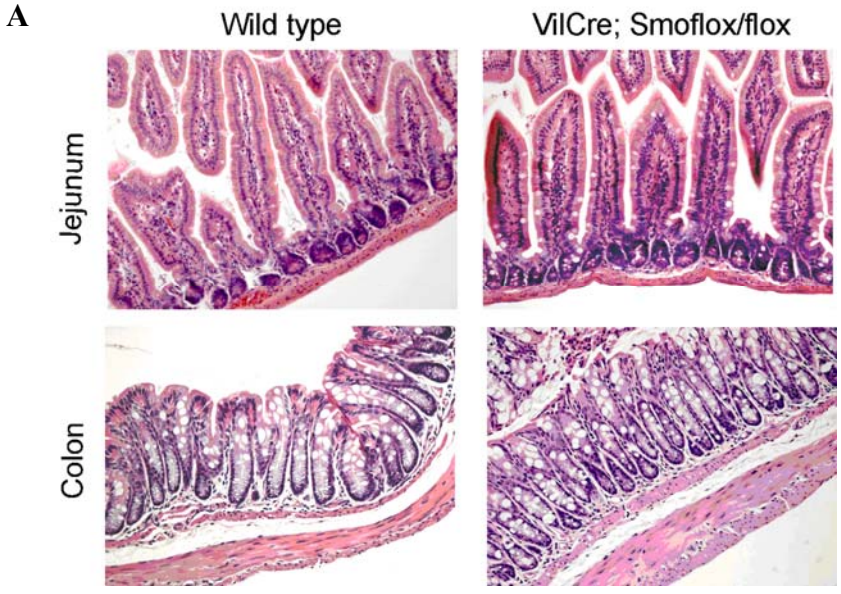

B

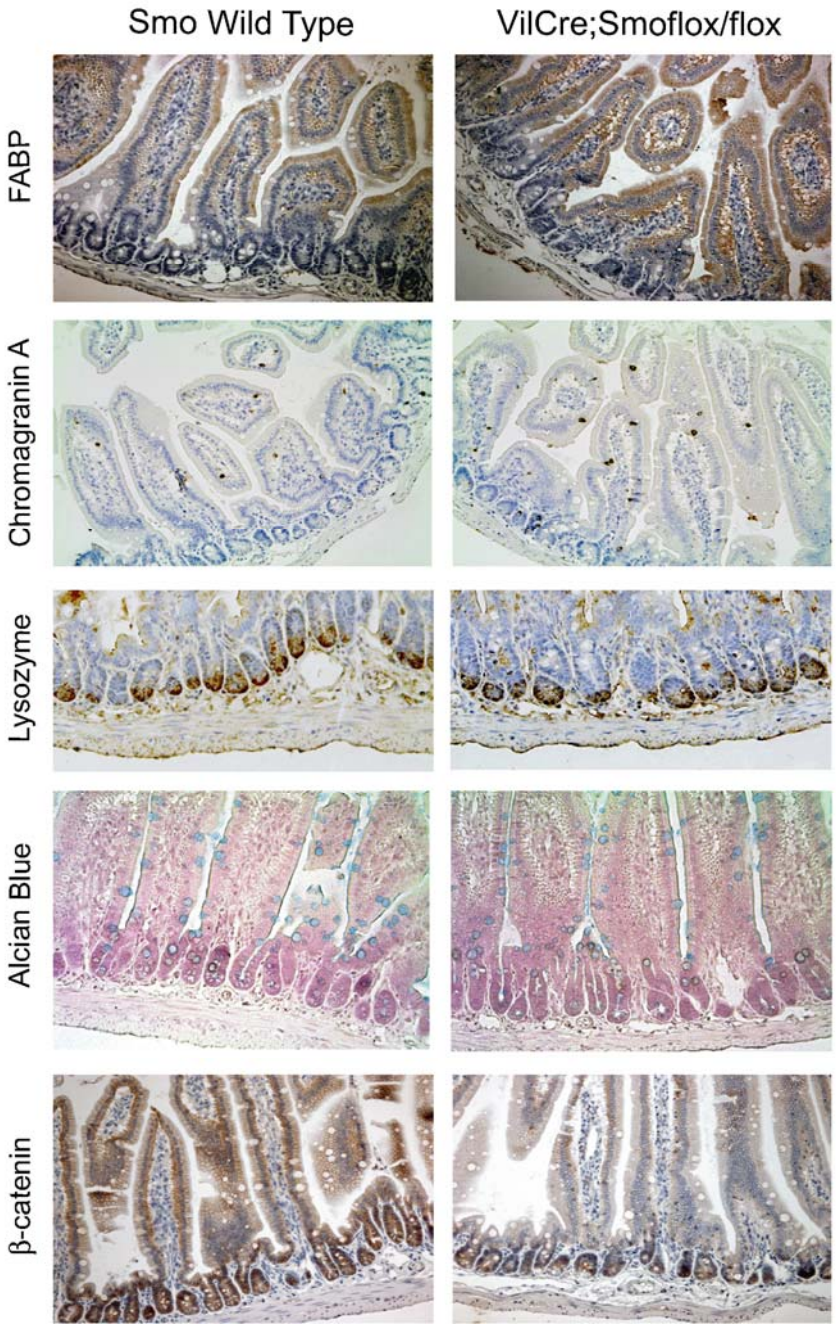

Figure 6. Normal Intestinal Development in Conditional *Smo* KO Mice. (A) H&E staining showing normal small intestine and colon morphology in *VilCre;Smo*$^{flox/flox}$ mice. (B) Normal epithelial cell differentiation and Wnt signaling in *VilCre;Smo*$^{flox/flox}$ mice.

Expression Analysis of Genes Deregulated in *Villin-Cre;Ihh$^{flox/flox}$* Mice

To investigate the molecular mechanisms underlying the disruption of the ISC niche and how it leads to abnormal ISC development, we performed expression array analysis of colon samples from control and *Villin-Cre;Ihh$^{flox/flox}$* mice. Statistical analysis identified 508 transcripts, including 298 named genes up-regulated and 532 transcripts, including 429 named genes down-regulated in *Villin-Cre;Ihh$^{flox/flox}$* mice (Table S1). As expected, all known targets of Hh signaling, such as *Gli1*, *Ptch* and *Hhip*, were significantly down-regulated in colon samples of the mutant mice (Figure 7A).

Among the genes that were up-regulated in mutant mice were Wnt targets, including *c-Myc*, *Sox-9* and *MMP7*, as well as the ISC marker *Lgr5* (Figure 7B). Furthermore, comparison of genes up-regulated in *Villin-Cre;Ihh$^{flox/flox}$* mice with Lgr5 stem cell genes identified several genes that overlap, including *Lgr5*, *Acot1*, *Adora1*, *Sox9*, *Soat1*, and *Slc12a2* (Figure 7B) (5). Genes involved in gut hormones (*CCK* and *glucagon*), reflecting changes in enteroendocrine cells as well as goblet cell marker genes (*Spdef*, *Spink4*, *Muc2*, *Gcnt3*, and *Foxa3*) were up-regulated in *Villin-Cre;Ihh$^{flox/flox}$* mice (Figure 7C), which is consistent with the expansion of secretory lineage cells observed in the mutants. Intriguingly, several MMPs (*MMP3*, *MMP7*, *MMP8* and *MMP10*) which are known to degrade ECM proteins and connective tissues were all up-regulated in mutant colon samples (Figure 7D).

Interestingly, the most prominent genes down-regulated in the mutant mice encode proteins that help support and maintain the ISC niche (Figure 7D and 7E). For example, genes that may provide structural support to ISCs such as genes involved in smooth muscle development (*Myh10*, *Myh11*, *myocardin*, *Mef2c*, and *desmin*, etc.) were

down-regulated in *Ihh* mutant colons (Figure 7E). Furthermore, genes encoding ECM proteins (multiple isoforms of *collagen*, and *laminin*; as well as *fibronectin, osteoglycin, versican*, *nidogen 1, Ecm2, etc*) which provide support, organization and mechanical signals to the niche were extensively down-regulated in *Villin-Cre;Ihh*$^{flox/flox}$ mice (Figure 7D). Additionally, several integrins (*Itga1*, *Itga8*, *Itga9*, *Itgav*, *Itgb6*) which attach epithelial cells to the ECM and mediate epithelial cell-matrix interactions were also down-regulated in mutant mice (Figure 7D). Overall, the expression analysis demonstrates that mesenchymal ISC niche components are compromised when Ihh is deleted in the intestine, supporting the hypothesis that disruption of the mesenchymal ISC niche may be the key mechanism that leads to abnormal epithelial cell development in *Villin-Cre;Ihh*$^{flox/flox}$ mice.

We next analyzed the signaling pathways that have been implicated in gut development including, Notch, BMP and Ras/MAPK pathway genes. We found that the BMP pathway was one of the major targets for Ihh signaling during gut morphogenesis (Figure 7F). For example, BMPs including *BMP2*, *BMP4* and *BMP5* were all down-regulated. BMP antagonists showed a more complicated pattern of expression: some were up-regulated, such *Gremlin1* and *Chordin-like-2*, while others were down-regulated, such as *Gremlin2* and *Twsg1*. Nevertheless, analysis of transcriptional targets of BMP signaling, including *ID1*, *ID2*, and *ID4*, revealed that all these genes were down-regulated in the mutant mice, suggesting an overall decrease in BMP signaling in conditional *Ihh* knockout mice.

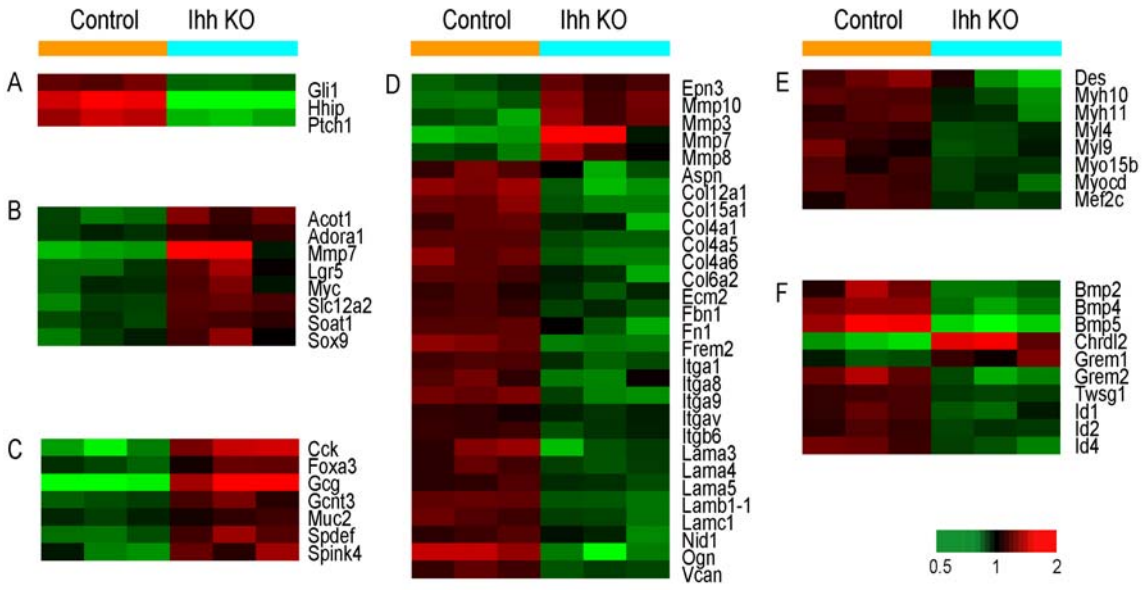

Figure 7. Genes differentially expressed in colon tissues from control and *Villin-Cre;Ihh*$^{flox/flox}$ mice. Heat maps of genes which are differentially expressed in control and *Ihh* KO mice are displayed by functional categories: (A): Hh target genes; (B) Wnt target and ISC-related genes; (C) Globet cell and enteroendocrine-related genes; (D) ECM-related genes; (E) Muscle-related genes; (F) BMP signaling pathway genes.

Inactivation of Ihh Disrupts Stromal Compartment

Given that the gene expression profiling data suggested that the smooth muscle character and ECM of the niche undergo marked changes in *Villin-Cre;Ihh*$^{flox/flox}$ mice, we decided to investigate how the loss of Hh signaling directly affects expression of muscle and ECM-related genes in ISEMFs. Quantitative RT-PCR performed on ISEMFs treated with the Gli transcription inhibitor GANT61 found a significant down-regulation of *Mef2c* and *Myocd*, two transcription factors known to regulate smooth muscle development (Figure 8A). These results are consistent with the microarray analysis, suggesting cultured ISEMFs closely resemble the *in vivo* situation. Furthermore, these findings imply that Hh signals may promote the differentiation of fibroblasts towards a myofibroblast phenotype in the intestine. We next examined the ability of ISEMFs to produce matrix proteins in

the absence of Hh signals. Expression of *laminin4* was significantly down-regulated in GANT61 treated ISEMFs (Figure 8A), while other ECM genes such as *fibronectin* and *collagen* showed no significant change (data not shown). Strikingly, MMPs, including *MMP-3* and *MMP-10* were significantly up-regulated by 3.3 and 14-fold, respectively, in GANT61 treated ISEMFs (Figure 8A). These data suggest that loss of Hh signaling amplifies the expression of MMPs in intestinal stromal cells, potentially leading to the degradation of ECM components.

The finding that MMPs are strongly up-regulated while ECM genes are down-regulated in the absence of Ihh suggested that ECM components may be significantly compromised in *Villin-Cre;Ihh*$^{flox/flox}$ mice. In normal colon, collagen IV expression was detected throughout the lamina propria. In mutant mice, collagen IV staining was significantly reduced in the colon (Figure 8B). Another basement membrane protein, laminin, was expressed in the lamina propria with intense staining at the epithelial-mesenchymal interface corresponding to the basement membrane in control colon. In contrast, laminin staining appeared diffusely weak and completely absent from the basement membrane in the mutant mice (Figure 8B). Thus, inactivation of Ihh in the gut leads to the down-regulation of ECM genes and matrix protein degradation, resulting in a weaker ECM that is vulnerable to crypt expansion.

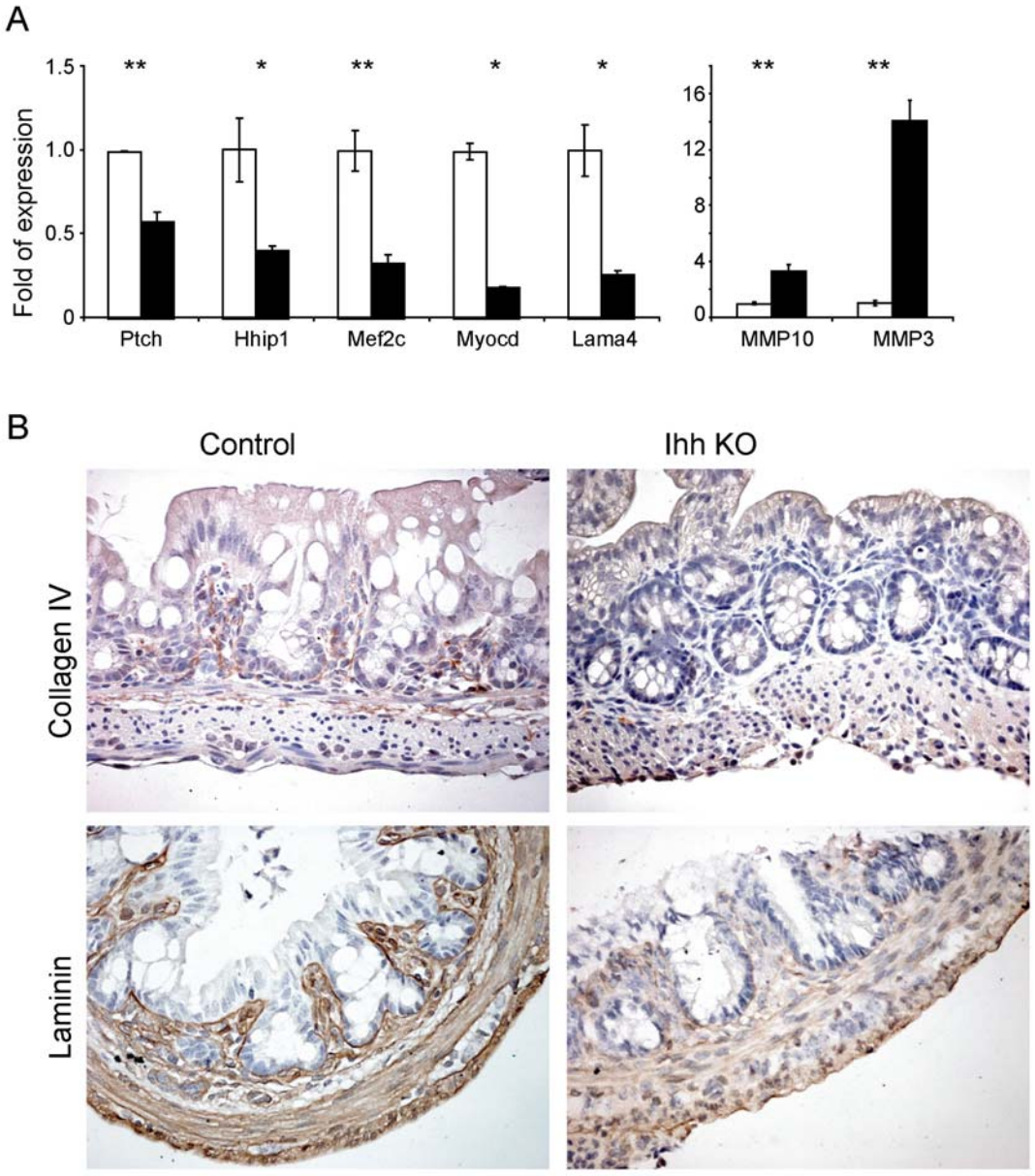

Figure 8. Disruption of Stromal Compartment upon Ihh Loss. (A) Quantitative RT-PCR analysis of *Ptch1*, *Hhip*, *Mef2c*, *Myocd*, *Lama4*, *MMP10* and *MMP3* expression in 18Co cells after GANT61 treatment. *, $P < 0.05$; **, $P < 0.01$. (B) Extracellular matrix molecules collagen IV and laminin are expressed in the stromal cells and basement membrane of the crypt in control colon. In *Ihh* mutant mice, there is decreased expression of both collagen IV and laminin.

Discussion

Hh signaling is one of the key pathways that are required for proper gut morphogenesis. Initial analysis suggested that Hh functions in an autocrine fashion and regulates Paneth cell differentiation and colonic epithelial cell growth (30, 31). However, several recent studies support that Hh signaling, in most cases, including during intestinal development, functions in a paracrine manner by directly regulating surrounding stromal cells (20, 32). In this study, we showed that depletion of Ihh in gut epithelial cells leads to disruption of the ISC niche, which subsequently leads to deregulated ISC self-renewal and abnormal epithelial cell differentiation. As a control, deletion of the required Hh signaling receptor Smo in gut epithelial cells caused no morphological phenotypes. These results provide, for the first time, functional evidence that Hh signaling is strictly paracrine during intestinal morphogenesis.

Pericryptic ISEMF cells are believed to be the key ISC niche cells. On the other hand, cells within the muscularis mucosae layer, despite its vicinity to the ISCs, are not known to be involved in ISC niche maintenance. In fact, muscularis mucosae cells are so poorly studied that little evidence exists describing its precise functional role, although some reports suggest that cells within the muscularis mucosae may participate in regulating gut motility (33). In our current study, we find that muscularis mucosae cells within the mouse small intestine are predominantly myofibroblast cells, as those cells were α-SMA positive and desmin negative. In contrast, SMCs are the major component in the mouse colon muscularis mucosae layer. We found the development of muscularis mucosae cells are strictly dependent on epithelial Ihh signaling, as deletion of Ihh leads to total ablation of the muscularis mucosae both in the colon and the small intestine. Our

studies suggest that loss of the muscularis mucosae layer may contribute to ISC expansion and deregulation of intestinal epithelial cell differentiation. These results provide, for the first time, genetic evidence of a possible functional role for the muscularis mucosae as an important component of the ISC niche and demonstrate that the muscularis mucosae together with pericryptic myofibroblasts regulate ISC self-renewal and differentiation.

The epithelial phenotypes we observed in the conditional *Ihh* knockout mice are overall consistent with other mouse models that disrupt Hh signaling during gut morphogenesis, such as mice overexpressing the Hh inhibitor Hhip, or mice with a conditional deletion of Ptch1 (22, 23). However, none of these studies addressed the critical question of whether paracrine Hh signaling affects ISC self-renewal or whether the epithelial phenotypes are due to the disruption of trans-amplifying/progenitor cells near the crypt base. Our study showed that in conditional *Ihh* knockout mice, there is a clear expansion of the ISC compartment, demonstrating that Hh regulates ISC cell fate by modulating its niche. In addition, previous studies have suggested that the mesenchymal ISC niche is a source of Wnt and functions primarily to maintain ISC proliferation. Here, we discover another dimension of niche function, which is to restrict crypt size and prevent abnormal stimulation. Thus, a delicate balance between the proliferative and restrictive activity by the ISC niche likely exists to refine the shape, size and function of the gut epithelium to form proper crypt-villus structures. Our analysis of ISCs is based on the quick-cycling $Lgr5^{+}$ ISC population located at the crypt base. Further studies will be necessary to determine if there are any changes in $Bmi\text{-}1^{+}$ stem cells at the +4 position upon intestinal deletion of Ihh. The descending gradient of Bmi-1-expressing cells from

the proximal to distal end of the small intestine, however, opposes the ascending gradient of Ihh expression as well as the degree of phenotypic changes observed in the *Ihh* mutants. Thus, it is possible that Bmi-1^{+} stem cells may not be affected by Ihh loss in the intestine.

As mentioned above, we noticed the severity of morphological changes that occurred in *Ihh* conditional knockout mice followed a gradient along the proximal to distal axis of the gut, with the mildest phenotypes in the duodenum, and the more severe phenotypes occurring distally in regions of the colon. The morphological changes we observed affected both stromal and epithelial cells. For example, we found that deletion of Ihh consistently reduced the number of pericryptal myofibroblasts in the colon, whereas in the small intestine, pericryptal myofibroblasts were typically maintained. However, myofibroblasts in the region between pericryptal myofibroblasts and the muscularis mucosae were generally decreased, although somewhat variable. The more pronounced phenotypes in the colon may reflect recent findings that show there is decreased Shh levels in the colon compared to the small intestine (20). In other words, little to no Hh is available to maintain myofibroblasts in the colon when Ihh is deleted, while the small intestine still has some crypt Shh which may contribute to myofibroblast proliferation and less severe phenotypes. Clearly, further studies are needed to address the contribution of Shh signaling in regulating the ISC niche.

What are the molecular mechanisms behind the expansion of the ISC compartment upon Ihh loss during gut morphogenesis? Our analyses indicate that Ihh likely regulates ISC self-renewal and cell fate determination via multiple mechanisms. Consistent with previous reports (34, 35), we find Ihh is a key regulator of BMP

signaling in gut mesenchymal cells. Our studies showed that loss of Ihh leads to the deregulation of multiple BMPs and BMP antagonists, with the overall consequence of reduced BMP signaling in the gut. The reduction of BMP signaling in the ISC niche upon Ihh deletion could constitute one possible mechanism that leads to the described phenotype, as BMP signaling normally acts to inhibit ISC self-renewal and repress crypt formation in the gut, while reduced BMP signaling causes an expansion of intestinal stem/progenitor cells and ectopic crypt formation (14, 36).

Nevertheless, the reduced BMP signaling does not account for all the phenotypes observed in conditional *Ihh* knockout mice. For example, in *villin-noggin* mice in which BMP signaling is completely abrogated, no morphological alternations are detected till 4 weeks of age (36). Other factors that likely contribute to the severe phenotypes seen in mutant mice are the complete loss of muscularis mucosae cells and the disruption of the ECM that surrounds ISCs. One can image muscularis mucosae cells likely provide solid structural support for ISCs at the crypt base. It is also likely that muscularis mucosae cells secrete additional factors that maintain proper ISC number and crypt structure such as the growth factor *Pdgfc* (Platelet derived growth factor C) and the Wnt antagonist *Sfrp2* (Secreted frizzled-related protein 2), two down-regulated genes identified by microarray analysis in conditional *Ihh* knockout mice. In addition, via our expression array analysis, we found profound loss of ECM gene expression in conditional *Ihh* knockout mice at RNA levels. The ECM components were further impaired by the up-regulation of MMPs, the major enzymes that degrade ECM proteins. Altogether, these niche changes provide a pro-growth microenvironment for ISCs, promoting ISC expansion and subsequent expansion of the transit amplifying compartment. These findings imply a very interesting

possibility that Ihh deletion, resulting in the loss of structural ECM integrity and the loss of the muscularis mucosae may precede colon cancer invasion and metastasis. In line with this hypothesis, recent data show that the Hh signaling components Gli1, Gli2, and Ptch are expressed in benign human colonic tissue samples, but are significantly reduced or lost in malignant colonic samples (37). Taken together, we show that paracrine signaling of Ihh is essential for muscularis mucosae perpetuation. Its loss leads to a severe disruption of the ISC niche architecture and the subsequent down-regulation of BMP signaling causes the observed phenotype of stem cell compartment expansion, uncontrolled proliferation and inhibition of differentiation, cumulating in neoplastic transformation.

Experimental Procedures

Mice

The *Ihh*$^{flox/flox}$ mice were kindly provided to us by Dr. Beate Lanske of Harvard University (38). *Villin-Cre* mice (24) and *Smo*$^{flox/flox}$ mice (39) were obtained from the Jackson Laboratory. *Ihh*$^{flox/flox}$ and *Villin-Cre* mice were mated and the offspring were backcrossed to generate *Villin-Cre;Ihh*$^{flox/flox}$ mice. Genotyping was performed by polymerase chain reaction on genomic DNA from tail clips as previously described (24, 38). The *Villin-Cre:Ihh*$^{flox/flox}$ pups suffer early lethality and were sacrificed when they displayed lethargy and inability to feed. All mice were housed, fed, and treated in accordance with protocols approved by the committee for animal research at the University of California, San Francisco.

Histology, Immunohistochemistry, Immunoflorescence and *in Situ* Hybridization

Animals were euthanized and their intestine was removed and flushed with PBS. Samples collected from the intestine were either immediately frozen for RNA extraction or fixed overnight in 4% paraformaldehyde. Fixed tissue samples were embedded in paraffin. Five micron sections were placed on slides, deparaffinized, rehydrated and stained with hematoxylin and eosin to observe cell morphology. Antigen retrieval was performed for immunostaining by microwaving the slides for 10 minutes in 10mM sodium citrate buffer (pH 6.0) followed by a 20 minute cooling period at room temperature. Immunohistochemistry staining was conducted using the ABC kit (Vector Laboratories, Burlingame, CA) as previously described (15). For immunofluorescene staining, slides were subsequently blocked in 3% normal goat serum and incubated with the primary antibody. Goat anti-mouse conjugated to Alexa 568, goat anti-mouse conjugated to FITC and goat anti-rabbit conjugated to Alexa 594 were used as secondary antibodies at a dilution of 1:500 (Invitrogen). The slides were mounted with Vectashield mounting medium containing DAPI (Vector Laboratories). Images were acquired using the Olympus BX51 fluorescence microscope. For double immunofluorescence staining the two primary antibody procedures were performed separately in succession. Primary antibodies and their dilutions were as follows: mouse anti-β-catenin, 1:200 (BD Bioscience); goat anti-Ihh, 1:400 (Santa Cruz Biotechnology); rabbit anti-Ki67, 1:150 (SP4); rabbit anti-desmin, 1:80; rabbit anti-chromogranin A, 1:400 (Lab vision); mouse anti-villin, 1:100 (Immunotech); mouse anti-SMA, 1:50 (DAKO); rabbit anti-Sox9, 1:200 (Millipore); rabbit anti-Fabp, 1:50 (Novus Biologicals); rat anti-CD44v6, 1:800 (Bender MedSystems); rabbit anti-collagen IV, 1:100 (Millipore); rabbit anti-lamanin, 1:100

(NeoMarkers). For Alcian Blue staining, rehydrated paraffin sections were stained for 30 minutes at room temperature in 1% Alcian Blue solution, pH2.5 (Newcommer Supply). Slides were then washed in water, and counterstained with nuclear fast red. Olfm4 in situ hybridization was performed as previously described (6).

Electron Microscopy

Intesinal tissue was thinly sliced (2-3mm thick) and placed in Karnovsky's fixative: 0.8% paraformaldehyde, 2.8 % glutaraldehyde in 0.1M Sodium cacodylate buffer pH 7.4 at room temperature for 2-4 hours before storing at 4°C. Fixed tissue was then rinsed in water, post-fixed in 2% OsO_4 and stained en bloc with Uranyl acetate before being dehydrated in ethanol, cleared with propylene oxide and embedded in Eponate 12 (Ted Pella Co). Thick sections (1 micron) were cut and stained with Toludine Blue, examined under a light microscope to select the areas for thin sections. Thin sections (`70-90 nm) were cut on a Leica ultracut UCT microtome (Bannock, Il), stained with Uranyl acetate and Reynold's Lead to enhance the contrast and examined under a Phlilips Tecnai 10 electron microscope (Eidhoven, Netherland).

Microarrays and data analysis

Three sets of colon tissues were harvested from *Villin-Cre:Ihh$^{flox/flox}$* pups and their control littermates. Total RNA was isolated using Trizol reagent, and hybridized to Affymetrix Gene 1.0 ST mouse arrays. The raw data are available at Gene Expression Omnibus (GEO, http://www.ncbi.nlm.nih.gov/projects/geo) under the accession no.

GSE18393. Paired Significance Analysis of Microarrays (SAM) (40) was performed to identify genes differentially expressed in control and mutant colon samples.

Cell Culture and treatment

Two primary intestinal ISEMF cell lines were used in the study: 18Co cells were purchased from ATCC, and IMF11B cells were established from histologically normal margins of surgically resected ileal (IMF) tissue using the outgrowth method described (41). The myofibroblast phenotype was verified by immunohistochemistry and flow cytometry as described (42). The primary myofibroblasts were cultured in DMEM that was supplemented with 10% NuSerum, 200 μM L-glutamine penicillin (50 U/ml), and streptomycin (50 μg/ml). GANT61 was purchased from Alexis Biochemicals and dissolved in DMSO to the final concentration of 10mM. The WST-1 assay (Roche) was used to quantify cell grow per manufacturer's instruction. The quantification of apoptosis was performed using the Caspase-Glo 3/7 Assay kit (promega) according the manufacturer's instruction. In both assays, 18Co and IMF11B cells were seated in 96 well plates and treated with DMSO or 10μM GANT61 for 72 hours. For BrdU labeling, cells were cultured on glass slides, treated with DMSO or Gant61 for 48 hours, and incubated with 10μM BrdU for 4 hours. Cells were then fixed in 4% paraformaldehyde, denatured with 2N HCl for 30 minutes at 37^{o}C, and neutralized with 0.1M pH8.5 Boric acid buffer. Cells were incubated with mouse anti-BrdU antibody, 1:200 (Lab Vision). The primary antibody binding was detected with goat anti-mouse antibody conjugated to Alexa 568 (Invitrogen). The slides were mounted with Vectashield mounting medium containing DAPI (Vector Laboratories). Images were acquired using the Olympus BX51

fluorescence microscope. 18Co cells were treated for 48 hours with GANT61 for quantitative RT-PCR studies.

Real-Time Quantitative Reverse-Transcription Polymerase Chain Reaction

Total RNA was extracted from frozen intestinal tissues or cultured ISEMF cells using Trizol (Invitrogen) and digested with DNase I to remove genomic DNA contamination. SYBR green based real-time RT-PCR was carried out as described (15) and rRNA or GAPDH was used as an internal control. The primer pair sequences are available in Table S2.

Statistical Analysis

Student's *t*-test was used to evaluate statistical significance. Values of $P < 0.05$ were considered significant. Data are expressed as means ± SD.

Acknowledgments:

We thank Dr. Beate Lanske of Harvard University for providing us with the *Ihh*$^{flox/flox}$ mice; and Sandra Huling of the UCSF Liver Center for histology and electron microscopy support. Authors declare no conflicts of interests. This work is supported in part by NIH grants R21DK-069309 to X.C. and R01DK55783 to D.W.P, a grant from the Research Grants Council of the Hong Kong Special Administrative Region, China (Project No. HKU7524/06M) to S.Y.L. and X.C, a grant from Strategic Research Theme on Cancer from The University of Hong Kong to S.Y.L. C.K. is supported by a stem cell fellowship provided by the California Institute for Regenerative Medicine; and D.E.S is supported by Deutsche Forschungsgemeinschaft (DFG, Sta1065/1-1).

References

1. Barker, N., van de Wetering, M. & Clevers, H. (2008) *Genes Dev* **22**, 1856-64.
2. van der Flier, L. G. & Clevers, H. (2009) *Annu Rev Physiol* **71**, 241-60.
3. Barker, N., van Es, J. H., Kuipers, J., Kujala, P., van den Born, M., Cozijnsen, M., Haegebarth, A., Korving, J., Begthel, H., Peters, P. J. & Clevers, H. (2007) *Nature* **449**, 1003-7.
4. Sangiorgi, E. & Capecchi, M. R. (2008) *Nat Genet* **40**, 915-20.
5. van der Flier, L. G., van Gijn, M. E., Hatzis, P., Kujala, P., Haegebarth, A., Stange, D. E., Begthel, H., van den Born, M., Guryev, V., Oving, I., van Es, J. H., Barker, N., Peters, P. J., van de Wetering, M. & Clevers, H. (2009) *Cell* **136**, 903-12.
6. van der Flier, L. G., Haegebarth, A., Stange, D. E., van de Wetering, M. & Clevers, H. (2009) *Gastroenterology* **137**, 15-7.
7. Potten, C. S., Booth, C., Tudor, G. L., Booth, D., Brady, G., Hurley, P., Ashton, G., Clarke, R., Sakakibara, S. & Okano, H. (2003) *Differentiation* **71**, 28-41.
8. Zhu, L., Gibson, P., Currle, D. S., Tong, Y., Richardson, R. J., Bayazitov, I. T., Poppleton, H., Zakharenko, S., Ellison, D. W. & Gilbertson, R. J. (2009) *Nature* **457**, 603-7.
9. Snippert, H. J., van Es, J. H., van den Born, M., Begthel, H., Stange, D. E., Barker, N. & Clevers, H. (2009) *Gastroenterology* **136**, 2187-2194 e1.
10. Gregorieff, A., Pinto, D., Begthel, H., Destree, O., Kielman, M. & Clevers, H. (2005) *Gastroenterology* **129**, 626-38.
11. Walker, M. R., Patel, K. K. & Stappenbeck, T. S. (2009) *J Pathol* 217, 169-80.
12. Powell, D. W., Mifflin, R. C., Valentich, J. D., Crowe, S. E., Saada, J. I. & West, A. B. (1999) *Am J Physiol* **277**, C183-201.
13. Powell, D. W., Adegboyega, P. A., Di Mari, J. F. & Mifflin, R. C. (2005) *Am J Physiol Gastrointest Liver Physiol* **289**, G2-7.
14. He, X. C., Zhang, J., Tong, W. G., Tawfik, O., Ross, J., Scoville, D. H., Tian, Q., Zeng, X., He, X., Wiedemann, L. M., Mishina, Y. & Li, L. (2004) *Nat Genet* **36**, 1117-21.
15. Kosinski, C., Li, V. S., Chan, A. S., Zhang, J., Ho, C., Tsui, W. Y., Chan, T. L., Mifflin, R. C., Powell, D. W., Yuen, S. T., Leung, S. Y. & Chen, X. (2007) *Proc Natl Acad Sci U S A* **104**, 15418-23.
16. Sato, T., Vries, R. G., Snippert, H. J., van de Wetering, M., Barker, N., Stange, D. E., van Es, J. H., Abo, A., Kujala, P., Peters, P. J. & Clevers, H. (2009) *Nature* **459**, 262-5.
17. Ootani, A., Li, X., Sangiorgi, E., Ho, Q. T., Ueno, H., Toda, S., Sugihara, H., Fujimoto, K., Weissman, I. L., Capecchi, M. R. & Kuo, C. J. (2009) *Nat Med* **15**, 701-6.
18. van den Brink, G. R. (2007) *Physiol Rev* 87, 1343-75.
19. Ramalho-Santos, M., Melton, D. A. & McMahon, A. P. (2000) *Development* **127**, 2763-72.

20. Kolterud, A., Grosse, A. S., Zacharias, W. J., Walton, K. D., Kretovich, K. E., Madison, B. B., Waghray, M., Ferris, J. E., Hu, C., Merchant, J. L., Dlugosz, A. A., Kottmann, A. H. & Gumucio, D. L. (2009) *Gastroenterology* **137**, 618-28.
21. Bitgood, M. J. & McMahon, A. P. (1995) *Dev Biol* **172**, 126-38.
22. Madison, B. B., Braunstein, K., Kuizon, E., Portman, K., Qiao, X. T. & Gumucio, D. L. (2005) *Development* **132**, 279-89.
23. van Dop, W. A., Uhmann, A., Wijgerde, M., Sleddens-Linkels, E., Heijmans, J., Offerhaus, G. J., van den Bergh Weerman, M. A., Boeckxstaens, G. E., Hommes, D. W., Hardwick, J. C., Hahn, H. & van den Brink, G. R. (2009) *Gastroenterology* **136**, 2195-2203 e1-7.
24. Madison, B. B., Dunbar, L., Qiao, X. T., Braunstein, K., Braunstein, E. & Gumucio, D. L. (2002) *J Biol Chem* **277**, 33275-83.
25. Lauth, M., Bergstrom, A., Shimokawa, T. & Toftgard, R. (2007) *Proc Natl Acad Sci U S A* **104**, 8455-60.
26. Wong, M. H., Rubinfeld, B. & Gordon, J. I. (1998) *J Cell Biol* **141**, 765-77.
27. van de Wetering, M., Sancho, E., Verweij, C., de Lau, W., Oving, I., Hurlstone, A., van der Horn, K., Batlle, E., Coudreuse, D., Haramis, A. P., Tjon-Pon-Fong, M., Moerer, P., van den Born, M., Soete, G., Pals, S., Eilers, M., Medema, R. & Clevers, H. (2002) *Cell* **111**, 241-50.
28. Karam, S. M. (1999) *Front Biosci* **4**, D286-98.
29. Wang, L. C., Nassir, F., Liu, Z. Y., Ling, L., Kuo, F., Crowell, T., Olson, D., Davidson, N. O. & Burkly, L. C. (2002) *Gastroenterology* **122**, 469-82.
30. van den Brink, G. R., Bleuming, S. A., Hardwick, J. C., Schepman, B. L., Offerhaus, G. J., Keller, J. J., Nielsen, C., Gaffield, W., van Deventer, S. J., Roberts, D. J. & Peppelenbosch, M. P. (2004) *Nat Genet* **36**, 277-82.
31. Varnat, F., Heggeler, B. B., Grisel, P., Boucard, N., Corthesy-Theulaz, I., Wahli, W. & Desvergne, B. (2006) *Gastroenterology* **131**, 538-53.
32. Yauch, R. L., Gould, S. E., Scales, S. J., Tang, T., Tian, H., Ahn, C. P., Marshall, D., Fu, L., Januario, T., Kallop, D., Nannini-Pepe, M., Kotkow, K., Marsters, J. C., Rubin, L. L. & de Sauvage, F. J. (2008) *Nature* **455**, 406-10.
33. Uchida, K. & Kamikawa, Y. (2007) *J Smooth Muscle Res* **43**, 157-77.
34. Roberts, D. J., Johnson, R. L., Burke, A. C., Nelson, C. E., Morgan, B. A. & Tabin, C. (1995) *Development* **121**, 3163-74.
35. Sukegawa, A., Narita, T., Kameda, T., Saitoh, K., Nohno, T., Iba, H., Yasugi, S. & Fukuda, K. (2000) *Development* **127**, 1971-80.
36. Haramis, A. P., Begthel, H., van den Born, M., van Es, J., Jonkheer, S., Offerhaus, G. J. & Clevers, H. (2004) *Science* **303**, 1684-6.
37. Alinger, B., Kiesslich, T., Datz, C., Aberger, F., Strasser, F., Berr, F., Dietze, O., Kaserer, K. & Hauser-Kronberger, C. (2009) *Virchows Arch* **454**, 369-79.
38. Razzaque, M. S., Soegiarto, D. W., Chang, D., Long, F. & Lanske, B. (2005) *J Pathol* **207**, 453-61.
39. Long, F., Zhang, X. M., Karp, S., Yang, Y. & McMahon, A. P. (2001) *Development* **128**, 5099-108.
40. Tusher, V. G., Tibshirani, R. & Chu, G. (2001) *Proc Natl Acad Sci U S A* **98**, 5116-21.

41. Mahida, Y. R., Beltinger, J., Makh, S., Goke, M., Gray, T., Podolsky, D. K. & Hawkey, C. J. (1997) *Am J Physiol* **273**, G1341-8.
42. Saada, J. I., Pinchuk, I. V., Barrera, C. A., Adegboyega, P. A., Suarez, G., Mifflin, R. C., Di Mari, J. F., Reyes, V. E. & Powell, D. W. (2006) *J Immunol* **177**, 5968-79.

Supplemental Information

Figure S1A

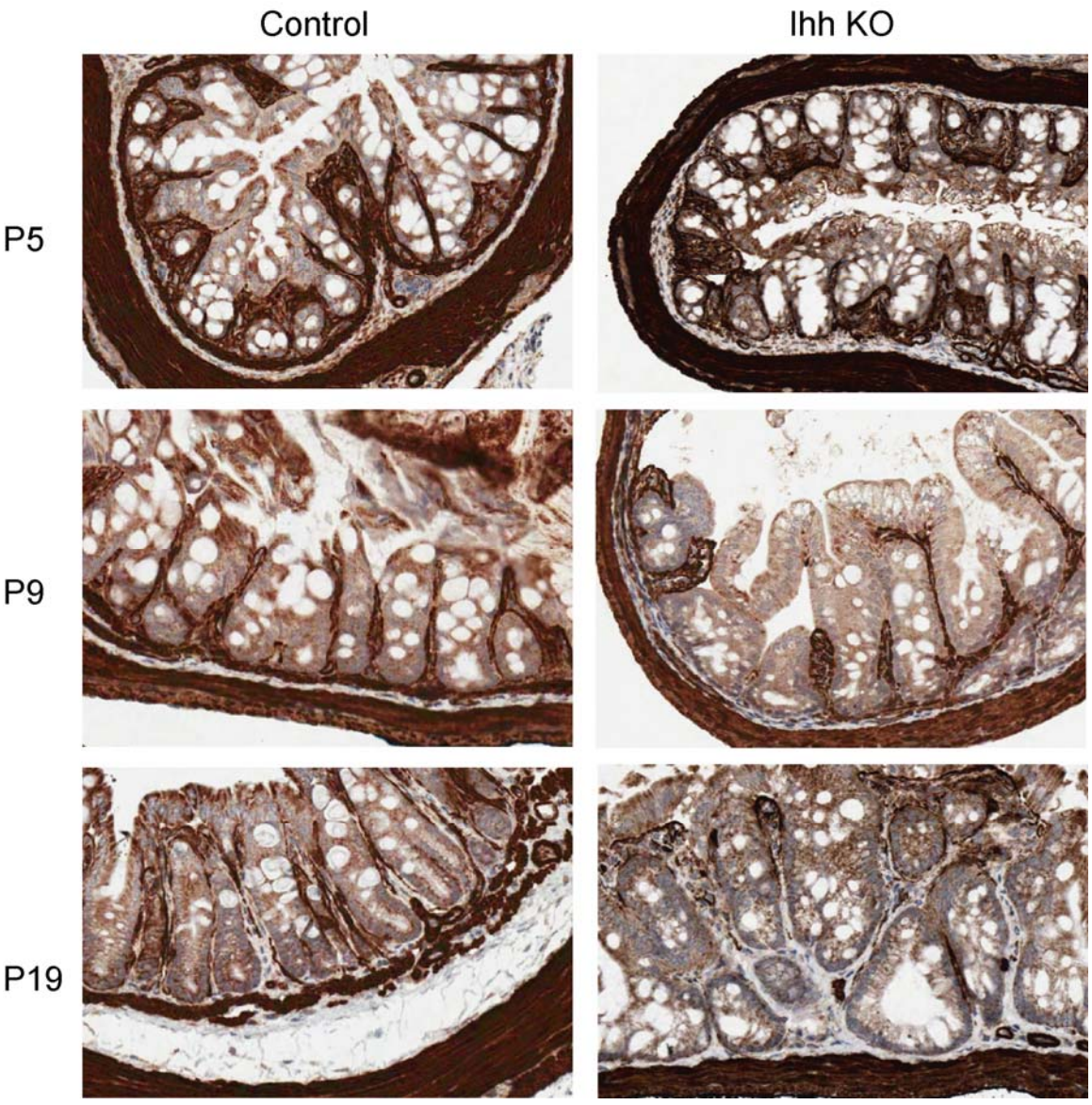

Figure S1B

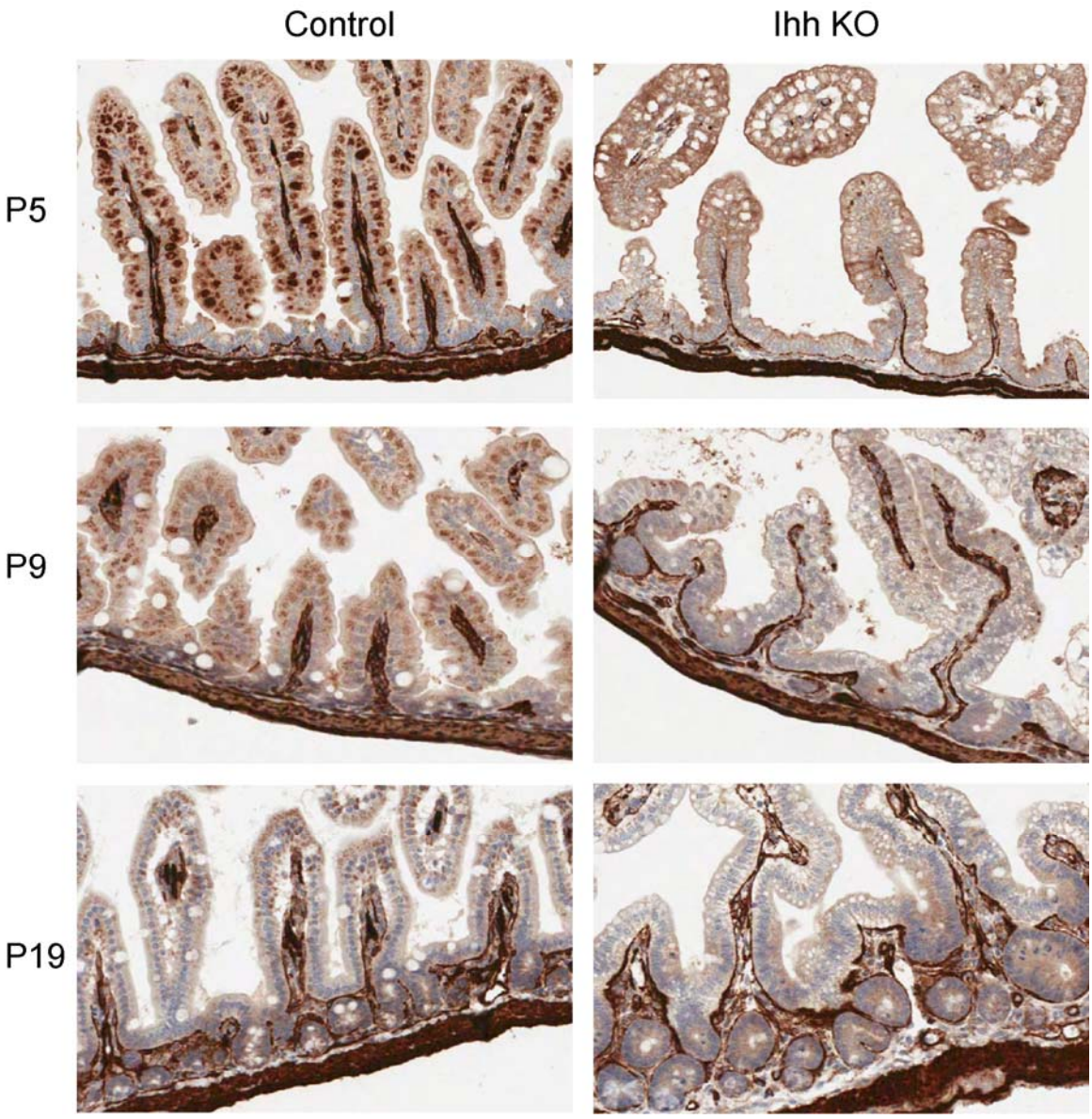

Figure S1. Loss of ISC Niche Cells in *Villin-Cre;Ihh*$^{flox/flox}$ Mice through Postnatal Development. α-SMA staining of colon (1A) and jejunum (1B) in control and *Ihh* KO mice at different ages (P5, P9 and P19).

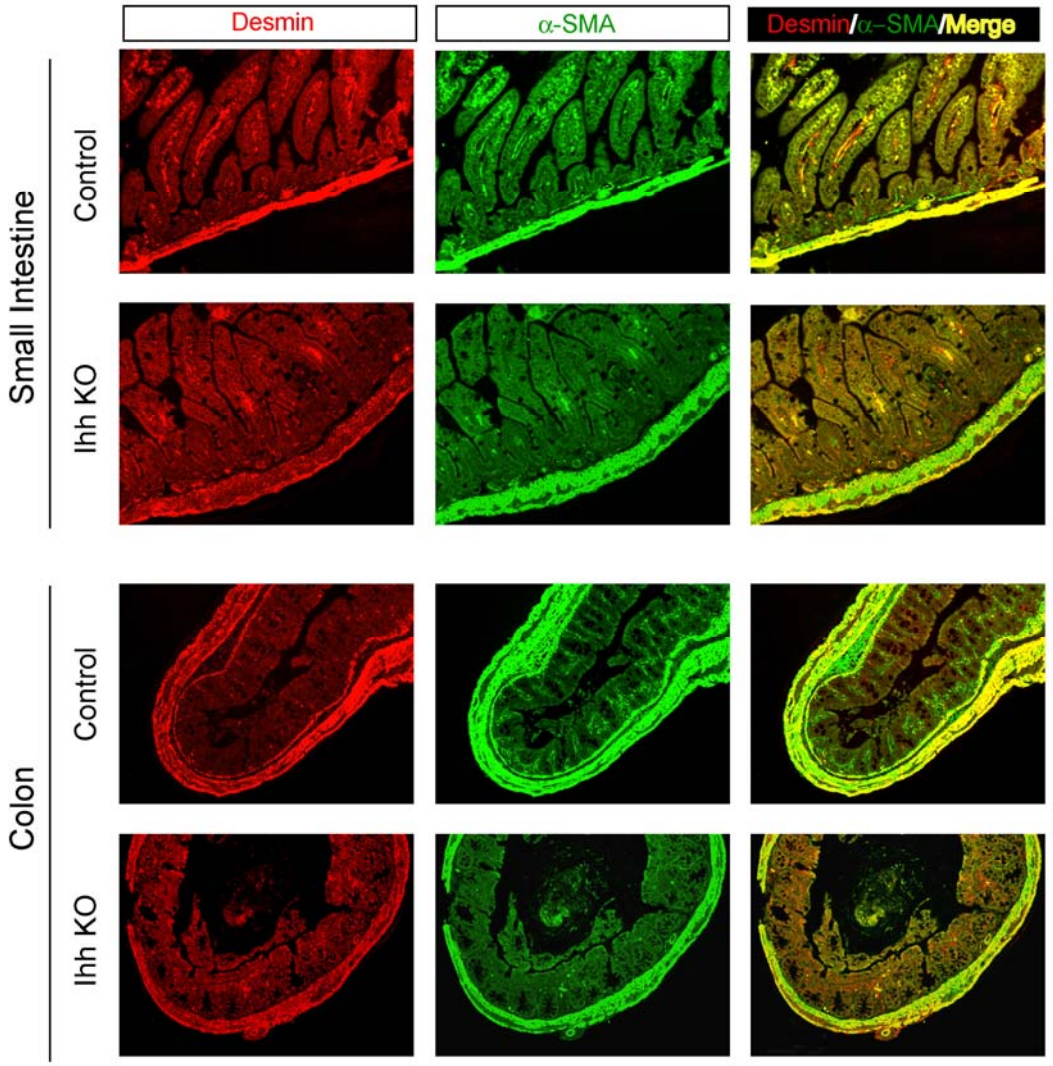

Figure S2. Loss of ISC Niche Cells in *Villin-Cre;Ihh$^{flox/flox}$* Mice. The figure shows the individual color channels of double immunofluorescent staining of SMA (green) and desmin (red) to distinguish ISEMF cells and SMCs in the small intestine and colon in control and Ihh mutant mice.

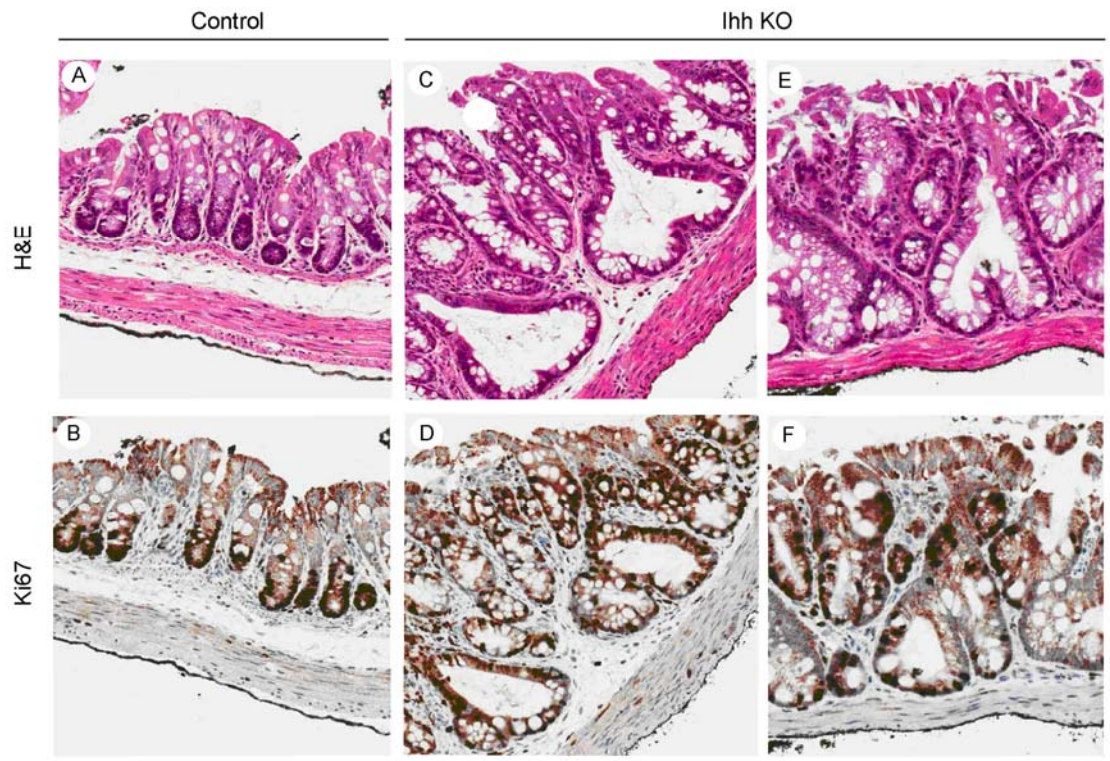

Figure S3. Abnormal Intestinal Epithelial Phenotypes in Colon Tissues of *Villin-Cre;Ihh*$^{flox/flox}$ Mice. (A) Control mice exhibit crypts that are uniform in size and shape with (B) Ki67 positive cells restricted to crypt bottoms. Note goblet cells are present in the upper two-thirds of the crypt (A); (C, E) *Ihh* KO mice display dilated, distorted crypts with increased goblet cells spanning the whole crypt. Note the mutant mice have increase incidences of crypt fission; (D, F) In *Ihh* KO mice, Ki67 immunostaining is detected in regions along the entire crypt length.

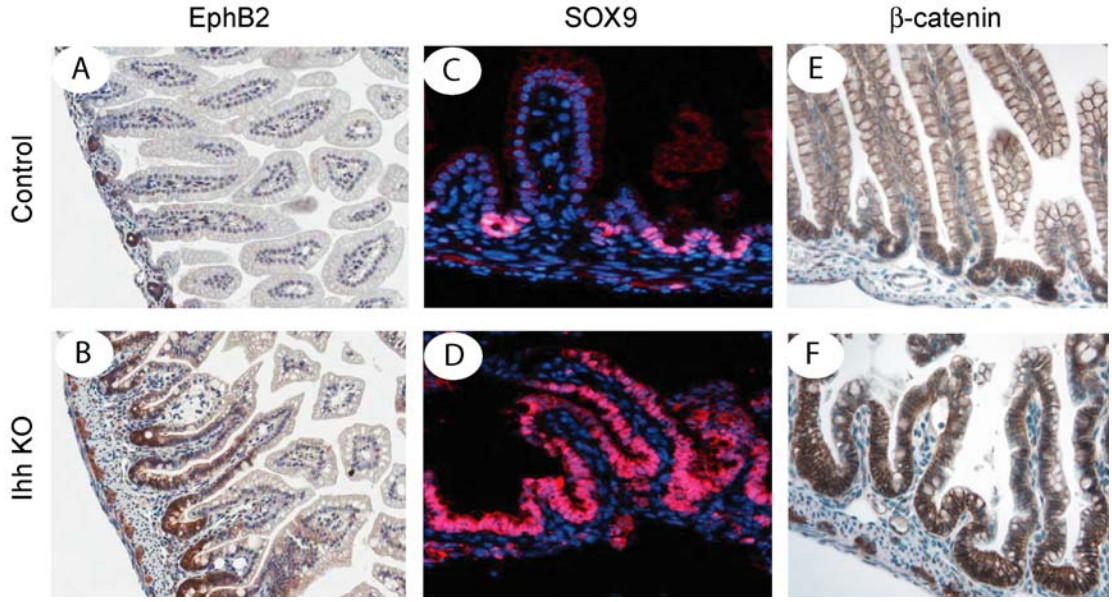

Figure S4: Abnormal Activation of Wnt/β-catenin Signaling in *Villin-Cre;Ihh*$^{flox/flox}$ Mice. (A-D) Small intestinal sections showing immunostaining of Wnt/β-catenin target genes (EphB2 and Sox9) is expanded in *Ihh* KO mice (B, D) compared to control (A, C). Cytoplasmic and nuclear β-catenin staining detected in *Ihh* KO mice (F), while control mice (E) predominantly displayed membrane β-catenin staining in the small intestine.

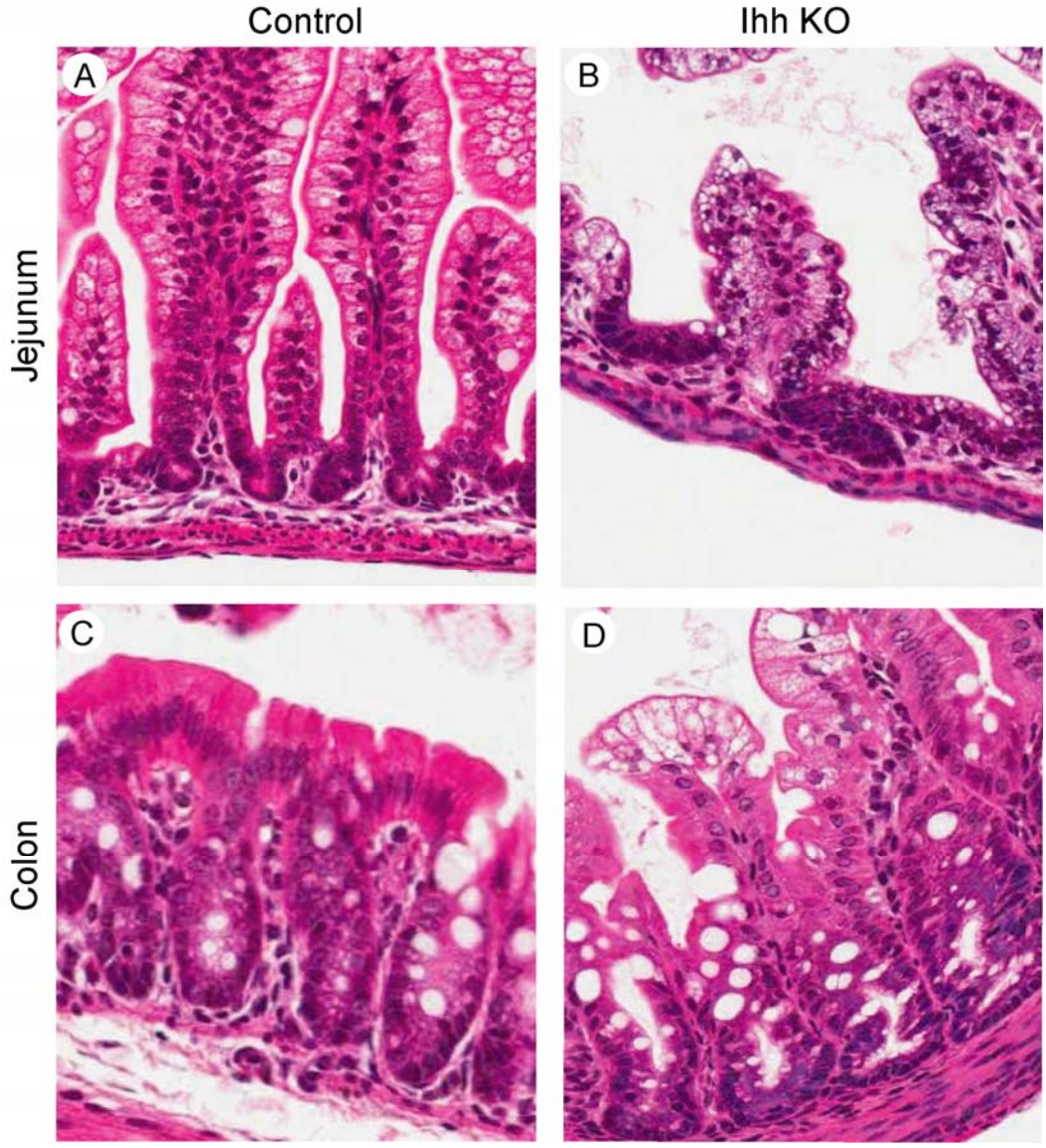

Figure S5. Vacuolation of enterocytes in *Villin-Cre;Ihh*$^{flox/flox}$ Mice. H&E staining of control (A, C) and conditional *Ihh* KO (B, D) mice showing the failure of enterocyte maturation with arrest in the vacuolated cell stage in the jejunum and colon of conditional *Ihh* KO mice.

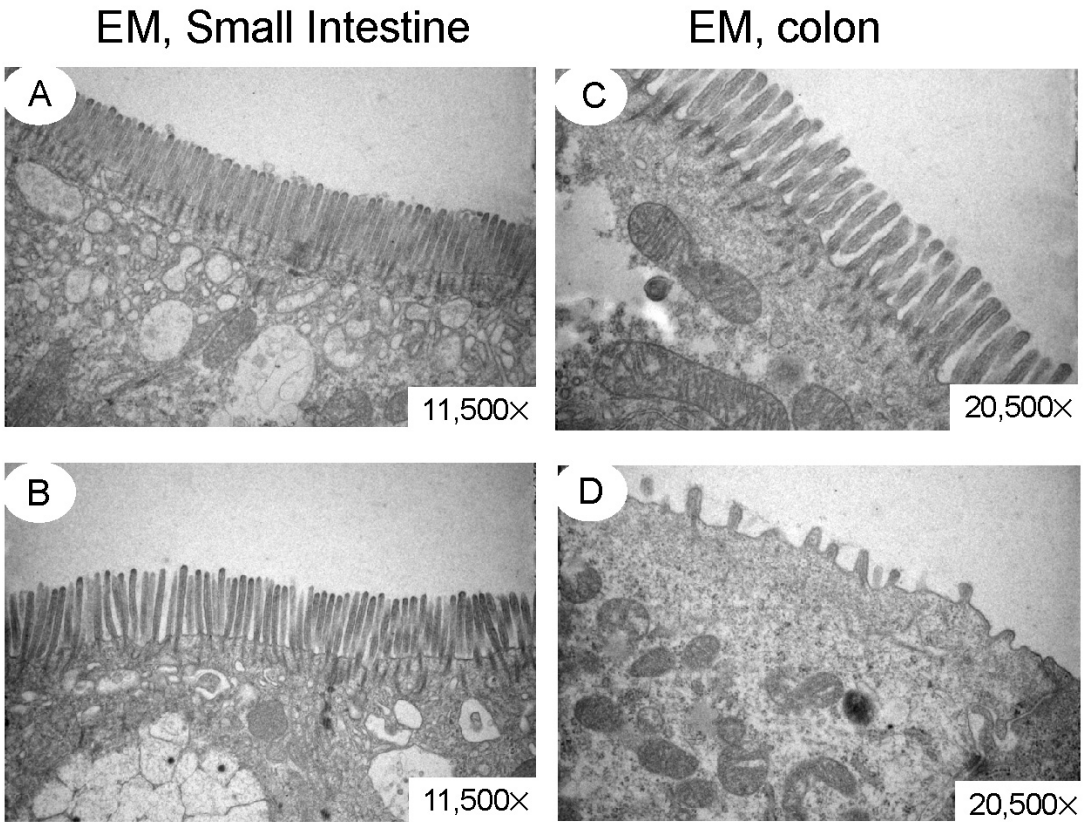

Figure S6. Transmission Electron Microscopy of the Microvillar Brush Border. Representative transmission electron micrographs of the apical membrane of epithelial cells isolated from the small intestine (A and B) and colon (C and D) of control (A and C) and *Villin-Cre;Ihh*$^{flox/flox}$ mice (B and D);

Table S1. Genes Differentially Expressed in *Villin-Cre;Ihh*$^{flox/flox}$ Mice versus Control Mice (Full List). For all genes scored, the fold change was calculated by dividing the mutant value by the control value. Paired Significance Analysis of Microarrays (SAM) was performed to identify genes differentially expressed in control and mutant colon samples.

Genes Down-regulated in Conditional *Ihh* Mutant Mice versus Control Mice

Gene Title	Gene Symbol	Fold Change
RIKEN cDNA 1110001D15 gene	1110001D15Rik	0.31
RIKEN cDNA 1190002N15 gene	1190002N15Rik	0.66
RIKEN cDNA 1200009O22 gene	1200009O22Rik	0.59
RIKEN cDNA 1700025G04 gene	1700025G04Rik	0.69
RIKEN cDNA 1700029G01 gene	1700029G01Rik	0.70
RIKEN cDNA 1810010M01 gene	1810010M01Rik	0.64
RIKEN cDNA 1810011H11 gene	1810011H11Rik	0.73
RIKEN cDNA 1810041L15 gene	1810041L15Rik	0.52
RIKEN cDNA 2010003K11 gene	2010003K11Rik	0.69
RIKEN cDNA 2010011I20 gene	2010011I20Rik	0.77
RIKEN cDNA 2010110P09 gene	2010110P09Rik	0.59
RIKEN cDNA 2810022L02 gene	2810022L02Rik	0.79
RIKEN cDNA 4631426J05 gene	4631426J05Rik	0.71
RIKEN cDNA 4833424O15 gene	4833424O15Rik	0.67
RIKEN cDNA 4930503L19 gene	4930503L19Rik	0.73
RIKEN cDNA 9230105E10 gene	9230105E10Rik	0.73
RIKEN cDNA 9930111J21 gene	9930111J21Rik	0.74
RIKEN cDNA 9930111J21 gene	9930111J21Rik	0.75
RIKEN cDNA A430107O13 gene	A430107O13Rik	0.52
alanine and arginine rich domain containing protein	Aard	0.62
ATP-binding cassette, sub-family G (WHITE), member 2	Abcg2	0.71
ABI gene family, member 3 (NESH) binding protein	Abi3bp	0.45
ankyrin repeat and BTB (POZ) domain containing 2	Abtb2	0.72
alkaline ceramidase 1	Acer1	0.65
actin, alpha, cardiac muscle 1	Actc1	0.54
actin, gamma 2, smooth muscle, enteric	Actg2	0.64
activin A receptor, type II-like 1	Acvrl1	0.71
a disintegrin and metallopeptidase domain 19 (meltrin beta)	Adam19	0.70
a disintegrin and metallopeptidase domain 23	Adam23	0.68
ADAM-like, decysin 1	Adamdec1	0.40
a disintegrin-like and metallopeptidase type1 motif, 18	Adamts18	0.70
a disintegrin-like and metallopeptidase type1 motif, 19	Adamts19	0.68
a disintegrin-like and metallopeptidase type1 motif, 9	Adamts9	0.60
a disintegrin-like and metallopeptidase type1 motif, 9	Adamts9	0.61
a disintegrin-like and metallopeptidase type1 motif, 9	Adamts9	0.61
a disintegrin-like and metallopeptidase type1 motif, 9	Adamts9	0.61
a disintegrin-like and metallopeptidase type1 motif, 9	Adamts9	0.63
a disintegrin-like and metallopeptidase type1 motif, 9	Adamts9	0.73

ArfGAP with dual PH domains 2	Adap2	0.71
AF4/FMR2 family, member 3	Aff3	0.73
angiotensinogen (serpin peptidase inhibitor, clade A, member 8)	Agt	0.48
aryl-hydrocarbon receptor	Ahr	0.71
aryl-hydrocarbon receptor repressor	Ahrr	0.73
allograft inflammatory factor 1	Aif1	0.77
A kinase (PRKA) anchor protein 6	Akap6	0.74
aldehyde dehydrogenase 2, mitochondrial	Aldh2	0.67
arachidonate 12-lipoxygenase	Alox12	0.78
amyotrophic lateral sclerosis 2 (juvenile) chromosome region, cnd 4	Als2cr4	0.70
angiopoietin-like 7	Angptl7	0.62
ankyrin repeat domain 37	Ankrd37	0.59
ankyrin repeat and sterile alpha motif domain containing 4B	Anks4b	0.78
anoctamin 1, calcium activated chloride channel	Ano1	0.40
annexin A6	Anxa6	0.71
amine oxidase, copper containing 3	Aoc3	0.56
adaptor-related protein complex 1, sigma 2 subunit	Ap1s2	0.81
adenomatosis polyposis coli down-regulated 1	Apcdd1	0.74
apelin receptor	Aplnr	0.65
apolipoprotein L 10a	Apol10a	0.56
aquaporin 4	Aqp4	0.57
aquaporin 8	Aqp8	0.41
Rho GTPase activating protein 28	Arhgap28	0.45
arrestin, beta 1	Arrb1	0.78
ankyrin repeat and SOCS box-containing 2	Asb2	0.65
achaete-scute complex homolog 2 (Drosophila)	Ascl2	0.69
asporin	Aspn	0.63
ATPase, Na+/K+ transporting, alpha 2 polypeptide	Atp1a2	0.76
ATPase, Ca++ transporting, plasma membrane 4	Atp2b4	0.59
AXL receptor tyrosine kinase	Axl	0.77
bradykinin receptor, beta 2	Bdkrb2	0.68
bone gamma-carboxyglutamate protein, related sequence 1	Bglap-rs1	0.54
bone gamma carboxyglutamate protein 1	Bglap1	0.62
bone morphogenetic protein 2	Bmp2	0.55
bone morphogenetic protein 4	Bmp4	0.49
bone morphogenetic protein 5	Bmp5	0.27
BTB (POZ) domain containing 3	Btbd3	0.69
calcium channel, voltage-dependent, alpha2/delta subunit 3	Cacna2d3	0.73
calbindin 2	Calb2	0.54
calcitonin-related polypeptide, beta	Calcb	0.77
calcitonin receptor-like	Calcrl	0.63
caldesmon 1	Cald1	0.67
CAP, adenylate cyclase-associated protein, 2 (yeast)	Cap2	0.58
calpain 2	Capn2	0.73
carbonic anhydrase 3	Car3	0.43
carbonic anhydrase 4	Car4	0.38
calsequestrin 1	Casq1	0.66
caveolin 1, caveolae protein	Cav1	0.62
carbonyl reductase 3	Cbr3	0.73

coiled-coil domain containing 3	Ccdc3	0.50
coiled-coil domain containing 68	Ccdc68	0.73
cholecystokinin A receptor	Cckar	0.52
CD34 antigen	Cd34	0.75
CD74 antigen	Cd74	0.55
CD93 antigen	Cd93	0.69
cadherin 11	Cdh11	0.77
cadherin 13	Cdh13	0.80
cadherin 5	Cdh5	0.75
cadherin 6	Cdh6	0.64
cyclin-dependent kinase inhibitor 1A (P21)	Cdkn1a	0.51
cyclin-dependent kinase inhibitor 2B (p15, inhibits CDK4)	Cdkn2b	0.52
carbohydrate (chondroitin 6/keratan) sulfotransferase 3	Chst3	0.77
creatine kinase, brain	Ckb	0.70
chloride channel calcium activated 3	Clca3	0.46
C-type lectin domain family 14, member a	Clec14a	0.71
chloride intracellular channel 5	Clic5	0.53
clusterin	Clu	0.52
calponin 1	Cnn1	0.61
contactin 3	Cntn3	0.76
collagen, type XII, alpha 1	Col12a1	0.46
collagen, type XV, alpha 1	Col15a1	0.55
collagen, type IV, alpha 1	Col4a1	0.64
collagen, type IV, alpha 5	Col4a5	0.63
collagen, type IV, alpha 6	Col4a6	0.54
collagen, type VI, alpha 2	Col6a2	0.64
carboxypeptidase A6	Cpa6	0.59
carboxypeptidase X 2 (M14 family)	Cpxm2	0.37
crystallin, alpha B	Cryab	0.66
colony stimulating factor 1 (macrophage)	Csf1	0.71
cystathionase (cystathionine gamma-lyase)	Cth	0.60
cathepsin E	Ctse	0.66
CUG triplet repeat, RNA binding protein 2	Cugbp2	0.76
chemokine (C-X3-C) receptor 1	Cx3cr1	0.73
chemokine (C-X-C motif) ligand 14	Cxcl14	0.47
chemokine (C-X-C motif) receptor 7	Cxcr7	0.61
cytochrome P450, family 2, subfamily c, polypeptide 40	Cyp2c40	0.59
cytochrome P450, family 2, subfamily c, polypeptide 55	Cyp2c55	0.48
cytochrome P450, family 2, subfamily c, polypeptide 67	Cyp2c67	0.65
cytochrome P450, family 2, subfamily c, polypeptide 68	Cyp2c68	0.49
cytochrome P450, family 2, subfamily d, polypeptide 13	Cyp2d13	0.58
cytochrome P450, family 2, subfamily s, polypeptide 1	Cyp2s1	0.64
cytochrome P450, family 3, subfamily a, polypeptide 44	Cyp3a44	0.69
cytochrome P450, family 4, subfamily f, polypeptide 14	Cyp4f14	0.60
cytochrome P450, family 4, subfamily f, polypeptide 16	Cyp4f16	0.51
DNA segment, human D4S114	D0H4S114	0.74
DNA segment, Chr 10, ERATO Doi 610, expressed	D10Ertd610e	0.72
dishevelled associated activator of morphogenesis 2	Daam2	0.69
disabled homolog 2 (Drosophila)	Dab2	0.71

dachshund 1 (Drosophila)	Dach1	0.58
discoidin, CUB and LCCL domain containing 2	Dcbld2	0.67
discoidin domain receptor family, member 2	Ddr2	0.66
DENN/MADD domain containing 5A	Dennd5a	0.73
desmin	Des	0.56
deiodinase, iodothyronine, type I	Dio1	0.46
dystrophia myotonica-protein kinase	Dmpk	0.62
deoxyribonuclease 1-like 3	Dnase1l3	0.58
dedicator of cytokinesis 4	Dock4	0.79
docking protein 5	Dok5	0.80
dipeptidylpeptidase 10	Dpp10	0.65
dysferlin	Dysf	0.74
DAZ interacting protein 1	Dzip1	0.64
DAZ interacting protein 1	Dzip1	0.79
RIKEN cDNA E030049G20 gene	E030049G20Rik	0.61
RIKEN cDNA E030049G20 gene	E030049G20Rik	0.74
RIKEN cDNA E130203B14 gene	E130203B14Rik	0.62
early B-cell factor 1	Ebf1	0.80
extracellular matrix protein 2, female organ and adipocyte specific	Ecm2	0.74
endothelin receptor type A	Ednra	0.69
epidermal growth factor-containing fibulin-like extracellular matrix protein 1	Efemp1	0.44
ephrin B2	Efnb2	0.74
predicted gene, EG638904	EG638904	0.73
predicted gene, EG665033	EG665033	0.58
EGF-like, fibronectin type III and laminin G domains	Egflam	0.57
EMI domain containing 1	Emid1	0.70
echinoderm microtubule associated protein like 1	Eml1	0.57
endonuclease domain containing 1	Endod1	0.64
enolase 3, beta muscle	Eno3	0.51
ectonucleotide pyrophosphatase/phosphodiesterase 2	Enpp2	0.38
endothelial PAS domain protein 1	Epas1	0.63
Eph receptor A7	Epha7	0.68
avian erythroblastosis virus E-26 (v-ets) oncogene related	Erg	0.80
E26 avian leukemia oncogene 1, 5' domain	Ets1	0.75
fatty acid desaturase 1	Fads1	0.57
family with sequence similarity 105, member A	Fam105a	0.73
family with sequence similarity 162, member B	Fam162b	0.64
family with sequence similarity 171, member B	Fam171b	0.74
FAT tumor suppressor homolog 3 (Drosophila)	Fat3	0.54
FAT tumor suppressor homolog 3 (Drosophila)	Fat3	0.64
FAT tumor suppressor homolog 3 (Drosophila)	Fat3	0.66
FAT tumor suppressor homolog 3 (Drosophila)	Fat3	0.67
FAT tumor suppressor homolog 4 (Drosophila)	Fat4	0.42
fibrillin 1	Fbn1	0.71
Fc fragment of IgG binding protein	Fcgbp	0.61
fibroblast growth factor 9	Fgf9	0.59
filamin, alpha	Flna	0.69
fibronectin 1	Fn1	0.63

fibronectin type III domain containing 1	Fndc1	0.55
forkhead box F1a	Foxf1a	0.60
forkhead box F2	Foxf2	0.42
forkhead box L1	Foxl1	0.71
Fraser syndrome 1 homolog (human)	Fras1	0.60
Fras1 related extracellular matrix protein 2	Frem2	0.51
follistatin-like 1	Fstl1	0.70
Fyn proto-oncogene	Fyn	0.77
frizzled homolog 4 (Drosophila)	Fzd4	0.65
gamma-aminobutyric acid (GABA-A) receptor, subunit alpha 2	Gabra2	0.72
growth arrest specific 5	Gas5	0.74
globoside alpha-1,3-N-acetylgalactosaminyltransferase 1	Gbgt1	0.80
gamma-glutamyl hydrolase	Ggh	0.63
gamma-glutamyl hydrolase	Ggh	0.63
gamma-glutamyltransferase 1	Ggt1	0.57
GLI-Kruppel family member GLI1	Gli1	0.58
glycine receptor, beta subunit	Glrb	0.70
glycosyltransferase 25 domain containing 2	Glt25d2	0.74
gene model 967, (NCBI)	Gm967	0.71
guanine nucleotide binding protein (G protein), alpha inhibiting 1	Gnai1	0.67
G protein-coupled receptor 177	Gpr177	0.74
G protein-coupled receptor 37	Gpr37	0.77
glutathione peroxidase 8 (putative)	Gpx8	0.77
growth factor receptor bound protein 14	Grb14	0.71
gremlin 2 homolog, cysteine knot superfamily (Xenopus laevis)	Grem2	0.50
glutamate receptor ionotropic, NMDA3A	Grin3a	0.52
gasdermin C2	Gsdmc2	0.60
gasdermin C3	Gsdmc3	0.53
glutathione S-transferase, alpha 3	Gsta3	0.60
glycophorin C	Gypc	0.72
histocompatibility 2, class II antigen A, beta 1	H2-Ab1	0.53
hyaluronan synthase 2	Has2	0.76
Hedgehog-interacting protein	Hhip	0.22
hemicentin 1	Hmcn1	0.59
hemicentin 1	Hmcn1	0.60
hemicentin 1	Hmcn1	0.62
hemicentin 1	Hmcn1	0.63
hemicentin 1	Hmcn1	0.66
hemicentin 1	Hmcn1	0.66
hemicentin 1	Hmcn1	0.67
hemicentin 1	Hmcn1	0.69
hemicentin 1	Hmcn1	0.69
hemicentin 1	Hmcn1	0.69
hemicentin 1	Hmcn1	0.71
hemicentin 1	Hmcn1	0.73
hemicentin 1	Hmcn1	0.75
HtrA serine peptidase 1	Htra1	0.51
hormonally upregulated Neu-associated kinase	Hunk	0.75
inhibitor of DNA binding 1	Id1	0.67

inhibitor of DNA binding 2	Id2	0.73
inhibitor of DNA binding 4	Id4	0.61
insulin-like growth factor binding protein 2	Igfbp2	0.54
immunoglobulin superfamily, member 9	Igsf9	0.57
interleukin 34	Il34	0.77
integrin alpha 1	Itga1	0.67
integrin alpha 8	Itga8	0.64
integrin alpha 9	Itga9	0.54
integrin alpha V	Itgav	0.81
integrin beta 6	Itgb6	0.75
iodotyrosine deiodinase	Iyd	0.61
potassium voltage gated channel, Shab-related subfamily, member 2	Kcnb2	0.80
potassium voltage-gated channel, Shal-related family, member 3	Kcnd3	0.57
potassium inwardly-rectifying channel, subfamily J, member 16	Kcnj16	0.53
kinase insert domain protein receptor	Kdr	0.66
Kruppel-like factor 4 (gut)	Klf4	0.71
kelch-like 23 (Drosophila)	Klhl23	0.71
kallikrein related-peptidase 15	Klk15	0.40
laminin, alpha 3	Lama3	0.55
laminin, alpha 4	Lama4	0.68
laminin, alpha 5	Lama5	0.74
laminin B1 subunit 1	Lamb1-1	0.59
laminin, gamma 1	Lamc1	0.64
leptin receptor	Lepr	0.67
leprecan-like 1	Leprel1	0.50
lectin, galactose binding, soluble 1	Lgals1	0.73
lin-7 homolog A (C. elegans)	Lin7a	0.74
LIM domain only 3	Lmo3	0.64
latrophilin 3	Lphn3	0.52
LIM domain containing preferred translocation partner in lipoma	Lpp	0.77
leucine rich repeat containing 61	Lrrc61	0.73
latent transforming growth factor beta binding protein 1	Ltbp1	0.66
latent transforming growth factor beta binding protein 4	Ltbp4	0.61
latexin	Lxn	0.78
v-maf musculoaponeurotic fibrosarcoma oncogene family, protein B	Mafb	0.66
MAM domain containing 2	Mamdc2	0.68
mucolipin 3	Mcoln3	0.72
mast cell protease 1	Mcpt1	0.35
mast cell protease 2	Mcpt2	0.39
myocyte enhancer factor 2C	Mef2c	0.75
meprin 1 alpha	Mep1a	0.66
meprin 1 beta	Mep1b	0.71
microfibrillar associated protein 5	Mfap5	0.47
monoglyceride lipase	Mgll	0.74
MON2 homolog (yeast) /// Eph receptor B6	Mon2 /// Ephb6	0.78
major histocompatibility complex, class I-related	Mr1	0.66
metallothionein 2	Mt2	0.59
myotubularin related protein 11	Mtmr11	0.65
MAX dimerization protein 1	Mxd1	0.63

v-myc myelocytomatosis viral related oncogene	Mycn	0.61
myc target 1	Myct1	0.71
myosin, heavy polypeptide 10, non-muscle	Myh10	0.64
myosin, heavy polypeptide 11, smooth muscle	Myh11	0.68
myosin, light polypeptide 4	Myl4	0.72
myosin, light polypeptide 9, regulatory	Myl9	0.73
myosin XVB	Myo15b	0.75
myocardin	Myocd	0.68
myomesin 1	Myom1	0.60
neural cell adhesion molecule 1	Ncam1	0.47
nexilin	Nexn	0.65
nidogen 1	Nid1	0.71
NK2 transcription factor related, locus 3 (Drosophila)	Nkx2-3	0.61
neuromedin U	Nmu	0.37
natriuretic peptide receptor 2	Npr2	0.71
NAD(P)H dehydrogenase, quinone 1	Nqo1	0.43
nuclear receptor subfamily 2, group F, member 1	Nr2f1	0.75
neuregulin 1	Nrg1	0.59
5' nucleotidase, ecto	Nt5e	0.46
neurotrophin 3	Ntf3	0.51
nuclear RNA export factor 7	Nxf7	0.72
osteoglycin	Ogn	0.37
olfactory receptor 165	Olfr165	0.32
olfactory receptor 178	Olfr178	0.77
olfactory receptor 558	Olfr558	0.72
purinergic receptor P2Y, G-protein coupled, 14	P2ry14	0.57
par-6 partitioning defective 6 homolog gamma (C. elegans)	Pard6g	0.73
protocadherin 20	Pcdh20	0.58
protocadherin 7	Pcdh7	0.65
Purkinje cell protein 4	Pcp4	0.74
proprotein convertase subtilisin/kexin type 6	Pcsk6	0.70
phosphodiesterase 7B	Pde7b	0.73
platelet-derived growth factor, C polypeptide	Pdgfc	0.70
platelet derived growth factor receptor, alpha polypeptide	Pdgfra	0.75
PDZ and LIM domain 3	Pdlim3	0.62
PDZ domain containing 2	Pdzd2	0.68
phosphatidylinositol 3 kinase, regulatory subunit, polypeptide 3 (p55)	Pik3r3	0.73
phosphatidylinositol-5-phosphate 4-kinase, type II, alpha	Pip4k2a	0.72
paired-like homeodomain transcription factor 1	Pitx1	0.51
protein kinase inhibitor, alpha	Pkia	0.73
plasminogen activator, urokinase	Plau	0.47
pleckstrin homology domain containing, family G member 1	Plekhg1	0.68
pleckstrin homology domain containing, family H member 2	Plekhh2	0.67
phospholamban	Pln	0.74
plastin 3 (T-isoform)	Pls3	0.79
phospholipid transfer protein	Pltp	0.66
plasmalemma vesicle associated protein	Plvap	0.65
plexin C1	Plxnc1	0.76
plexin D1	Plxnd1	0.66

prostate transmembrane protein, androgen induced 1	Pmepa1	0.70
peripheral myelin protein 22	Pmp22	0.60
periostin, osteoblast specific factor	Postn	0.67
phosphatidic acid phosphatase type 2B	Ppap2b	0.63
protein phosphatase 1, regulatory (inhibitor) subunit 3B	Ppp1r3b	0.68
phosphatidylinositol-3,4,5-trisphosphate-dependent Rac factor 2	Prex2	0.62
prickle-like 2 (Drosophila)	Prickle2	0.72
protein kinase C, delta binding protein	Prkcdbp	0.69
protein kinase D1	Prkd1	0.68
protein kinase, cGMP-dependent, type I	Prkg1	0.73
prion protein dublet	Prnd	0.47
patched homolog 1	Ptch1	0.37
prostaglandin E receptor 1 (subtype EP1)	Ptger1	0.46
prostaglandin-endoperoxide synthase 1	Ptgs1	0.63
protein tyrosine phosphatase, non-receptor type 14	Ptpn14	0.79
protein tyrosine phosphatase, receptor type, B	Ptprb	0.71
protein tyrosine phosphatase, receptor type, M	Ptprm	0.67
polymerase I and transcript release factor	Ptrf	0.66
peroxidasin homolog (Drosophila)	Pxdn	0.60
muscle glycogen phosphorylase	Pygm	0.65
quaking	Qk	0.77
retinoic acid induced 2	Rai2	0.70
receptor (calcitonin) activity modifying protein 2	Ramp2	0.70
RAS related protein 2a	Rap2a	0.76
retinoic acid receptor, beta	Rarb	0.74
RAS-like, family 11, member B	Rasl11b	0.74
ribonucleoprotein, PTB-binding 2	Raver2	0.53
regulator of calcineurin 2	Rcan2	0.72
RCSD domain containing 1	Rcsd1	0.74
RAS-like, estrogen-regulated, growth-inhibitor	Rerg	0.65
regulator of G-protein signalling 10	Rgs10	0.55
regulator of G-protein signaling 5	Rgs5	0.70
regulator of G-protein signaling 5	Rgs5	0.73
ring finger protein 152	Rnf152	0.68
roundabout homolog 1 (Drosophila)	Robo1	0.61
roundabout homolog 4 (Drosophila)	Robo4	0.76
ribosomal protein S6 kinase, polypeptide 2	Rps6ka2	0.77
serum amyloid A 1 /// serum amyloid A 2	Saa1 /// Saa2	0.20
sal-like 1 (Drosophila)	Sall1	0.58
sterile alpha motif domain containing 5	Samd5	0.77
sterile alpha motif domain containing 9-like	Samd9l	0.76
scavenger receptor class B, member 1	Scarb1	0.70
stearoyl-Coenzyme A desaturase 2	Scd2	0.41
schwannomin interacting protein 1 /// predicted gene, EG208426	Schip1 /// EG208426	0.67
scinderin	Scin	0.65
sodium channel, voltage-gated, type II, alpha 1	Scn2a1	0.73
sodium channel, nonvoltage-gated 1 alpha	Scnn1a	0.63
secreted and transmembrane 1B	Sectm1b	0.69

secreted, (semaphorin) 3A	Sema3a	0.45
serine (or cysteine) peptidase inhibitor, clade B, member 9e	Serpinb9e	0.68
secreted frizzled-related protein 2	Sfrp2	0.49
sarcoglycan, epsilon	Sgce	0.79
SH3-binding domain glutamic acid-rich protein	Sh3bgr	0.74
solute carrier family 11 (proton-coupled divalent metal ion transporters), 2	Slc11a2	0.60
solute carrier family 13 (sodium-dependent dicarboxylate transporter), 2	Slc13a2	0.54
solute carrier family 16 (monocarboxylic acid transporters), member 9	Slc16a9	0.73
solute carrier family 17 (sodium phosphate), member 4	Slc17a4	0.55
solute carrier family 39 (zinc transporter), member 2	Slc39a2	0.61
solute carrier family 3, member 1	Slc3a1	0.38
solute carrier family 40 (iron-regulated transporter), member 1	Slc40a1	0.65
solute carrier family 46, member 1	Slc46a1	0.46
solute carrier family 6 (neurotransmitter transporter), member 14	Slc6a14	0.70
solute carrier family 8 (sodium/calcium exchanger), member 1	Slc8a1	0.73
solute carrier family 9 (sodium/hydrogen exchanger), member 9	Slc9a9	0.68
solute carrier organic anion transporter family, member 2a1	Slco2a1	0.46
SLIT and NTRK-like family, member 6	Slitrk6	0.46
MAD homolog 6 (Drosophila)	Smad6	0.68
small muscle protein, X-linked	Smpx	0.74
snail homolog 2 (Drosophila)	Snai2	0.69
synuclein, alpha interacting protein (synphilin)	Sncaip	0.78
sorting nexin 18	Snx18	0.80
sorbin and SH3 domain containing 1	Sorbs1	0.69
spermatogenesis associated glutamate (E)-rich protein 7, pseudogene 1	Speer7-ps1	0.52
Spi-B transcription factor (Spi-1/PU.1 related)	Spib	0.70
sparc/osteonectin, cwcv and kazal-like domains proteoglycan 3	Spock3	0.57
small proline-rich protein 2E	Sprr2e	0.74
sushi-repeat-containing protein, X-linked 2	Srpx2	0.46
beta galactoside alpha 2,6 sialyltransferase 2	St6gal2	0.72
STEAP family member 4	Steap4	0.54
serine/threonine kinase 10	Stk10	0.76
serine/threonine kinase 36 (fused homolog, Drosophila)	Stk36	0.77
storkhead box 2	Stox2	0.65
storkhead box 2	Stox2	0.71
syntaxin binding protein 1	Stxbp1	0.59
sulfotransferase family, cytosolic, 1C, member 2	Sult1c2	0.67
syncollin	Sycn	0.60
synaptotagmin XIII	Syt13	0.77
tachykinin receptor 2	Tacr2	0.57
T-box 2	Tbx2	0.59
transcription elongation factor A (SII)-like 6	Tceal6	0.74
transcription factor 4	Tcf4	0.65
tet oncogene 1	Tet1	0.65
tet oncogene 1	Tet1	0.66
tet oncogene 1	Tet1	0.68
transglutaminase 3, E polypeptide	Tgm3	0.28
tyrosine kinase with immunoglobulin-like and EGF-like domains 1	Tie1	0.74
tissue inhibitor of metalloproteinase 3	Timp3	0.69

transmembrane protein 47	Tmem47	0.64
transmembrane and tetratricopeptide repeat containing 1	Tmtc1	0.68
tensin 4	Tns4	0.69
tripartite motif-containing 12	Trim12	0.59
transient receptor potential cation channel, subfamily A, member 1	Trpa1	0.58
tetratricopeptide repeat domain 28	Ttc28	0.68
tubulin tyrosine ligase-like family, member 7	Ttll7	0.77
twisted gastrulation homolog 1 (Drosophila)	Twsg1	0.71
vasohibin 2	Vash2	0.79
versican	Vcan	0.68
WAP four-disulfide core domain 1	Wfdc1	0.60
wingless-related MMTV integration site 4	Wnt4	0.70
wingless-related MMTV integration site 5A	Wnt5a	0.62
WSC domain containing 2	Wscd2	0.71
X-linked lymphocyte-regulated 4B	Xlr4b	0.61
X-linked lymphocyte-regulated 4C	Xlr4c	0.64
zinc finger E-box binding homeobox 2	Zeb2	0.63
zinc finger protein 536	Zfp536	0.51
zinc finger protein 791	Zfp791	0.74
zinc finger protein, multitype 2	Zfpm2	0.76

Genes Up-regulated in Conditional *Ihh* Mutant Mice versus Control Mice

Gene Title	Gene Symbol	Fold Change
RIKEN cDNA 1300002K09 gene	1300002K09Rik	1.46
RIKEN cDNA 1600029D21 gene	1600029D21Rik	2.61
RIKEN cDNA 1700001L05 gene	1700001L05Rik	1.37
RIKEN cDNA 1700019H03 gene	1700019H03Rik	1.54
RIKEN cDNA 1810010D01 gene	1810010D01Rik	1.30
RIKEN cDNA 1810033B17 gene	1810033B17Rik	1.53
RIKEN cDNA 2010002N04 gene	2010002N04Rik	1.66
RIKEN cDNA 2010106E10 gene	2010106E10Rik	2.87
RIKEN cDNA 2210407C18 gene	2210407C18Rik	2.77
RIKEN cDNA 2210417D09 gene	2210417D09Rik	1.50
RIKEN cDNA 2310016C08 gene	2310016C08Rik	1.60
RIKEN cDNA 4732429D16 gene	4732429D16Rik	1.39
RIKEN cDNA 4833403I15 gene	4833403I15Rik	1.46
RIKEN cDNA 4921506M07 gene	4921506M07Rik	1.30
RIKEN cDNA 4933409K07 gene	4933409K07Rik	1.73
RIKEN cDNA 4933409K07 gene	4933409K07Rik	1.72
RIKEN cDNA 4933409K07 gene	4933409K07Rik	1.66
RIKEN cDNA 4933409K07 gene	4933409K07Rik	1.72
RIKEN cDNA 4933409K07 gene	4933409K07Rik	1.53
RIKEN cDNA 4933409K07 gene	4933409K07Rik	1.46
RIKEN cDNA 4933409K07 gene	4933409K07Rik	1.42
RIKEN cDNA 5330417C22 gene	5330417C22Rik	1.46
RIKEN cDNA 5330438D12 gene	5330438D12Rik	1.32

RIKEN cDNA 6330406I15 gene	6330406I15Rik	1.38
RIKEN cDNA 9030619P08 gene	9030619P08Rik	1.96
RIKEN cDNA 9130221D24 gene	9130221D24Rik	1.47
RIKEN cDNA A230067G21 gene	A230067G21Rik	1.34
alpha-1,4-N-acetylglucosaminyltransferase	A4gnt	2.54
acetyl-Coenzyme A carboxylase beta	Acacb	1.35
acyl-CoA thioesterase 1	Acot1	1.71
acyl-CoA thioesterase 2	Acot2	1.41
acyl-CoA synthetase family member 2	Acsf2	1.73
acyl-CoA synthetase family member 2	Acsf2	1.71
adenylate cyclase 8	Adcy8	1.80
alcohol dehydrogenase 1 (class I)	Adh1	1.70
alcohol dehydrogenase 5 (class III), chi polypeptide	Adh5	1.33
adenosine A1 receptor	Adora1	1.31
angiotensin II receptor, type 2	Agtr2	1.34
aldo-keto reductase family 1, member B8	Akr1b8	1.82
aminolevulinic acid synthase 2, erythroid	Alas2	1.30
arachidonate 5-lipoxygenase activating protein	Alox5ap	1.53
alpha-kinase 1	Alpk1	1.29
amphiphysin	Amph	1.34
angiopoietin-like 4	Angptl4	2.03
ankyrin repeat domain 22	Ankrd22	1.61
annexin A13	Anxa13	1.43
aquaporin 1	Aqp1	1.66
aquaporin 3	Aqp3	2.20
amphiregulin	Areg	1.70
arginase type II	Arg2	1.66
asparagine synthetase	Asns	1.52
asparaginase homolog (S. cerevisiae)	Aspg	1.46
atonal homolog 1 (Drosophila)	Atoh1	1.32
ATPase, H+ transporting, lysosomal accessory protein 2	Atp6ap2	1.35
AU RNA binding protein/enoyl-coenzyme A hydratase	Auh	1.28
expressed sequence AW551984	AW551984	1.57
UDP-GlcNAc:betaGal beta-1,3-N-acetylglucosaminyltransferase 6	B3gnt6	2.45
beta-1,4-N-acetyl-galactosaminyl transferase 2	B4galnt2	1.71
UDP-Gal:betaGlcNAc beta 1,4-galactosyltransferase, 4	B4galt4	1.38
beta-site APP-cleaving enzyme 2	Bace2	1.31
cDNA sequence BC021891	BC021891	1.42
betaine-homocysteine methyltransferase 2	Bhmt2	1.47
B-cell linker	Blnk	1.30
B-box and SPRY domain containing	Bspry	1.28
bone marrow stromal cell antigen 1	Bst1	1.67
RIKEN cDNA C130090K23 gene	C130090K23Rik	1.54
C1GALT1-specific chaperone 1	C1galt1c1	1.35
C1q and tumor necrosis factor related protein 7	C1qtnf7	1.30
complement component 3	C3	2.07
complement component 4B (Childo blood group)	C4b	1.75
carbonic anyhydrase 12	Car12	1.55
caspase 14	Casp14	1.40
carbonyl reductase 2	Cbr2	1.76
cystathionine beta-synthase	Cbs	1.47

coiled-coil domain containing 101	Ccdc101	1.31
cholecystokinin	Cck	2.62
chemokine (C-C motif) ligand 25	Ccl25	1.63
chemokine (C-C motif) ligand 6	Ccl6	1.39
chemokine (C-C motif) ligand 9	Ccl9	1.80
chemokine (C-C motif) receptor 2	Ccr2	1.74
CD14 antigen	Cd14	1.32
CD177 antigen	Cd177	5.29
CD24a antigen	Cd24a	1.89
CD55 antigen	Cd55	1.63
carcinoembryonic antigen-related cell adhesion molecule 10	Ceacam10	5.34
CCAAT/enhancer binding protein (C/EBP), delta	Cebpd	1.52
cystic fibrosis transmembrane conductance reg. homolog	Cftr	1.44
cell growth regulator with EF hand domain 1	Cgref1	1.56
chromodomain helicase DNA binding protein 7	Chd7	1.37
chromodomain helicase DNA binding protein 7	Chd7	1.24
chromodomain helicase DNA binding protein 7	Chd7	1.26
chitinase 3-like 1	Chi3l1	2.03
chordin-like 2	Chrdl2	2.82
chloride channel calcium activated 2	Clca2	1.80
chloride channel calcium activated 4	Clca4	1.47
claudin 2	Cldn2	2.13
claudin 4	Cldn4	1.52
C-type lectin domain family 4, member d	Clec4d	1.59
colipase, pancreatic	Clps	1.62
colony stimulating factor 3 receptor (granulocyte)	Csf3r	1.46
cubilin (intrinsic factor-cobalamin receptor)	Cubn	1.71
chemokine (C-X-C motif) ligand 5	Cxcl5	2.51
cytochrome P450, family 2, subfamily j, polypeptide 5	Cyp2j5	1.51
delta-like 1 homolog (Drosophila)	Dlk1	2.48
dual oxidase 2	Duox2	1.66
dual oxidase maturation factor 2	Duoxa2	1.66
dual specificity phosphatase 4	Dusp4	1.51
dynein cytoplasmic 1 intermediate chain 1	Dync1i1	1.39
EF-hand calcium binding domain 5	Efcab5	1.37
predicted gene, EG245472	EG245472	1.32
predicted gene, EG434181	EG434181	1.29
predicted gene, EG665783	EG665783	1.41
epidermal growth factor	Egf	1.44
enoyl-Coenzyme A, hydratase/3-hydroxyacyl Coenzyme A dehydrogenase	Ehhadh	1.65
eukaryotic translation initiation factor 1A	Eif1a	1.26
eukaryotic translation initiation factor 2B, subunit 1 (alpha)	Eif2b1	1.33
embigin	Emb	1.32
ectonucleotide pyrophosphatase/phosphodiesterase 3	Enpp3	1.44
ectonucleoside triphosphate diphosphohydrolase 7	Entpd7	1.29
epsin 3	Epn3	1.50
epiregulin	Ereg	1.68
ecotropic viral integration site 1	Evi1	1.46
extracellular proteinase inhibitor	Expi	1.65
coagulation factor XIII, A1 subunit	F13a1	1.71

coagulation factor III	F3	1.35
family with sequence similarity 55, member B	Fam55b	2.27
family with sequence similarity 57, member A	Fam57a	1.65
Fc receptor, IgG, low affinity IIb	Fcgr2b	1.67
fibroblast growth factor 15	Fgf15	3.54
FK506 binding protein 5	Fkbp5	3.02
forkhead box A3	Foxa3	1.48
formyl peptide receptor 2 /// formyl peptide receptor 3	Fpr2 /// Fpr3	1.50
FERM domain containing 3	Frmd3	1.87
fucosyltransferase 2	Fut2	1.50
FXYD domain-containing ion transport regulator 3	Fxyd3	1.47
FXYD domain-containing ion transport regulator 4	Fxyd4	1.64
UDP-N-acetyl-alpha-D-galactosamine:polypeptide N-acetylgalactosaminyltransferase 3	Galnt3	1.55
glucagon	Gcg	3.98
glucosaminyl (N-acetyl) transferase 3, mucin type	Gcnt3	1.53
guanine deaminase	Gda	2.01
glycerophosphodiester phosphodiesterase domain 1	Gdpd1	1.63
GTP binding protein	Gem	1.43
gene model 1123, (NCBI)	Gm1123	1.38
gene model 379, (NCBI)	Gm379	1.61
gene model 73, (NCBI)	Gm73	1.47
GDP-mannose 4, 6-dehydratase	Gmds	1.52
glycoprotein 49 A	Gp49a	2.26
G protein-coupled receptor 120	Gpr120	1.46
glutathione peroxidase 2	Gpx2	1.47
gene regulated by estrogen in breast cancer protein	Greb1	1.34
gremlin 1	Grem1	1.41
grainyhead-like 3 (Drosophila)	Grhl3	1.33
guanylate cyclase 2c	Gucy2c	1.32
guanylate kinase 1	Guk1	1.39
hemoglobin alpha, adult chain 1	Hba-a1	1.62
hemoglobin alpha, adult chain 2	Hba-a2	1.60
hepatocyte growth factor activator	Hgfac	1.61
hypoxia inducible factor 3, alpha subunit	Hif3a	1.99
high mobility group AT-hook 2	Hmga2	1.41
3-hydroxy-3-methylglutaryl-Coenzyme A synthase 2	Hmgcs2	1.63
hepatocyte nuclear factor 4, gamma	Hnf4g	1.56
HOP homeobox	Hopx	1.46
haptoglobin	Hp	2.16
4-hydroxyphenylpyruvic acid dioxygenase	Hpd	1.67
interferon induced transmembrane protein 1	Ifitm1	1.66
interferon induced transmembrane protein 1	Ifitm1	1.64
insulin-like growth factor 2 receptor	Igf2r	1.31
interleukin 1 beta	Il1b	3.50
interleukin 1 receptor, type I	Il1r1	1.45
interleukin 8 receptor, beta	Il8rb	3.03
insulin-like 5	Insl5	1.93
insulin receptor-related receptor	Insrr	1.63
inositol 1,3,4,5,6-pentakisphosphate 2-kinase	Ippk	1.33
interleukin-1 receptor-associated kinase 3	Irak3	1.41

integrin alpha M	Itgam	1.44
potassium channel, subfamily K, member 1	Kcnk1	1.61
potassium voltage-gated channel, subfamily Q, member 1	Kcnq1	1.40
keratin 18	Krt18	1.51
LAG1 homolog, ceramide synthase 6	Lass6	1.50
lipopolysaccharide binding protein	Lbp	1.66
lipocalin 2	Lcn2	2.34
leucine-rich repeat LGI family, member 1	Lgi1	1.42
leucine rich repeat containing G protein coupled receptor 5	Lgr5	1.60
leukocyte immunoglobulin-like receptor, subfamily B, 4	Lilrb4	1.84
similar to Heparanase-2 (Hpa2)	LOC545291	1.39
lactoperoxidase	Lpo	1.49
lactotransferrin	Ltf	1.41
lymphocyte antigen 6 complex, locus A	Ly6a	1.72
lymphocyte antigen 6 complex, locus D	Ly6d	2.08
maternally expressed 3	Meg3	1.97
matrix Gla protein	Mgp	2.98
mohawk homeobox	Mkx	1.36
matrix metallopeptidase 10	Mmp10	1.77
matrix metallopeptidase 3	Mmp3	1.81
matrix metallopeptidase 7	Mmp7	2.49
matrix metallopeptidase 8	Mmp8	1.59
membrane protein, palmitoylated 3 (MAGUK p55 subfamily 3)	Mpp3	1.53
mucin 1, transmembrane	Muc1	1.45
mucin 2	Muc2	1.27
myelocytomatosis oncogene	Myc	1.39
nuclear factor, interleukin 3, regulated	Nfil3	1.57
nuclear factor of kappa light polypeptide gene enhancer in B-cells inhibitor	Nfkbiz	1.34
NADPH oxidase activator 1	Noxa1	1.87
neuritin 1	Nrn1	1.43
neurotensin	Nts	1.82
nuclear protein 1	Nupr1	2.06
olfactory receptor 1463	Olfr1463	1.38
olfactory receptor 624	Olfr624	1.29
oncostatin M receptor	Osmr	1.74
organic solute transporter beta	Ostb	2.24
predicted gene, OTTMUSG00000000971	OTTMUSG00000000971	2.28
predicted gene, OTTMUSG00000002043	OTTMUSG00000002043	1.43
pappalysin 2	Pappa2	2.23
pappalysin 2	Pappa2	1.92
pappalysin 2	Pappa2	1.56
phosphoenolpyruvate carboxykinase 1, cytosolic	Pck1	1.58
proprotein convertase subtilisin/kexin type 1	Pcsk1	1.71
phosphodiesterase 8B	Pde8b	1.74
phosphodiesterase 9A	Pde9a	1.38
protein disulfide isomerase associated 5	Pdia5	1.32
pyruvate dehydrogenase kinase, isoenzyme 4	Pdk4	2.74
peroxisomal delta3, delta2-enoyl-Coenzyme A isomerase	Peci	1.38
period homolog 1 (Drosophila)	Per1	1.38
peroxisomal biogenesis factor 11a	Pex11a	1.43

peptidoglycan recognition protein 1	Pglyrp1	1.66
phytanoyl-CoA hydroxylase	Phyh	1.26
polymeric immunoglobulin receptor	Pigr	1.46
proviral integration site 3	Pim3	1.31
phospholipase A2, group IIF	Pla2g2f	1.74
phospholipase A2, group VII	Pla2g7	1.60
plasminogen activator, tissue	Plat	2.20
plasminogen activator, urokinase receptor	Plaur	1.74
pleckstrin homology domain containing, family H member 1	Plekhh1	1.42
phospholipid scramblase 1	Plscr1	1.43
phospholipid scramblase 1	Plscr1	1.36
phosphomannomutase 2	Pmm2	1.39
peptidylprolyl isomerase F (cyclophilin F)	Ppif	1.34
peroxiredoxin 6	Prdx6	1.39
protease, serine, 22	Prss22	1.33
prostate stem cell antigen	Psca	1.94
peptide YY	Pyy	1.60
quiescin Q6 sulfhydryl oxidase 2	Qsox2	1.44
Ras association (RalGDS/AF-6) domain family member 4	Rassf4	1.55
regenerating islet-derived 3 beta	Reg3b	6.22
regenerating islet-derived 3 gamma	Reg3g	5.71
regenerating islet-derived family, member 4	Reg4	2.74
resistin like beta	Retnlb	5.44
resistin like gamma	Retnlg	2.17
Rho-guanine nucleotide exchange factor	Rgnef	1.27
RNA imprinted and accumulated in nucleus	Rian	1.78
receptor-interacting serine-threonine kinase 3	Ripk3	1.51
ring finger protein 39	Rnf39	1.28
rabphilin 3A-like (without C2 domains)	Rph3al	1.28
radical S-adenosyl methionine domain containing 1	Rsad1	1.45
S100 calcium binding protein A8 (calgranulin A)	S100a8	2.86
S100 calcium binding protein A9 (calgranulin B)	S100a9	1.95
sphingosine-1-phosphate receptor 3	S1pr3	1.40
sodium channel, nonvoltage-gated 1 beta	Scnn1b	1.80
serine (or cysteine) peptidase inhibitor, clade A, 3N	Serpina3n	2.44
secreted frizzled-related protein 1	Sfrp1	1.73
serum/glucocorticoid regulated kinase 1	Sgk1	1.36
sphingomyelin synthase 2	Sgms2	1.45
serine hydroxymethyltransferase 1 (soluble)	Shmt1	1.42
SID1 transmembrane family, member 1	Sidt1	2.20
signal-regulatory protein beta 1	Sirpb1	1.77
solute carrier family 10, member 2	Slc10a2	2.24
solute carrier family 12, member 2	Slc12a2	1.60
solute carrier family 12, member 8	Slc12a8	1.47
solute carrier family 18 (vesicular monoamine), member 1	Slc18a1	1.80
solute carrier family 19 (sodium/hydrogen exchanger), 1	Slc19a1	1.30
solute carrier family 27 (fatty acid transporter), member 2	Slc27a2	2.29
solute carrier family 35 (CMP-sialic acid transporter),1	Slc35a1	1.40
solute carrier family 39 (zinc transporter), member 4	Slc39a4	2.81
solute carrier family 39 (metal ion transporter), member 8	Slc39a8	1.89
solute carrier family 5 (sodium-dependent vitamin transporter), 6	Slc5a6	1.53

solute carrier family 6 (neurotransmitter transporter), 19	Slc6a19	1.60
solute carrier family 7 (cationic amino acid transporter, y+ system), 11	Slc7a11	1.41
solute carrier family 9 (sodium/hydrogen exchanger), member 3	Slc9a3	2.46
solute carrier family 9 (sodium/hydrogen exchanger), member 4	Slc9a4	1.27
secretory leukocyte peptidase inhibitor	Slpi	2.11
SPARC related modular calcium binding 2	Smoc2	1.49
sterol O-acyltransferase 1	Soat1	1.41
suppressor of cytokine signaling 3	Socs3	1.43
SRY-box containing gene 9	Sox9	1.47
SAM pointed domain containing ets transcription factor	Spdef	1.74
serine peptidase inhibitor, Kazal type 4	Spink4	1.73
small proline-rich protein 1A	Sprr1a	2.61
serglycin	Srgn	1.46
signal sequence receptor, delta	Ssr4	1.36
ST3 beta-galactoside alpha-2,3-sialyltransferase 5	St3gal5	1.65
stefin A2	Stfa2	1.74
stefin A2 like 1 /// stefin A2	Stfa2l1 /// Stfa2	4.57
stefin A3	Stfa3	1.61
sulfotransferase family 1A, phenol-preferring, member 1	Sult1a1	2.01
tachykinin 1	Tac1	1.82
tumor-associated calcium signal transducer 2	Tacstd2	1.93
T-cell activation GTPase activating protein 1	Tagap1	1.37
TRAF-interacting protein with forkhead-associated domain	Tifa	2.16
tissue inhibitor of metalloproteinase 1	Timp1	1.85
transmembrane 4 superfamily member 4	Tm4sf4	1.61
transmembrane 4 superfamily member 5	Tm4sf5	1.62
transmembrane channel-like gene family 5	Tmc5	1.44
transmembrane emp24 protein transport domain containing 5	Tmed5	1.40
transmembrane protein 56	Tmem56	1.62
transmembrane and immunoglobulin domain containing 1	Tmigd1	1.59
transmembrane protease, serine 11a	Tmprss11a	1.26
transmembrane protease, serine 2	Tmprss2	1.50
tumor necrosis factor, alpha-induced protein 8-like 1	Tnfaip8l1	1.35
tumor necrosis factor receptor superfamily, member 11b	Tnfrsf11b	1.34
tumor necrosis factor receptor superfamily, member 23	Tnfrsf23	1.40
tumor necrosis factor receptor superfamily, member 8	Tnfrsf8	1.40
triggering receptor expressed on myeloid cells 1	Trem1	1.61
tripartite motif-containing 71	Trim71	1.37
transient receptor potential cation channel, subfamily M, member 6	Trpm6	2.10
twinfilin, actin-binding protein, homolog 1 (Drosophila)	Twf1	1.40
twinfilin, actin-binding protein, homolog 1 (Drosophila)	Twf1	1.31
UDP-N-acetylglucosamine pyrophosphorylase 1	Uap1	1.34
UDP glucuronosyltransferase 2 family, polypeptide B35	Ugt2b35	1.50
uroplakin 1B	Upk1b	1.48
vav 3 oncogene	Vav3	1.53
vasoactive intestinal peptide receptor 1	Vipr1	1.36
vomeronasal 2, receptor 68	Vmn2r68	1.32
vanin 1	Vnn1	3.38
V-set and immunoglobulin domain containing 2	Vsig2	1.49
zinc finger and BTB domain containing 16	Zbtb16	1.62

Table S2. Primer Sequences

Primers for Genotyping		
Primer	Forward	Reverse
flIhh	AGCACCTTTTTTCTCGACTGCCTG	TGTTAGGCCGAGAGGGATTTCGTG
fSmo	CCACTGCGAGCCTTTGCGCTAC	CCCATCACCTCCGCGTCGCA
VillinCre	GTGTGGGACAGAGAACAAACC	ACATCTTCAGGTTCTGCGGG

Murine Primers for Quantitative RT-PCR		
Primer	Forward	Reverse
GAPDH	GGAGTTGCTGTTGAAGTCGCA	GGAGTTGCTGTTGAAGTCGCA
Ihh	CCATCTTCATCCCAGCCTTCG	CACCCCCAACTACAATCCCG
Ptch1	TACGTGGAGGTGGTTCATCA	CACCAACACCAAGAGCAAGA
Gli1	CCTGGTGGCTTTCATCAACT	TCATCTGAGGTGGGAATCCT

Human Primers for Quantitative RT-PCR		
Primer	Forward	Reverse
GAPDH	GAAGGTGAAGGTCGGAGTC	GAAGATGGTGATGGGATTTC
Ptch1	GGTGGCTTCTCTAGGTGTCG	TACCCTGAGGTTCCAGCATC
Hhip1	CCCACACTTCAACAGCACCA	GCACATCTGCCTGGATCGT
Mef2c	ATGCCATCAGTGAATCAAAGGAT	CTGGTAAAGTAGGAGTTGCTACG
Myocd	GCACTGCACAGAACTCAGGAG	CCGCTTTCAATAAGCACGTCC
Lama4	GCAGTGGAAATTCAGATCCCA	TAACCGCAGGTCATCAGTCAG
MMP10	TGCTCTGCCTATCCTCTGAGT	TCACATCCTTTTCGAGGTTGTAG
MMP3	AGTCTTCCAATCCTACTGTTGCT	TCCCCGTCACCTCCAATCC

Chapter 4

Conclusion

Implications

Reciprocal signaling events between the gut epithelium and the underlying mesenchyme are essential for proper intestinal development, regional patterning, maintenance of the stem cell population, and homeostasis. Significant advances have been made towards identifying the location (epithelium and/or mesenchyme) of signaling molecules in the intestine, but many questions remain about the specific signals that emanate from or target the mesenchymal intestinal stem cell (ISC) niche and how signaling pathways coordinately control intestinal morphogenesis, ISC self-renewal and differentiation. The work presented in this thesis provides new insights toward the definition of the mesenchymal ISC niche. In particular, we have identified new secreted niche factors that influence epithelial cell behavior and determine that Indian hedgehog (Ihh), an epithelial-to-mesenchymal signal, maintains the niche environment and indirectly controls ISC fate. Furthermore, our findings highlight the dual nature of the ISC niche in that it acts to both promote and restrict ISC self-renewal.

We performed expression profiling of the normal human colon and identified nine hundred sixty-nine cDNA clones that were differentially expressed between the top and bottom crypt compartments. Two clusters of genes were found up-regulated in crypt bottoms. The first cluster consisted of genes associated with cell proliferation and cell cycle regulation. It is conceivable that among the genes included in this cluster are candidate ISC markers. In fact, Olfm4, which we showed to be enriched in crypt bottoms was recently identified as a definitive ISC marker (1). Determining the staining pattern of these genes in the crypt will further clarify the specific role each gene plays (e.g., proliferation, stem cell renewal, maturation of Paneth cells (in the small intestine)). The

second cluster consisted of genes that encode secretory proteins and genes involved in extracellular matrix organization. Among the genes identified in this cluster were three BMP antagonists, Gremlin 1, Gremlin 2, and Chordin-like 1. *In situ* hybridization and RT-PCR revealed that these BMP antagonists are expressed by intestinal subepithelial myofibroblasts and smooth muscle cells at the crypt base. Further experimentation demonstrated that Gremlin 1 concurrently activates Wnt signaling and inhibits differentiation in intestinal epithelial cells. Taken together, these results suggest BMP antagonists are secreted ISC niche factors that coordinate with Wnt signals to promote ISC self-renewal.

The identification of BMP antagonists as ISC niche factors raised the question of what signals may act on the ISC niche and direct paracrine regulators of stem cell activity. Here we show that Indian hedgehog (Ihh) regulates the expression of BMP signaling components and is required for the proper development of the ISC niche. Inactivation of intestinal epithelial Ihh in mice resulted in loss of the muscularis mucosae in the small intestine and colon, reduced myofibroblasts around the crypt base, and a compromised ECM. Furthermore, BMP signaling, which is believed to block crypt formation, was reduced in Ihh-deficient mice. Disruption of the ISC niche subsequently led to an increase in ISC numbers, enlarged crypts, increased incidences of crypt fission, and *de novo* crypts. In regions along the colon of Ihh-deficient mice where the muscularis mucosae remained intact, the size and shape of crypts were normal with proliferating cells restricted to the bottom. This finding suggests that the function of the muscularis mucosae may extend beyond contractile activity and include a previously unrecognized role as an ISC niche element that acts together with myofibroblasts to

restrain crypt expansion and prevent abnormal stimulation of ISCs. Until now, no study has distinguished between the effects of Ihh on ISCs versus the progenitor compartment. This is the first demonstration that Ihh controls ISC numbers. Furthermore, we show Ihh-mediated regulation of ISCs is paracrine, rather than cell-autonomous, as inactivation of Hh signaling in intestinal epithelial cells results in no obvious epithelial or mesenchymal defects, including changes in ISC numbers. Finally, we provide novel mechanistic evidence that Ihh modulates ISC fate via the deregulation of BMP signaling and the disruption of extracellular matrix proteins that surround ISCs.

Future Perspectives

Does loss of Ihh in the gut promote colorectal cancer? Abnormal activation of the Hh pathway has been implicated in multiple tumor types, including basal cell carcinoma, medulloblastoma, pancreatic adenocarcinomas, prostrate and ovarian cancer (2-5). However, involvement of the Hh pathway in colorectal cancer remains unclear and controversial with numerous conflicting reports existing in the literature. Expression analysis of key members of the Hh signaling pathway in colon cancer cell lines (e.g., Colo205, Colo320, HT29, Caco-2, SW480) found no cell line that expressed all the components necessary to activate the Hh pathway (6). In agreement, Berman et al. showed that colon-derived tumor cell lines lacked expression of the Hh target gene Ptch and maintained viability *in vitro* and *in vivo* when treated with the Hh-specific antagonist cyclopamine (7). In contrast to these studies, Qualtrough et al. detected Ptch, Smo, and Gli1 in colon-derived tumor cell lines and observed increased apoptosis in colon tumor cells treated with cyclopamine (8). Nevertheless, as more evidence accumulates

suggesting that Hh signals target gut mesenchymal cells *in vivo*, the significance of Hh-responsiveness in colon tumor epithelial cells seems low. The recent finding that Hh-induced mesenchymal signals are required for the tumorigenesis of Hh-expressing cancers raises more questions about the relevance of *in vitro* cell experiments, as cell culture systems do not accurately recapitulate the *in vivo* microenvironment (9). Human pathological studies on colorectal cancer have produced conflicting reports as well. Tissue samples obtained from patients with familial adenomatous polyposis (FAP), a syndrome caused by the loss of APC expression, leading to uncontrolled Wnt activity and polyp formation, were shown to have loss of Ihh expression from dysplastic epithelial cells (10). In contrast to these results, Sonic hedgehog (Shh) expression was found to be up-regulated in hyperplastic polyps, adenomas, and adenocarcinomas of the colon (11). Most recently, analysis of benign and malignant colonic lesions showed that expression of Shh, Gli1, Gli2, and Ptch was maintained in benign lesions, whereas malignant lesions displayed reduced or lost expression of Hh signaling components (12).

The majority of colorectal tumors are characterized by their inability to regulate β-catenin/TCF-mediated transcription (13). Ihh has been shown to abrogate Wnt signaling in a colon cancer cell line and transgenic expression of the pan-hedgehog inhibitor, Hhip (hedgehog interacting protein) augments Wnt activity in the small intestine. In our study, we found that loss of intestinal Ihh increased activation of Wnt signaling and led to neoplastic transformation of the small intestinal and colonic epithelium in 4 week old mice. Furthermore, we observed Ihh-deficient mice have increased expression of matrix metalloproteinases (MMPs) and reduced expression of ECM proteins. The ECM imparts strength and acts as a physical barrier to migrating

cells. Additionally, it supports cell adhesion, induces differentiation, cell division, and apoptosis, and contributes to the architectural layout of the crypt-villus axis. Disruption of the ECM components can alter epithelial cell behavior towards uncontrolled cell growth and enhance the metastatic potential of neoplastic colonic cells. Our studies suggest that loss of Ihh may contribute to colorectal cancer, playing distinct roles during different stages of tumor development. Loss of Ihh results in increased expression of the Wnt pathway and increased nuclear β-catenin levels, leading to single crypt adenomas. In our microarray study, we detected marked increases in immuno-response genes, including cytokines, chemokines and their receptors (e.g., IL1b, IL1 receptor 1, CCL6, CCL9). Whether the increase in inflammatory stimuli, in concert with increased Wnt activity, is responsible for the development of tubular adenoma in the mutant mice remains to be addressed. Additionally, we observed a compromised ECM compartment, increased MMP expression, and loss of the muscularis mucosae in the mutant mice, a situation that favors cancer metastasis during late stages of colon cancer. Further studies will be necessary to determine whether Ihh loss accelerates cancer progression and metastasis. This question may be addressed by assessing the effect of the combined deletion of *Apc* and *Ihh*.

Is Ihh required for adult intestinal homeostasis? We have demonstrated that Ihh is required for the proper development of the mesenchymal compartment of the gut, including the establishment of the muscularis mucosae and structural integrity of the ECM; these mesenchymal changes, secondarily affect the epithelium and include dilated crypts, branching villi, increased proliferation, and aberrant differentiation. An important

question is once the mesenchymal compartment is formed, is Ihh signaling necessary to maintain it. For example, we show that MMPs are up-regulated in the colon of postnatal mice, but it is unknown whether loss of Ihh will have the same effect in the adult. MMPs are normally involved in intestinal remodeling during the postnatal stages of murine development, whereas in adult mice, intestinal morphogenesis is complete and MMP activity is reduced (14). Thus, Ihh may play a role in regulating MMP activity when MMP expression is induced during development, but not in adulthood when MMP expression is more stable. Another question that remains is how will Ihh signaling integrate with the signaling pathways that are active during intestinal homeostasis? These questions may be resolved by the conditional knockout of Ihh in adult mice. These mice may be generated by crossing $Ihh^{flox/flox}$ mice with AhCre mice (Cre transgrene is activated in intestinal epithelial cells and hepatocytes by the cytochrome P450 1A1 promoter after injection of β-naphthoflavone).

Does Ihh regulate gut motility? The enteric nervous system (ENS) acts together with gastrointestinal smooth muscle and pacemakers known as Interstitial Cells of Cajal (ICC) to propagate coordinated gut contractions (15). Abnormalities in the ENS, gut muscle, and ICCs may lead to gut motility disorders. A study by Ramalho-Santos et al. found that Ihh is involved in the development of the ENS and that *Ihh*-null mice display a phenotype with features resembling Hirschsprung's disease, a disorder characterized by the lack of ganglion cells in the colon, leading to severe chronic constipation (16). However, subsequent studies have found that Ihh is not a major gene in Hirschsprung's disease (17) and transgenic mice expressing Hhip exhibit no defects in neuronal

patterning (18). Furthermore, it was reported that enteric neurons lack Gli1 expression, indicating they do not respond to Hh signals (19). The conditional Ihh mutants from our study displayed distended stomachs and small intestines and yellow liquid stool or no stool in the colon. These pathological findings suggest that the mutant mice may have impaired gut motility. It is possible that this phenotype is due to indirect effects of Ihh on the ENS, such that Ihh indirectly disrupts the migration, differentiation, or proliferation of the neuron or glial cells that make up the ENS. However, because Ihh has been shown to target mesenchymal cells, it seems more likely that Ihh affects gut motility by regulating the development of smooth muscle cells or ICCs, which originate from the intestinal mesenchyme. Alterations in the position, number, and size of enteric neurons and ICCs may be examined by immunohistochemical analysis. These initial studies will provide new insights into the role of Ihh in the mechanisms of gut motility.

References

1. van der Flier, L. G., Haegebarth, A., Stange, D. E., van de Wetering, M. & Clevers, H. (2009) *Gastroenterology* **137,** 15-7.
2. Jiang, J. & Hui, C. C. (2008) *Dev Cell* **15,** 801-12.
3. Evangelista, M., Tian, H. & de Sauvage, F. J. (2006) *Clin Cancer Res* **12,** 5924-8.
4. Xie, J. (2005) *Future Oncol* **1,** 331-8.
5. Bhattacharya, R., Kwon, J., Ali, B., Wang, E., Patra, S., Shridhar, V. & Mukherjee, P. (2008) *Clin Cancer Res* **14,** 7659-66.
6. Chatel, G., Ganeff, C., Boussif, N., Delacroix, L., Briquet, A., Nolens, G. & Winkler, R. (2007) *Int J Cancer* **121,** 2622-7.
7. Berman, D. M., Karhadkar, S. S., Maitra, A., Montes De Oca, R., Gerstenblith, M. R., Briggs, K., Parker, A. R., Shimada, Y., Eshleman, J. R., Watkins, D. N. & Beachy, P. A. (2003) *Nature* **425,** 846-51.
8. Qualtrough, D., Buda, A., Gaffield, W., Williams, A. C. & Paraskeva, C. (2004) *Int J Cancer* **110,** 831-7.
9. Yauch, R. L., Gould, S. E., Scales, S. J., Tang, T., Tian, H., Ahn, C. P., Marshall, D., Fu, L., Januario, T., Kallop, D., Nannini-Pepe, M., Kotkow, K., Marsters, J. C., Rubin, L. L. & de Sauvage, F. J. (2008) *Nature* **455,** 406-10.
10. van den Brink, G. R., Bleuming, S. A., Hardwick, J. C., Schepman, B. L., Offerhaus, G. J., Keller, J. J., Nielsen, C., Gaffield, W., van Deventer, S. J., Roberts, D. J. & Peppelenbosch, M. P. (2004) *Nat Genet* **36,** 277-82.
11. Oniscu, A., James, R. M., Morris, R. G., Bader, S., Malcomson, R. D. & Harrison, D. J. (2004) *J Pathol* **203,** 909-17.
12. Alinger, B., Kiesslich, T., Datz, C., Aberger, F., Strasser, F., Berr, F., Dietze, O., Kaserer, K. & Hauser-Kronberger, C. (2009) *Virchows Arch* **454,** 369-79.
13. Morin, P. J., Sparks, A. B., Korinek, V., Barker, N., Clevers, H., Vogelstein, B. & Kinzler, K. W. (1997) *Science* **275,** 1787-90.
14. Powell, D. W., Adegboyega, P. A., Di Mari, J. F. & Mifflin, R. C. (2005) *Am J Physiol Gastrointest Liver Physiol* **289,** G2-7.
15. Burzynski, G., Shepherd, I. T. & Enomoto, H. (2009) *Neurogastroenterol Motil* **21,** 113-27.
16. Ramalho-Santos, M., Melton, D. A. & McMahon, A. P. (2000) *Development* **127,** 2763-72.
17. Garcia-Barcelo, M. M., Lee, W. S., Sham, M. H., Lui, V. C. & Tam, P. K. (2003) *Neurogastroenterol Motil* **15,** 663-8.
18. Madison, B. B., Braunstein, K., Kuizon, E., Portman, K., Qiao, X. T. & Gumucio, D. L. (2005) *Development* **132,** 279-89.
19. Kolterud, A., Grosse, A. S., Zacharias, W. J., Walton, K. D., Kretovich, K. E., Madison, B. B., Waghray, M., Ferris, J. E., Hu, C., Merchant, J. L., Dlugosz, A. A., Kottmann, A. H. & Gumucio, D. L. (2009) *Gastroenterology* **137,** 618-28.

Publishing Agreement

It is the policy of the University to encourage the distribution of all theses, dissertations, and manuscripts. Copies of all UCSF theses, dissertations, and manuscripts will be routed to the library via the Graduate Division. The library will make all theses, dissertations, and manuscripts accessible to the public and will preserve these to the best of their abilities, in perpetuity.

Please sign the following statement:

I hereby grant permission to the Graduate Division of the University of California, San Francisco to release copies of my thesis, dissertation, or manuscript to the Campus Library to provide access and preservation, in whole or in part, in perpetuity.

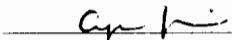

Author Signature

12/15/09

Date